Fabrication of an organic electrochemical transistor for the detection of *Escherichia coli* O157:H7 in liquid samples

by

Angelica Isabel Aguilar Vallejo

A thesis submitted in partial fulfillment of the requirements for the degree of

Master of Science

in

Materials Engineering

Department of Chemical and Materials Engineering

University of Alberta

Abstract

Escherichia coli O157:H7 is an enterohaemorrhagic bacteria which produces Shiga toxins 1 and 2; this strain is responsible for several outbreaks due to contaminated food and water. In order to prevent future outbreaks and maintain the public safe from infections, different microbiological techniques such as cell cultures and polymerase chain reaction (PCR) are routinely used pathogen detection. However, these techniques have some limitations, including the time required for analysis, requirements for sophisticated equipment, and the need for trained personnel. Alternatives that can contribute to the bacteria detection with faster response times and easy methodologies are highly desirable.

Biosensors are devices that can detect a biological analyte by sensing an interaction and transforming it into a measurable output signal. In order to discriminate between the target analyte and other elements found in a sample, high selectivity is required. In this work we propose using the bacteriophage (phage) PP01 as the bioreceptor for the detection of *E. coli* O157:H7, transducing this interaction by using an organic electrochemical transistor (OECT) as the sensing platform.

In this work OECTs were fabricated using a commercial pre-patterned indium tin oxide (ITO) substrate onto which a poly(3,4-ethylenedioxythiophene) polystyrene sulfonate (PEDOT:PSS)-based active channel was deposited. Different formulations of PEDOT:PSS were explored to develop a stable layer that exhibited high conductivity and good device performance. The organic solvent 2-isopropanol (IPA) was added as conductive enhancement agent, and (3-glycidyloxypropyl)trimethoxysilane (GOPS) was added as a cross-linker to increase the stability of the ink in water.

Gold gate electrodes were prepared by physisorption and chemical immobilization of phages PP01 through the MUA/EDC/NHS coupling. The chemical coupling and the attachment of phages was characterized through XPS, and the antimicrobial activity was evaluated by exposing the modified samples to *E.coli* O157:H7 in liquid and solid phase media. As for the gate electrode, the performance of the transistor was evaluated by using (1) a bare gold wire, and (2) a chemically modified gold wire with immobilized PP01 phages.

Output and transfer curves demonstrated that the transistor works as a depletion mode OECTs, where the best performance was observed when using tryptic soy broth as the electrolyte solution rather than phosphate buffered saline (PBS), reaching an OFF state at V_G= 1.0 V. For the measurement of different controls (media, target bacteria, non-target bacteria, and phage), transfer properties were measured over a timeframe of 30-60 min, showing that the transistor developed was stable through all measurements at room temperature. Using a gold wire with chemically-attached phage PP01 as the gate electrode, selective detection of *E. coli* O157:H7 (at a concentration of 10^8 CFU/mL in TSB medium) was demonstrated. This work aims to set the basis for a new generation of transistors in which phages are used as bioreceptors, and detect the presence of *E. coli* O157:H7 in liquid samples faster. This would provide a complementary test for the microbiological techniques widely used in water- and foodborne pathogen detection.

Acknowledgements

Throughout these three years, the number of names that I would like to show gratitude is too big. This project brought me more than knowledge; it brought me friends, colleagues, new skills, and a new life perspective.

I would like to say from the bottom of my heart a big thank you to my supervisors, Dr. Anastasia Elias and Dr. Dominic Sauvageau; this project wouldn't have been finished without your guidance and patience. As well, to Dr. Xihua Wang for accepting being part of my defense committee, and MSc. Marnie Jamieson for participating as chair of this defense. Also, to Dr. Hyun-Joong Chung for allowing me to use his lab resources without hesitation and to the trainers in the nanoFAB at the U. of A., where learning became an unforgettable experience.

To the incredible members in both Elias' and Sauvageau's lab, you have my gratitude and admiration. Especially I would like to show my appreciation in this section to Joshua Cunningham and Ana Arvizu who were my trainers and helpers whenever I needed. As well, to Meghana Jois for being the best classmate, best lab mate, and best friend.

Last but not least, my deepest gratitude goes to my family who always supported and encouraged this dreams since it was just an idea, and learned how to love me beyond the distance: my beautiful mom, my siblings and in-laws, my nieces, and nephew; and to my aunt Veronica who has always been present. To my friends who always kept in touch with me, and to all the church family who prayed for my success and well-being: thank you all.

And as we say in my country: ¡Viva Mexico!

Table of contents

List of Tables

List of Figures

Nomenclature and Abbreviations

Symbols

I_D	Drain current
V_D	Drain voltage
V_G	Gate voltage

Abbreviations

ALP	Alkaline phosphatase
C1	Capacitor 1
C2	Capacitor 2
CDC	US Centre for Disease Control and Prevention
CFU	Colony forming unit
DBSA	4-dodecylbenzenesulfonic acid
DI	Deionized water
DNA	Deoxyribonucleic acid
DEAC	Diffusely adherent
DPV	Differential pulse voltammetry
E. coli	*Escherichia coli*
EaggEC	Enteroaggregative
EDC	1-(3-dimethylaminopropyl)- ethylcarbodiimide hydrochloride
EDL	Electric double layer
EHEC	Enterohaemorrhagic
EIEC	Enteroinvasive
EIS	Electrochemical impedance spectroscopy
ECP	Extrinsically conducting polymers
EPEC	Enteropathogenic
ETEC	Enterotoxigenic
GCE	Glassy carbon electrode

GOPS	(3 glycidyloxypropyl)-trimethoxysilane
GOx	Glucose Oxidase
HTL	Hole transport layer
HUS	Hemolytic uremic syndrome
ICP	Intrinsically conducting polymers
IPA	Isopropanol
ITO	Indium tin oxide
LOD	Limit of detection
mTSB	TSB with 10 mM $MgSO_4 \cdot 7H_2O$
MUA	11-mercaptoundecanoic acid
MWCNTs	Multiwall carbon nanotubes
NB	Nutrient broth
NHS	N-hydroxysuccinimide
OD_{600}	Optical density at 600 nm
OECT	Organic electrochemical transistor
OFET	Organic field-effect transistors
OTFT	Organic thin film transistors
P3HT	Poly(3-hexylthiophene)
PANI	Polyaniline
PBS	Phosphate buffered saline
PCR	Polymerase chain reaction
PDMS	Polydimethylsiloxane
PEDOT:PSS	Poly(3,4-ethylenedioxythiophene) polystyrene sulfonate
PEI	Polyethylenimine
PFU	Plaque forming units
PP1-P2 NT	Poly(EDOT-COOH-co-EDOT-EG3) nanotubes
RT	Room temperature
SAM	Self-assembled monolayer
SFCA	Surfactant-free cellulose acetate membrane
SMU	Sourcemeter unit
Stx1	Shiga toxin 1

Stx2	Shiga toxin 2
SWCNT-SPE	Single-walled carbon nanotube-modified screen-printed electrode
TBS	Tryptic soy broth
TSA	Tryptic soy agar
U.S. EPA	United States Environmental Protection Agency
UV-O	Ultraviolet-Ozone
XPS	X-ray Photoelectron Spectroscopy
WHO	World Health Organization

Chapter 1. Introduction

1.1 Background and motivation

Safety is a non-negotiable priority to health, food, and the environment. Monitoring harmful species in systems such as livestock, food products, and drinking water is essential for preventing the spread of infectious disease. Several organizations, such as the United States Environmental Protection Agency (U.S. EPA) have established guidelines for testing and monitoring the presence of possible pathogens in both livestock and water. Pathogens, including some bacteria and viruses, are microorganisms able to infect humans and cause adverse reactions. According to the World Health Organization (WHO), contact with pathogens such as some strains of *Escherichia coli* and *Salmonella* through food and water ingestion causes approximately 2.2 million deaths per year around the world. One example is the well know *E. coli* O157:H7[1–3].

E. coli O157:H7 is a relatively new strain of *E. coli*: it was firstly reported in the 1980's. This foodborne bacteria is of high concern since infections of the human body with this strain can cause renal failure and hemolysis. In 2006, the presence of *E. coli* O157:H7 in raw spinach led to an outbreak in the United States, affecting 199 people in 26 states. Some patients were hospitalized due to kidney failure and three deaths were linked to the outbreak[4–6]. Impacted states and range of patients are shown schematically in Figure 1.1. In addition, contamination of drinking water with this bacteria has also been reported. In 2000, Canada experienced a very serious outbreak of *E. coli* in Walkerton, Ontario, caused by contaminated drinking water. Almost half of the town's population got ill and seven deaths linked during this event [7].

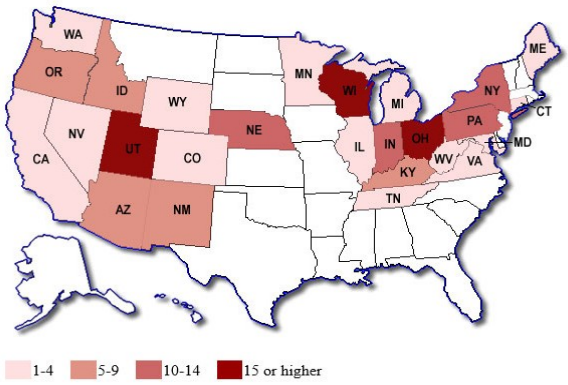

Figure 1.1. US map of case count of citizens infected with *E. coli* O157:H7 in raw spinach outbreak in 2006.[5]

In the province of Alberta, the highest rates of gastrointestinal illness are reported in rural areas in the southern region. This is linked to elevated livestock density and agricultural activity such as irrigation, which can lead to microbial contamination of water sources[8]. Also, the low availability of regular testing supplies in 67% of the farms in this area contributes to uncertainty regarding water quality.[8,9]

To date, reliable methods for the evaluation of bacteria in liquid samples are available as microbiological methods such as polymerase chain reaction (PCR) and cell culture. However, sophisticated equipment, expensive supplies, and trained personnel are required to perform the experiments; an example of these methods is described in the Standard Analytical Protocol for *Escherichia coli* O157:H7 in Water issued by the U.S. EPA[2]. Bringing an affordable and easy-to-use device for would decrease the probability of an outbreak (and its consequences)[10]. Electrochemical devices hold great potential for such applications.

Organic electrochemical transistors (OECTs) are an emerging platform for biosensing applications. An OECT is a three-terminal device consisting of a gate electrode, a source electrode and a drain electrode. In normal operation, a voltage bias between the source and drain causes current to flow through a semiconducting layer. When a voltage is applied to the gate electrode, the current between the source and drain electrodes is modulated.[11] An OECT can work in one of the two modes: depletion mode, consisting of transistor in which current normally flows until it is turned OFF by the gate voltage, and the accumulation mode, which works in the opposite way – devices that are normally OFF until they are triggered to turn ON by a gate voltage –[12]. They are easy to fabricate, have low operation voltage, and exhibit superior sensitivity in comparison to traditional electrochemical sensors. Recently they have been used to sense a variety of biomarkers, including cortisol, the stress hormone that is produced when an individual is under stress conditions[13]. In the work reported by Janardhanan *et al.* an OECT was fabricated by using indium tin oxide (ITO)-coated glass substrates, and two semiconducting layers: PEDOT:PSS as the underlayer and nanotubes made from a co-polymer PEDOT(EDOT-COOH-*co*-EDOT-EG3) to which for anti-cortisol antibodies were attached[13]. Figure 1.2 illustrates the different components of the transistor and the electrical characteristics of the device through the output and transfer curves.

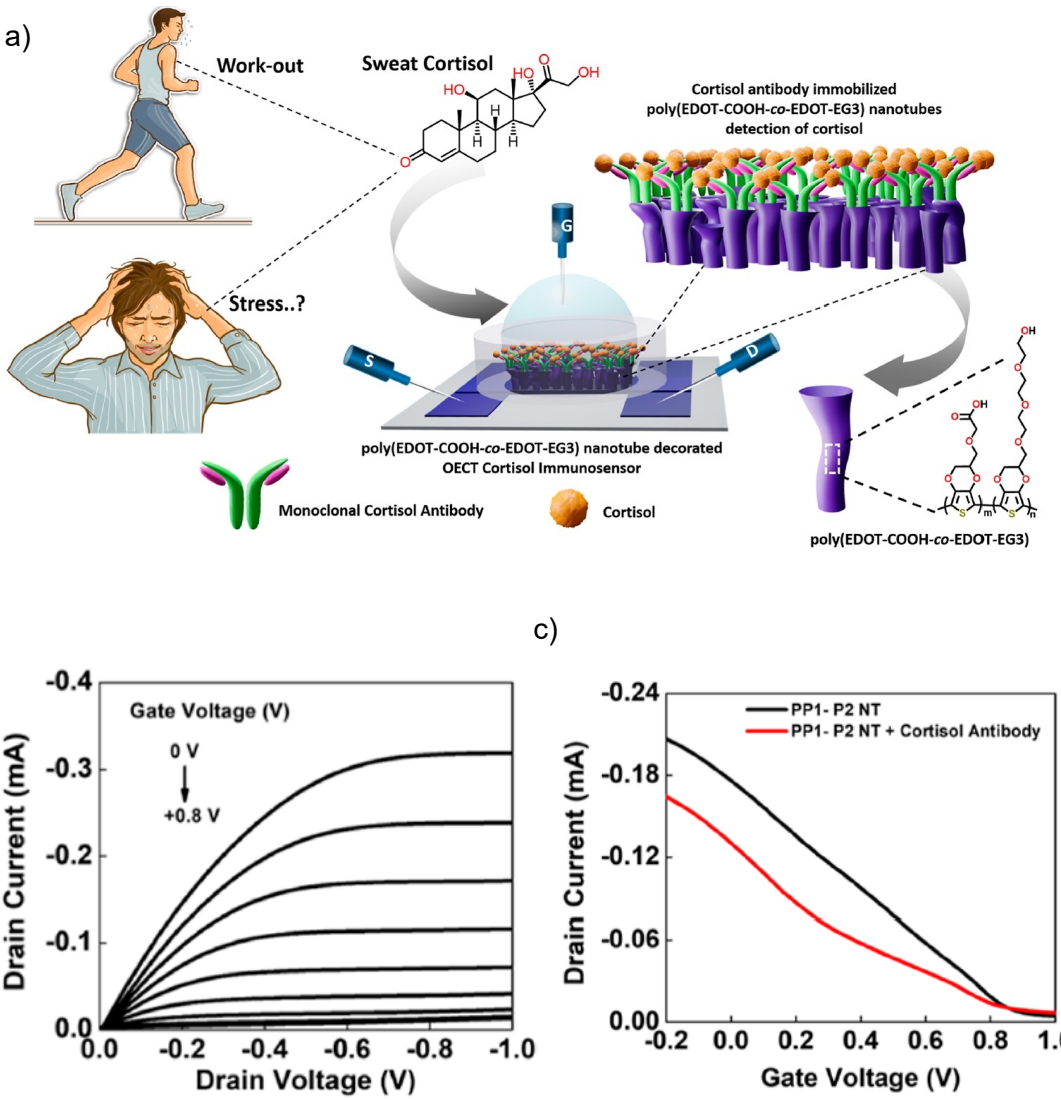

Figure 1.2.a) Representation of OECT and its respective components for the detection of cortisol in sweat: the gate electrode using an Ag/AgCl wire, the source and drain electrodes patterned by using ITO-coated glass substrate, and the anti-cortisol antibody as bioreceptor; b) output and c) transfer curves describing the depletion-mode of the OECT. When a positive gate bias is applied, the drain current will decrease when the voltage increases, reaching a saturation region while sweeping the drain voltage towards negative voltage. For the transfer curves, the drain current decreases when exposed to cortisol antibody due to formation of an insulation layer over the thin film area where the antibodies are attached. PP1-P2 NT: poly(EDOT-COOH-co-EDOT-EG3) nanotubes[13].

An important component of a biosensor is the bioreceptor, which is a biological element that is naturally sensitive to an specific target; examples of this are enzymes and antibodies[14]. However, these entities often have several disadvantages such as complications in maintaining the integrity of enzymes during immobilization and operation, and high cost and limited lifespan of antibodies.[15] Bacteriophages (phages) – which are viruses with the property to attach and infect a specific bacterial strain[16] – have been applied as bioreceptors in various bacteria sensing devices due to their robustness, high specificity for target cells, and easy and cost efficient production[17,18].

Because of their respective features, it is proposed to develop a new device combining OECT and phages for rapid and affordable pathogen detection, with the aim *E. coli* O157:H7 infections.

1.2 Objectives

The overall objective of this project is to fabricate a depletion-mode OECT using PEDOT:PSS thin films, followed by the tailoring of the thin film dimensions, and the chemical modification of a gold wire electrode for subsequent characterization of this device under different conditions and media. The goal for this work is to develop basic OECT devices with potential applications in the detection of the pathogen *E. coli* O157:H7 based on ionic changes due to interaction with PP01. A schematic depicting the design of this device is shown in Figure 1.3. It consists of a commercial, pre-patterned substrate, a reservoir to hold the sample made by PDMS, a thin film prepared by using PEDOT:PSS as the conducting layer (for the device channel), and a gold wire that will be used as the

gate electrode for this device. In order to achieve this objective, many technical challenges must be addressed.

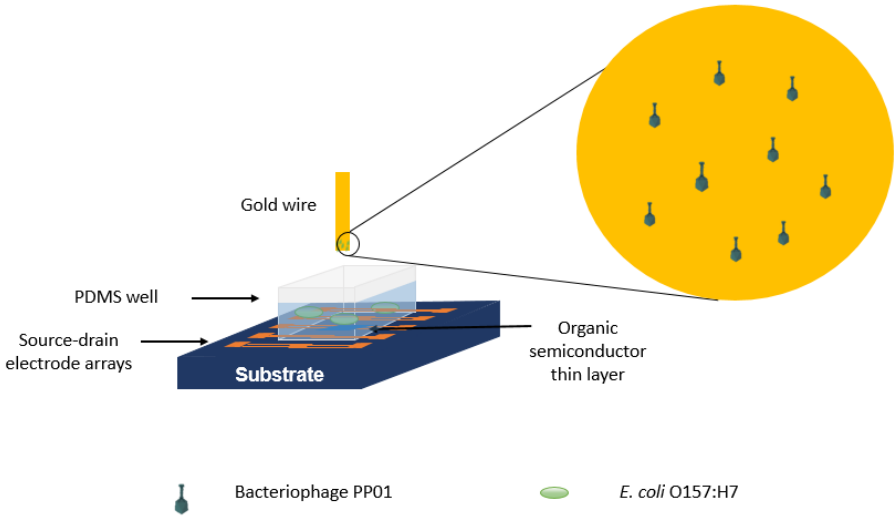

Figure 1.3. Representation of PEDOT:PSS-based OECT with phages chemically attached to the gold wire (i.e. the gate) for the recognition of *E. coli* O157:H7 in liquid samples.

For this work, the objectives are listed below:

a) To fabricate an OECT through spin-coating of a thin layer onto a pre-patterned ITO substrate;
    i. To select and optimize the appropriate PEDOT:PSS-based ink for the deposition in the substrate;
    ii. To optimize the length and width of the PEDOT:PSS thin film in accordance with transistor performance;
b) To characterize the thickness and resistivity of the PEDOT:PSS thin film that comprises the device channel;

c) To chemically attach the phage PP01 onto the gold wire to be used as the gate electrode in the device;
d) To evaluate the performance of the transistor for output and transfer curves in different media;
e) To evaluate the performance of the transistor in the selected aliquots, so as to identify suitable media for use in;
    i. Media alone;
    ii. Media and *E. coli* O157:H7;
f) To compare transistor performance in two different media, a non-nutrient medium and a nutrient medium;
g) To corroborate the selectivity of phage PP01 as bio-recognition element in presence of targeted and non-targeted bacteria.

1.3 Organization

In Chapter 2, background literature will be presented to support the hypothesis as well as to provide a deeper description of each element that comprises this project. Both fundamental concepts as well as relevant previous works found in literature will be described.

In Chapter 3, the materials and methods for the preparation of the transistor, the attachment of the phages to the gold wire surface, as well as selected characterization techniques and conditions for analyses will be described.

In Chapter 4, the results will be discussed in three sections. 1) Device fabrication: the characterization of PEDOT:PSS-based inks and their performance as conducting layer in

OECTs will be described. 2) Phage-immobilization on the sensing electrode: the attachment of phages to gold surfaces will be characterized. This includes investigating the EDC/NHS chemistry used for linker formation, and determining the antimicrobial activity of chemically attached phage PP01 onto gold surfaces in both solid and liquid media. 3) Device performance: In the final section, the effect of the medium on the transistor performance will be explored. Proof-of-concept results showing the detection of bacteria will be presented.

Chapter 2. Literature Review

2.1 *Escherichia coli*

E. coli is a Gram-negative bacteria first discovered by Theodor Esherich[4]. It is a member of the Enterobacteriaceae, and easily grows in warm environments (37 ºC). This bacterium can be pathogenic and non-pathogenic or commensal.

Non-pathogenic *E. coli* is naturally found in the digestive tract, performing tasks which are beneficial to the health of warm-blooded organisms such as helping in digestion of different nutrients. Pathogenic *E. coli* compromises the health of its host by producing illness such as diarrhea[4]. Water sources contaminated with *E. coli* are mainly produced when contaminated faecal matter gets in contact with water, implicitly representing poor or deficient sanitation, hence leading to a potential outbreak.[19]

In the literature, pathogenic *E. coli* are classified based on how they will react with the host organism and which symptoms are developed: (1) enteropathogenic (EPEC); (2) enteroaggregative (EaggEC); (3) enteroinvasive (EIEC); (4) enterotoxigenic (ETEC); (5) diffusely adherent (DEAC); and (6) enterohaemorrhagic (EHEC), which includes the serotype O157:H7[6]. EHEC *E. coli* O157:H7 produces the toxins Shiga toxins 1 and 2 (Stx1 and Stx2), causing diarrhea, hemorrhagic colitis, and hemolytic uremic syndrome (HUS)[6,20].

Usually, *E. coli* O157:H7 infections are related to foodborne-related outbreaks, such as drinking contaminated milk or raw food, rather than to consuming contaminated water. For foodborne cases, the US Centre for Disease Control and Prevention (CDC) reports that the time between the first infection and the report of an outbreak can take three to four weeks[21]. For *E. coli* bacteria, the symptoms typically appear 3-4 days after

the ingestion of contaminated meals. Subsequently, medical care, lab studies, and the involvement of public health authorities are required to formally declare an outbreak in a specific area[21]. In other words, the process is time consuming, risking the health of other individuals in the meantime. Due to this, it would be valuable to develop new approaches to find a new way to detect pathogenic *E. coli* O157:H7 in a faster and affordable way; namely through the design and engineering of biosensors [22].

2.2 Biosensors

A biosensor is defined as "a device that uses specific biochemical reactions mediated by isolated enzymes, immunosystems, tissues, organelles or whole cells to detect chemical compounds usually by electrical, thermal or optical signals"[23]. Each device consists of three components utilized to detect the presence of the analyte or target element present in a sample: (1) a biological recognition element, responsible for the detection and interaction with the target; (2) a transducer, the component capable of generating a measurable output signal, which can be fluorescent, electrochemical, etc[24]; and (3) a signal processing unit. A schematic of components making a biosensor is depicted in Figure 2.1. There are several characteristics that are desirable in a biosensor, such as sensitivity and selectivity, where the first one consists of recognizing and generating a signal when the target is found at a low concentration, and the second one consists of discriminating the target from foreign species in a sample .[25,26]

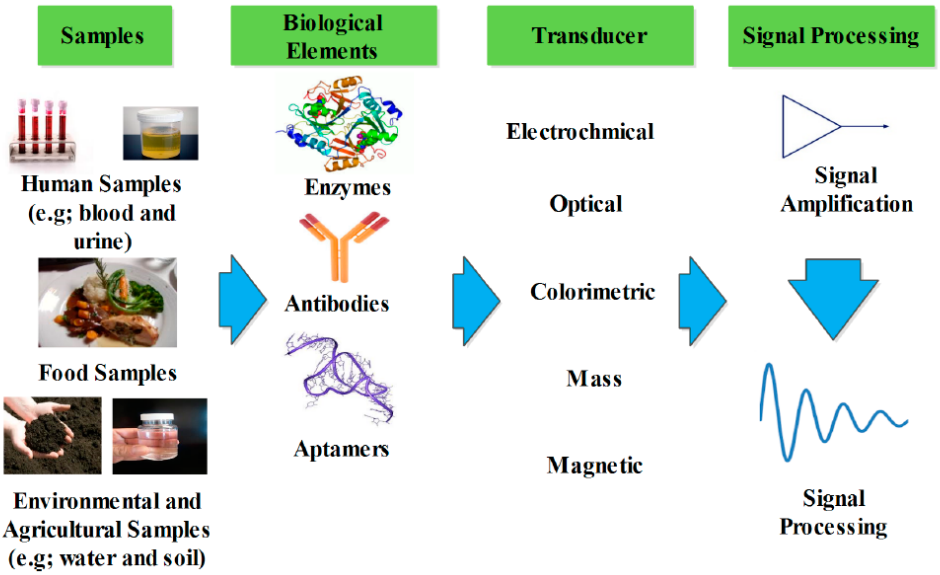

Figure 2.1. Components of a biosensor.[26]

2.3 Bacteriophages as biological receptors

A bioreceptor is a biological entity or molecule that is attach to the biosensing platform, which ideally must be capable of discriminating and interacting with a specific target of interest amongst other substances found in a sample or aliquot. Different receptors can be used in the design of biosensors; for instance the enzyme Glucose Oxidase (GOx) is often utilized in the generation of glucose biosensors[27]. Enzymes are complex proteins that acts as natural catalyzers for specific substances, such as, in this example, GOx catalyzing or transforming glucose into a different product[28]. For bacterial detection, elements such as *E. coli* biotin-modified aptamer probes are often used[29–31]. In the work reported by Liang *et al*[32]*,* an aptamer, a short single-stranded oligonucleotide, was used to detect the strain O157:H7 based on its high affinity towards the proteins found on the *E. coli* surface. However, some biological moieties require a very specific environment to preserve their stability, and hence, their performance. In addition, it is

often expensive to produce purified biomolecules (such as aptamers). A more stable species has been found to be effective on its performance as biological recognition element and relative cost-effective processing: phages.[33,34]

A phage is a virus targeting bacteria. It often has a natural affinity to a specific strain or even a serotype of bacteria. Receptors located at the bacterial surface are uniquely identified by these phages[35,36]. Historically, bacteriophages weren't recognized as viruses, rather this term was applied to pathogenic agents found putrefying organic matter, wound infection, and infectious diseases. However in 1915, Frederick W. Twort observed a "sporadic" disintegration of bacterial colonies, which he firstly referred as "glassy transformations"[37]. Two years later, Felix H. d'Herelle observed lysis of cultures of dysentery bacilli in both liquid and solid medium. In this publication on *Comptes Rendus de l' Academie des Sciences* (Reports from the Academy of Sciences), he proposed that this event was caused by an invisible micro-organism that, in addition to killing the bacteria, may also explain recovery and immunity from infectious diseases[35]. Two decades later, in 1940, the concept "bacteriophage" was acknowledged as reference to a virus. [35,37]

With respect to the mechanism of infection: once the phage recognizes the host bacterial cell, viral nuclei acid in injected into the host, leading to two possible cycles: (1) lytic cycle; and (2) lysogenic cycle. In the first process, the production of new progeny or new phages is performed by the bacterial machinery. An infected cell can produce around up to hundreds or thousands of new phages[37]. Phage progeny is released through breaking the cell membrane enabling infection of more bacteria. The lysogenic cycle consists of the injection of the viral DNA to the host and its integration into the bacterial

genome. The phage genome is then replicated it during cell division. Phages that possess this ability to carry out a lysogenic cycle are called temperate phages, which under certain circumstances such as for survival mechanism when they cannot sustain a lytic infection, can remain as temperate until the risk is gone and phages shift to lytic cycle[35,38]. Both mechanisms are summarized in Figure 2.2.

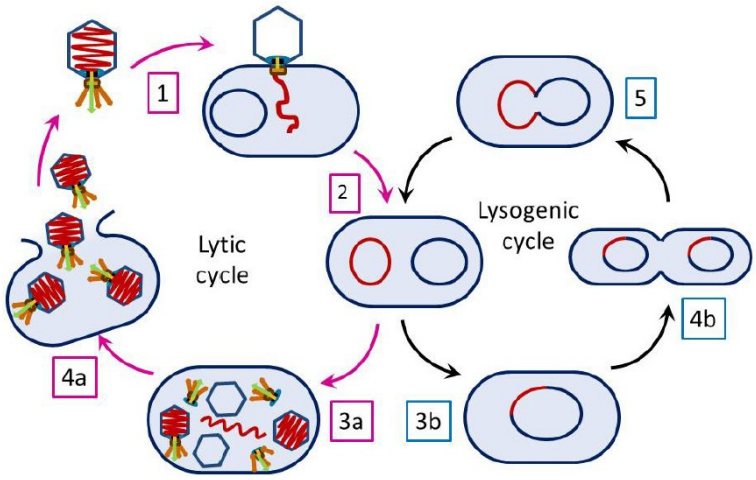

Figure 2.2. Schematic representation of lytic and lysogenic processes: 1) attachment and phage DNA infection; 2) viral DNA replication; 3a) synthesis of new phages; 3b) introduction of viral DNA into bacterial DNA; 4a) phage assembly and cell lysis; 4b) cell division process; 5) Formation of plasmids.[37]

This cost-effective production of phages through the lytic cycle, their natural robustness to temperature conditions and affinity to a specific strain make phages suitable for biosensing as recognition elements [37,39]

Phages can be found in different shapes and sizes, which is also important for the recognition of a particular bacteria[40]. In Figure 2.3, five different types of phage

morphologies are displayed. Phage PP01, the phage used in this work, closely resembles the T4 phage structure.

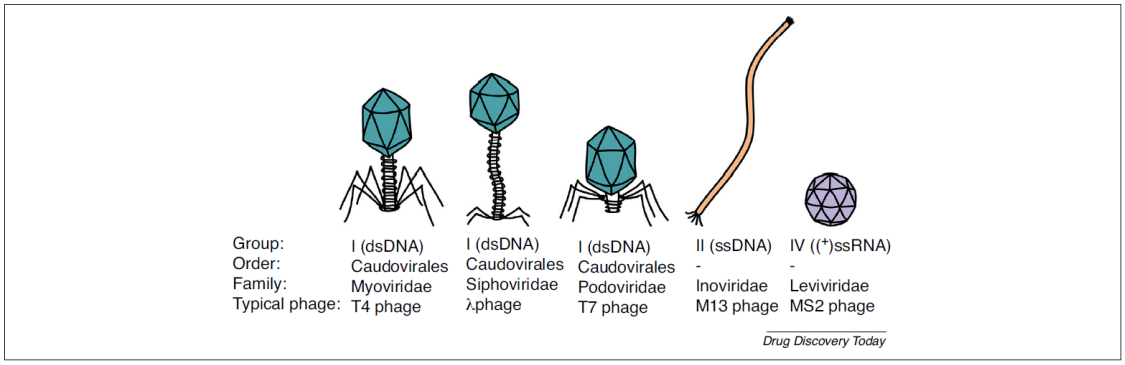

Figure 2.3. Schematics of different morphologies for bacteriophage families.[40]

2.3.1 Phage Immobilization

An important aspect of using phages for sensing purposes is to make sure that they are properly immobilized so the bacteria can be captured. For this, different approaches have been explored for both physisorption and chemical attachment methods.

Phages naturally possess surface charge that can be used to orient them in order to have the tail free for infection of the target. Using this natural property, Zhou *et al.* prepared an electrochemical biosensor where T2 phages were oriented through an induced field electric immobilization over positively charged polyethylenimine-functionalized multiwall carbon nanotubes[41]. Another example of physisorption was studied by Bone *et al.* where silica particles functionalized with 3-(aminopropyl) triethoxysilane (APTES) were used for electrostatic attachment of phages. This functionalization conferred a positive charge to the silica particles, allowing the phage capsid to bind and leaving the phage tail fibers free for infection[42]. Unlike for the work of

Zhou *et al.*, there was no induced electric field used to orientate the electrostatic interaction, rather the samples were incubated overnight in phosphate buffered saline (PBS) at 20 °C under shaking.

The second approach consists of chemical attachment of phages, where functional groups (carboxyl and amines) found on the surface of the phages are used for covalent bonding with a proposed linker. In this context, sugars such as cysteamine[43] and L-cysteine[44] have been used to form self-assembled monolayer (SAM) on gold surfaces ,since these sugars possess thiol functional groups (R-SH) that will bond with the metallic surface. For further efficiency of functional groups, glutaraldehyde was used as a cross-linker in both works. Another path investigated was described by Gervais *et al.* where phage T4 was genetically modified to produce biotinylated capsid heads which were covalently attached to streptavidin previously deposited on pre-cleaned gold surfaces[31]. Another common linker for biological entities uses the 1-(3-dimethylaminopropyl)-ethylcarbodiimide hydrochloride / N-hydroxysuccinimide (EDC/NHS)) chemistry. This method is applied in this project. To perform this coupling and form a linker on gold surfaces, a SAM that contains a free carboxylic group must be introduced onto the surface in order to link with EDC. 11-mercaptoundecanoic acid (MUA) is commonly used for this since it contains a thiol group on one end that binds to gold[45,46], and a carboxylic (–COOH) group on the other end of the molecule. Then, EDC reacts with the carboxyl group to form an active *o*-acylisourea intermediate that can subsequently react with NHS to form a semi-stable amide. This amide then undergoes bonding with the phages[47]. The description of this coupling is depicted in Figure 2.4.

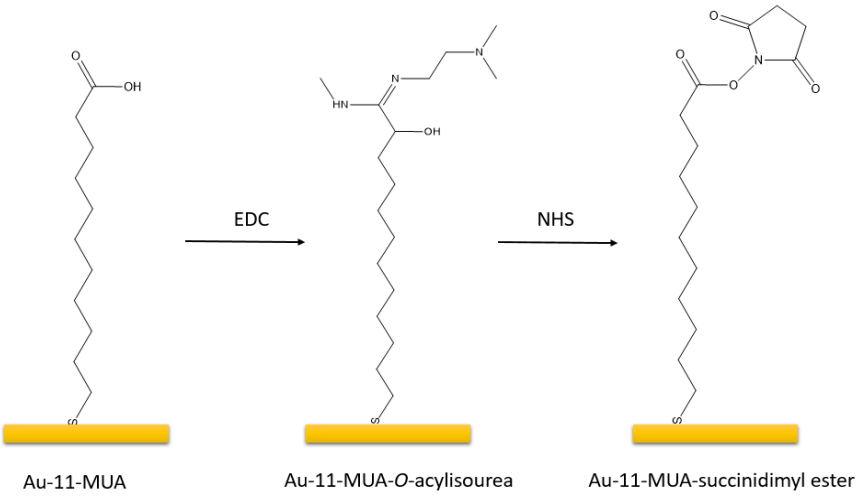

Figure 2.4. Representation of MUA/EDC/NHS coupling.

2.4 Transducers

The third element of a biosensor is the transducer, which is in charge of translating a reaction from the sensing area into a measurable signal[40]. Transducers can generate different types of signals, including fluorescent, magnetic, or electrochemical signals. The latter has several advantages over other transducing methods: it leads to fast-responsive systems, and it can be integrated into miniaturized microdevices that can form the basis of user-friendly portable biosensors. One well-known example is portable glucose sensors, where screen-printed electrodes comprises the conventional 3-electrode electrochemical systems for detection of glucose[48].

In recent years, OECTs have been demonstrated as efficient sensing platforms based on their signal amplification for small changes in the ionic environment, low voltage of operation as well as its biocompatibility[49,50].

2.5 Introduction to Organic Electronics

Organic electronics refers to modern electronics in which one (or more) of the components is a carbon-based material. The discovery of electrically conductive organic compounds, a partially conductive material obtained from anodic oxidation of aniline, was first reported in 1862 by Henry Letheby [51]. More than one hundred years later, in the late 1970s, Heeger, MacDiarmid, and Shirakawa discovered that polymer polyacetylene was highly conductive; these investigators were awarded the Nobel Prize in 2000 for this work. Since then, research in the field of organic electronics has increased due to several advantages that organic materials provide – including ease of tailoring and processing. These make them promising candidates for the replacement of conventional inorganic semiconductor, such as silicon, and some conducting materials to develop devices that are cost-effective with better mechanical flexibility devices. One area of specific interest is the study of organic thin-film transistors (OTFTs).[52]

2.6 Organic Thin Film Transistors

OTFTs are platforms that offer several advantages from conventional systems, starting from their inherent signal amplification, resulting in a higher sensitivity and lower limit of detection (LOD). Because of these features, in addition to low cost for organic semiconductor processing and miniaturization, OTFTs are good candidates for use as chemical and biological sensing devices.[53]

In general, the design of an OTFT consists of a three-electrode circuit, including the source, drain, and gate electrodes, and a thin film of an organic semiconductor deposited between the source and the drain, working as an active channel; the purpose

of this channel is to allow the current flow between electrodes that will be modulated by the voltage applied to the gate electrode[54]. Current changes can be used for sensing purposes since when a interaction occurs (attachment, electrostatic interaction), the surface charge changes, causing a change in the current registered.[55]

According to their structure and working principle, OTFTs are divided in two main categories: organic field-effect transistors (OFETs) and organic electrochemical transistors (OECTs) (Figure 2.5)[54]. In an OFET, a solid film of an organic semiconductor is separated from the gate electrode by either an insulator layer or a dielectric layer working as a parallel plate capacitor. When applying OFETs as biosensors the substrate, gate, and dielectric layer are deposited, followed by the deposition of the source/drain electrodes on which the bioreceptor will subsequently be immobilized. Once this step is finished, the modified electrodes are in contact with the analyte for a determined amount of time. The last part consists of covering the electrodes by the semiconductor film to evaluate the current change due to this interaction; one example of such a device is reported by Yan *et al.*[56] In OECTs, there is no dielectric layer separating the gate from the two other electrodes and the active layer. Rather, there is an electrolyte whose ions can penetrate the active channel and, thus, modulate its conductivity[57].

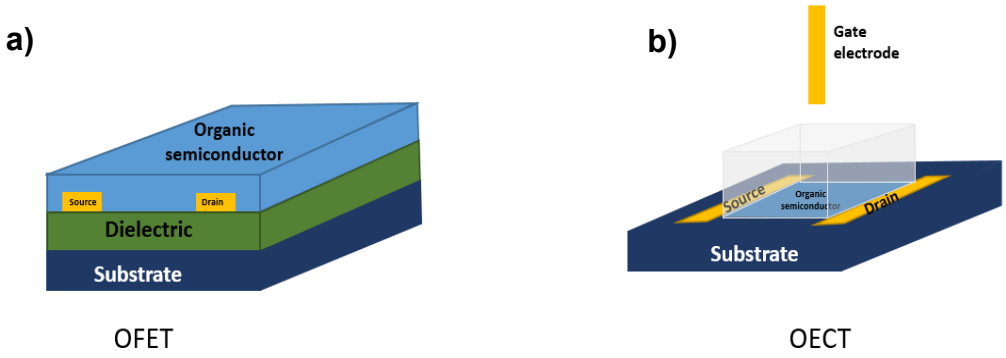

Figure 2.5. Representation of a) organic field effect and b) organic electrochemical transistor.

2.7 Organic Electrochemical Transistors

The first report on the fabrication of OECTs is attributed to Mark S. Wrighton in 1984 in which he introduced a “chemically derivatized microelectrode array” to amplify a signal with a small charge applied to this system.[58]

As described above, OECTs are a type of OTFT whose design is considered as a special form of OFET, consisting in a three-electrode array (metallic gate, source, and drain). The gate electrode is separated from the design of the transistor but is in contact with an electrolyte contained in a well[57]. In contrast with typical OFETs, the electrolyte, which has a high volumetric capacitance, is a substitute for the dielectric layer. As well, an organic semiconductor with high carrier mobility is in direct contact with the pair of drain and source electrodes. When a gate bias or gate voltage (V_G) is applied, ions migrate from the electrolyte and are injected in the semiconductor layer, causing either an increase or decrease of the conductivity of the active channel[59]. Depending on the nature of the organic semiconductor (including its structure), the doping type (whether it is p-type or n-type), the electron mobility, and the ion mobility, transistors may operate

either in accumulation mode or in depletion mode. When the transistor operates in accumulation mode, a negative gate bias is applied from the injection of anions, increasing the charge carrier mobility in the channel; whereas for the depletion mode, injected cations de-dope the semiconductor channel, decreasing the recorded current. Figure 2.6 shows the mechanism for both modes of operation and illustrates the variation in drain current (I_D) that occurs as V_G modulates the transport of the ions in the electrolyte. As a result of this mechanism, and the simultaneous transport of ionic and electronic charges, these devices present higher transdoconductance than OFETs, making them more suitable for biosensing since the range of operation is usually below 1 V[60,61]. Figure 2.7 shows the energy diagram of an OECT, where the electric double layer (EDL) between the gate and the electrolyte, and the electrolyte with the semiconductor are represented as capacitors (C1 and C2) that influence the effective gate voltage applied in the system. In this work, we will focus on depletion-mode devices.[54]

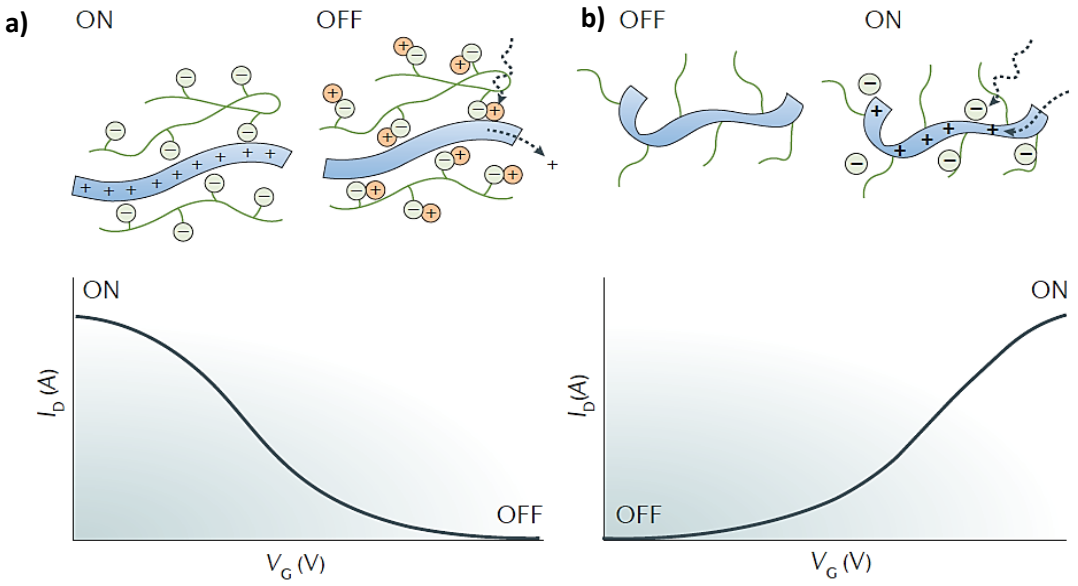

Figure 2.6. Schematics of a) depletion-mode transistor, where ions injected from the electrolyte compensate the doping areas in the backbone of the semiconductor, leading to a decrease in the current of the transistor; and b) accumulation-mode transistor, where ions introduced from the electrolyte increase the conductivity of the transistor [57].

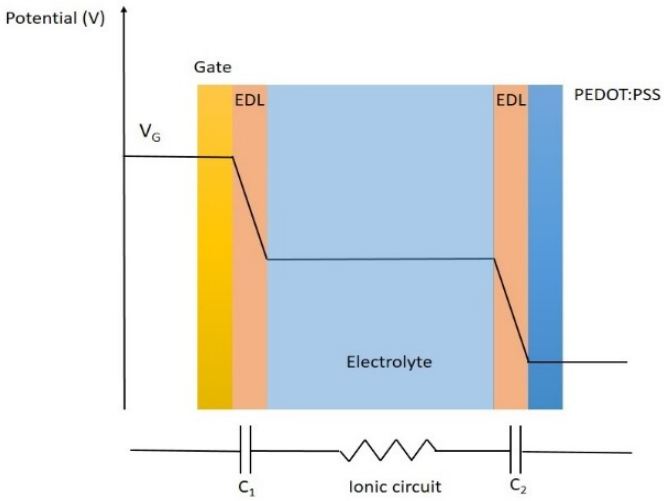

Figure 2.7. Energy diagram and ionic circuit for an OECT. V_G: gate voltage; EDL: electric double layer; C1, C2: capacitors one and two (gate-electrolyte and electrolyte-thin film).

2.7.1 Organic semiconductors for OECTs

Organic semiconductors are key components of OECTs since the working principle relies on the characteristics of the semiconductor, which operates by de-doping or by accumulation mode[62]. An organic semiconductor is a carbon-based compound that has the ability to conduct electricity in the form of both holes and electrons, and exhibits an electronic band gap. This conductivity is attributed to conjugated π bonds that allow the delocalization of the charge carriers via molecular orbitals. Polymeric semiconductors also have enabled the fabrication of a new class of flexible devices, since polymers are not as rigid as the traditional semiconductor material, silicon. In specific, for the purpose of bioelectronics devices, several features must be considered; for instance, biocompatibility (to avoid damage or death of the biological entities when in contact), and long-term stability (to assure the efficiency of the developed devices without presenting any fluctuation while performing a specific measurement or analysis)[63,64].

Conductive polymers are divided in two main categories: (1) extrinsically conducting polymers (ECP), which are made conductive through the addition of conductive materials, such as metallic particles, to a polymer matrix, and (2) intrinsically conducting polymers (ICP), whose structure confers them the ability to be naturally conductive, without adding any metallic additives[65]. Redox polymers are considered ICPs. One of the main advantages of ICPs is their ease of processing due their solubility and dispersion in different media (depending on their polarity)[65]. Some examples of these semiconductors are poly(3-hexylthiophene) (P3HT), poly(triarylamine), polyaniline, pentacene, and poly(3,4-ethylenedioxythiophene):poly(styrene sulfonic acid) (PEDOT:PSS)[54,63]. Their structure is depicted in Figure 2.8. During the next section the

fundamentals, properties an applications of PEDOT:PSS will be further discussed, as it is used in this thesis.

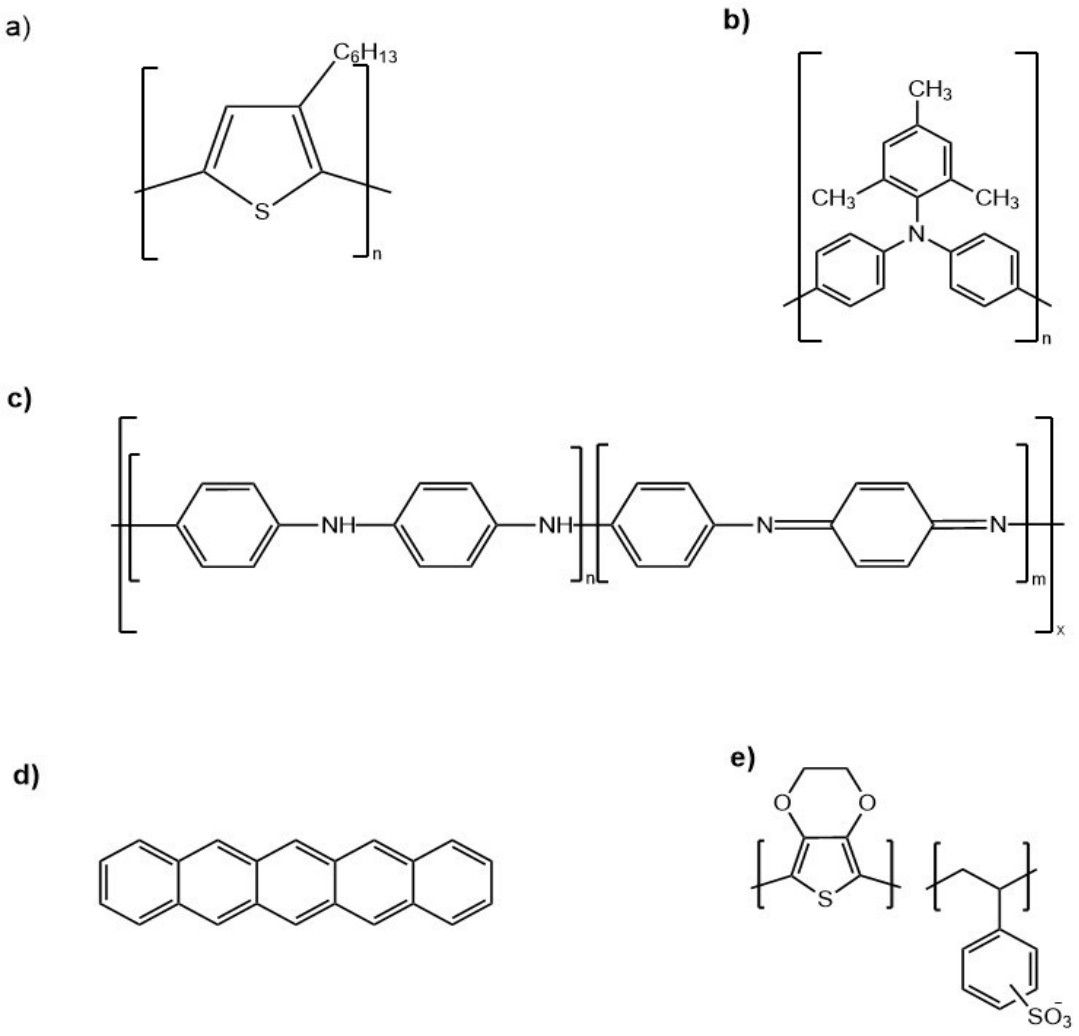

Figure 2.8. Chemical structure of a) poly(3-hexylthiophene) (P3HT); (b) poly(triarylamine); c) polyaniline (PANI); d) pentacene; and e) poly(3,4-ethylenedioxythiophene):poly(styrene sulfonic acid) (PEDOT:PSS).

2.7.2 Poly(3,4-ethylenedioxythiophene):poly(styrene sulfonic acid) (PEDOT:PSS)

PEDOT:PSS is a conductive polymer that has been widely used for the generation of new organic electronic devices due to its advantageous characteristics: (1) good water stability and dispersibility, (2) biocompatibility, (3) tailorable conductivity, (4) stretchability, and (5) good film-forming properties[66]. The formation of this polymer starts with the polymerization of the ionomers PEDOT and the polyanion PSS. Due to its hydrophilic properties, PSS wraps the hydrophobic PEDOT chains making nanoparticles in water. A certain portion of deprotonated styrene sulfonate units are found near the PEDOT chain working as dopants, compensating the positive charge of the backbone PEDOT[67,68].

When PEDOT:PSS is used as the organic semiconductor in an OECT, an applied gate voltage leads to ions from the electrolyte being injected into the film, changing its doping state, which results in a modulation of the current. This provides PEDOT:PSS with a ionic-to-electronic current transduction property[57]. Since this phenomenon does not require high voltages to perform the de-dedoping process, PEDOT:PSS-based devices have great potential for biological applications[57,69].

Different commercial formulations of PEDOT:PSS can be found depending on the needs of the device, such as PH1000, designed for applications where a high optical transparency and high conductivity is needed, as well as HTL Solar, a mixture applied for matching interfacial energy level in electronic devices such as organic photovoltaic cells[70].

At the time of writing, there were no reports of merging phages and PEDOT:PSS-based OECTs for the fabrication of biosensors. Relevant works for both elements will be reviewed in the next sections.

2.8 Bacteriophages as biological recognition elements in electrochemical systems

As mentioned in section 2.3, phages can be used as recognition elements in bacterial sensing. For the recognition of the bacteria *E. coli*, different phages, specific to different strains of the bacteria, have been explored. For instance, El-Moghazy *et al.* used phages as the recognition element in an electrochemical biosensor for *E. coli* BL21[71]. In their work, they modified the genome of phage T7 to induce the expression of alkaline phosphatase (ALP) during the infection process. The reaction of ALP with the substrate 1- naphtyl phosphate generates the electroactive compound 1-naphthol by desphosphorylation. This compound, when in contact with a single-walled carbon nanotube-modified screen-printed electrode (SWCNT-SPE), is oxidized which generates an electrical response measurable through differential pulse voltammetry (DPV). During the evaluation of the sensor, different parameters were analyzed for optimal conditions: phage concentration, nanotube concentration, substrate concentration, and the response time for measuring low concentrations. For example, when assessing a cell contamination of 1 colony forming units (CFU)/mL, the authors performed a pre-incubation step to increase the quantity of bacteria present before assessing the sample in the presence of a fixed titer of phages, demonstrating that the overall time for processing and measuring the sample was less than nine hours, a shorter time than conventional methods. As well, results showed that increasing the amount of both phages and the non-electroactive 1-naphthol did not translate to better performance. In the case of the phage, the current obtained could be compromised because of the competition between phage infection and expression of ALP. For the case of 1-naphthol, at concentrations above 2 mM, the current reaches a plateau region for enzymatic activity. From DPV curves (Figure 2.9), a linear

trend was found correlating the logarithmic concentration of the electroactive compound with potential, making it possible to apply this device in spinach leaves previously inoculated with the bacteria tested[71].

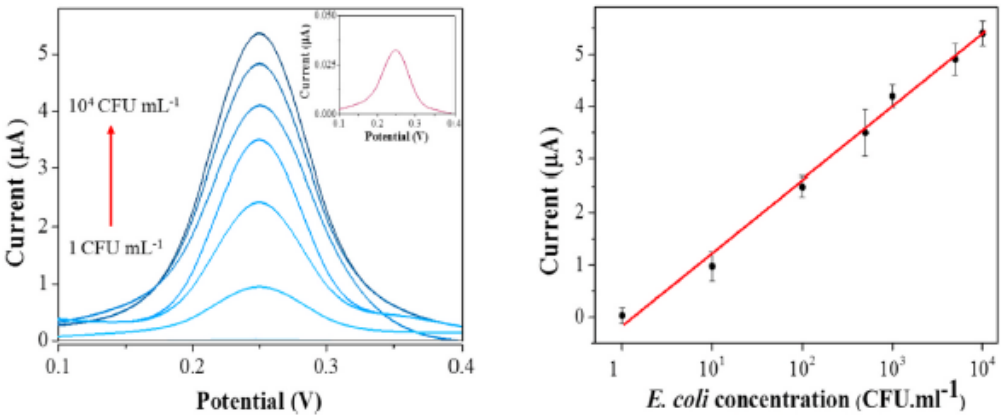

Figure 2.9. a) DPV response of phage-based electrochemical sensor in presence of different bacterial concentration; and b) calibration curve taken from current peaks from electrochemical evaluations for each concentration of *E. coli* [71].

In another electrochemical setup, a capacitance-based biosensor was reported by Ashianik *et al* [72]. Their device used biotinylated phage T4 immobilized on a glassy carbon electrode (GCE) that was chemically-modified with streptavidin/polyaniline. The conductivity of three different cases was evaluated through cyclic voltammetry (CV) it was evaluated: bare GCE, chemically immobilized electrode, and biotinylated phage T4 immobilized on the gold electrode. Results showed that the presence of oriented phage T4 on the electrode surface produced a reduction of the current and corresponding peaks on the voltammogram using $K_3[Fe(CN_6)]$ in PBS as probe solution. This showed the phages essentially acting as an insulator in comparison with polyaniline/glassy carbon

electrode (PANI/GCE), where PANI is well known for its electroactive characteristics, improving the electron transfer when present in an electrochemical system. To evaluate the selectivity of the biosensor, the device was exposed to different bacteria and the output signal was measured through changes in capacitance. During the test, it was demonstrated that the biggest difference in capacitance corresponded to the presence of *E. coli* compared to non-targeting bacteria (Figure 2.10)[72]. This demonstrates the capacity of the phage used to selectively interact with this *E. coli* strain amongst bacteria of other genera.

Phage T2 were also used as bioreceptors on glassy carbon electrodes (GCE) for the sensing of *E. coli* B, as reported by Zhou *et al*[41]. In this sensor, the negative charge of the phage capsid aligned the phage towards the positively charged GCE surface previously modified with multiwall carbon nanotubes (MWCNTs) functionalized with polyethylenimine (PEI). The effectiveness of the immobilization method and the decrease of the Nyquist arc when the concentration of *E. coli* B increases, which is related to the charge transfer resistance, were demonstrated through electrochemical impedance spectroscopy (EIS). This behavior was attributed to the incubation time of the electrode with *E. coli* B. The longer the incubation, the more bacteria were infected. During the infection, progeny phages were released in the medium, causing the bacteria to release intracellular material upon lysis, increasing the ionic concentration in the suspension. This resulted in decreasing the arc or charge transfer resistance of the electrode.[41]

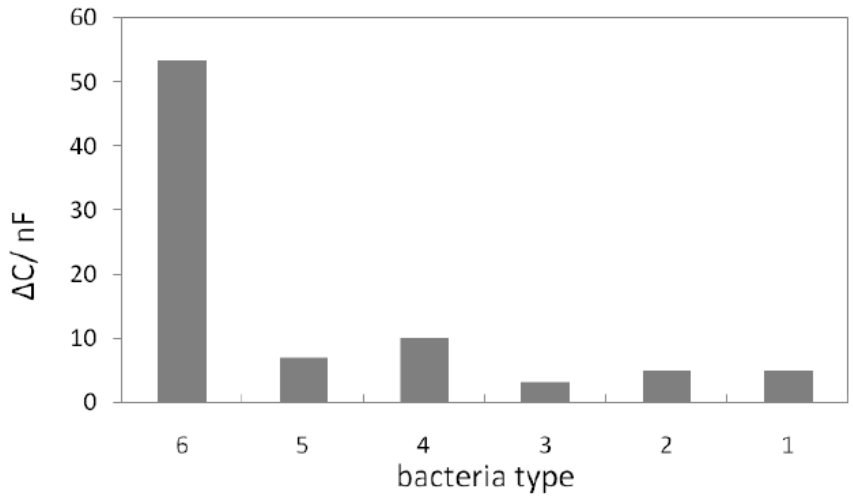

Figure 2.10. Capacitance difference response on selectivity tests for different bacteria: 1) *Staphylococcus aureus*; 2) *Kebsiellapneumoniae*; 3) *Shigelladysenteriae*; 4) *Vibrio cholera;* 5) *Salmonella typhiand*; and 6) *E. coli*.[72]

2.9 PEDOT-PSS based OECTs as sensing platforms for E. coli sensing

In literature, there are a variety of examples demonstrating the use of OECTs as biosensors. Some examples of these are glucose sensors[73] and sensors for different cells, such as epithelial cancer cells[55]. However, few studies report their use for the evaluation of the bacteria of interest, *E. coli*.

An inkjet-printed OECT using antibodies to sense *E. coli* was reported by Demuru *et al.*[74] In their work, a planar and flexible device was fabricated by using biocompatible materials, such as gold, for the gate, drain, and source electrodes, and PEDOT:PSS for the active channel (Figure 2.11). Functionalization of the surface with antibodies was performed through silanization of the gold gate. The medium standard nutrient broth (NB) was used as electrolyte solution, serving as both medium and for evaluation of the bacteria attachment. *E. coli* detection involved incubation for 2 h before measurements.

Cyclic voltammetry was used to characterize the electro-transfer resistance effect of both gate-antibody and gate-antibody-bacteria functionalization, proving the presence of both biological entities. As for evaluation of the OECT, the authors proposed that the antibody-bacteria interactions modified the electric double layer of the gate-electrolyte interface (Figure 2.11), which decreased the voltage drop caused by the EDL of this interface and increased the potential applied to the active channel, hence, decreasing the drain current of this channel. This means the presence (and concentration) of bacteria is related to the reduction of drain current for the transfer curves in comparison with measurements in medium alone[74].

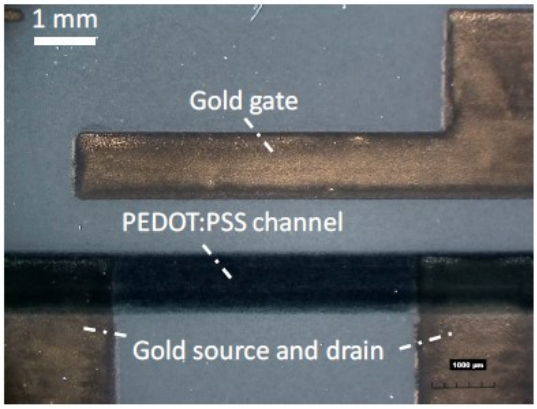

Figure 2.11. Image of a single inkjet-printed OECT[74]. © [2019]

For the evaluation of *E. coli* O157:H7, He *et al.* fabricated a PEDOT:PSS OECT using anti-*E. coli* antibodies that were attached to a chemically-treated PEDOT:PSS active layer[75]. In their work the devices were tested at different concentrations of the electrolyte (KCl in water) to study their effect on the curves during experiments. As well,

this study discussed the influence of the electrical properties of *E. coli* O157:H7 on the performance of the transistor.[75]

The authors studied the influence of selected concentrations of KCl at V_G = 0.4 V and V_D = -0.1 V applied on the transistor. The behavior of the transfer curves for each concentration was attributed to two main factors: the ionic strength of the solution and the calculated electric double layer (EDL) for each concentration of KCl. At lower concentrations, the ionic strength allowed the bacteria to have more negative charges on the surface; in addition, the thickness of the EDL was expected to be higher than the length of the antibodies attached, causing a higher gate voltage shift on the transfer curves in efforts to compensate the negative charge of the bacteria. On the other hand, at higher concentrations, calculations showed that there was no shift in voltage. This behavior, according to the authors, was attributed to both the increased ionic strength of the medium and the smaller EDL, which may screen the negative charge of the bacteria, making a weak interaction with the PEDOT:PSS active layer; hence, no significant shift in transfer curves. The device and relative shift changes of the gate voltage are depicted in Figure 2.12.[75]

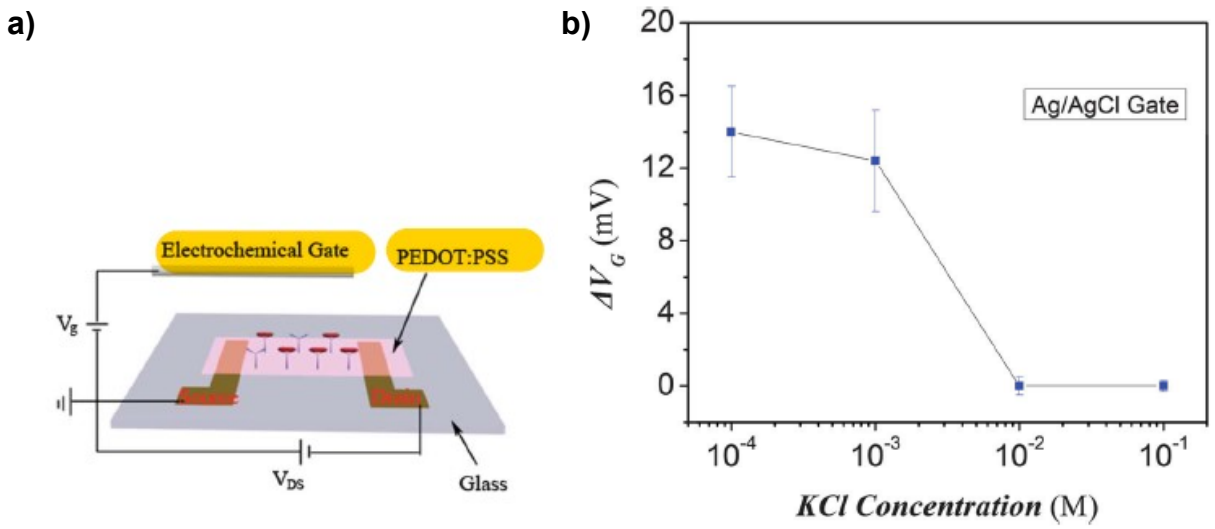

Figure 2.12. a) Schematic of OECT with anti-*E.coli* O157:H7 antibodies attached to pre-treated PEDOT:PSS active layer; b) calculated gate voltage shift in transfer curves for each KCl concentration.[75]

3. Experimental Procedures

3.1 Preparation of Organic Electrochemical Transistor

As mentioned before, the first challenge consisted of the preparation of a depletion-mode transistor by using PEDOT:PSS as the proposed semiconductor. The first step in the fabrication process was to manufacture the transistor, including interdigitated electrodes, and the PEDOT:PSS channel. For the preparation of the transistor, a pre-patterned interdigitated ITO substrate was purchased from Ossila® UK (Product code S161) with five pairs of source-drain electrodes; each pair contains three fingers with channel length of 50 μm and width of 30 mm and an overall glass substrate size of 20 mm x 15 mm[76]. A picture of the substrate is shown in Figure 3.1. Before the deposition of the thin layer, the substrate was cleaned by sonication, first in a diluted solution of Sparkleen® powder soap in deionized (DI) water for 20 min, then in DI water for 20 min, and then in acetone and isopropanol for 10 min each. After this, the substrate was dried under a nitrogen flow and the surface was further cleaned by using a Jetlight UV-O cleaner with a 190-nm lamp for UV-Ozone cleaning for 15 min.

Figure 3.1. Picture of ITO Glass substrate from Ossila® UK.[76]

The first ink evaluated in this project was pristine PEDOT:PSS suspension (483095, Sigma-Aldrich), which was previously sonicated for 30 min and spin-coated at different velocities (from 1500 to 4000 rpm) with a selected acceleration of 500 rpm/s^2 for 40 s and baked at 120 ºC on a hotplate. Consecutively, a pristine PEDOT:PSS PH1000 suspension (M122, Ossila©) was tested using the same range of spin rates but increasing the acceleration to 1500 rpm/s^2. Baking of this ink was done in a vacuum oven, performing alternate cycles of vacuum and nitrogen atmosphere three times at different temperatures depending on the ink studied.

The third mixture evaluated consisted of PEDOT:PSS PH1000, 5 (v/v)% glycerol (G9012, Sigma-Aldrich), 1(v/v)% (3 glycidyloxypropyl)-trimethoxysilane (GOPS, 440167, Sigma-Aldrich), and 0.5 (v/v)% 4-dodecylbenzenesulfonic acid (DBSA, 44198, Sigma-Aldrich). The thin films were prepared by spin coating at different velocities, increasing the acceleration to 1500 rpm/s^2 for 40 s. Ink baking was done by purging the vacuum oven three times with alternate vacuum and nitrogen atmosphere cycles and curing the samples at 140 ºC for 1 h.

For the final mixture and active channel deposition, a PEDOT:PSS ink was prepared from PH1000, a commercial emulsion consisting of PEDOT:PSS in water. PH1000 was mixed with isopropanol (99%) (A451-1, FischerSci) at a 1:1 volume ratio, followed by rigorous stirring at room temperature using a magnetic hotplate for 24 h. Typically, 0.99 ml of PEDOT:PSS emulsion was added to 0.99 ml of isopropanol. Subsequently, (3 glycidyloxypropyl)-trimethoxysilane (440167, Sigma-Aldrich) was added in a 2 (v/v)% proportion and the final mixture was then further mixed with a vortexer for 60 s to integrate this reagent to the final ink. The mixture was spin-coated onto the freshly

cleaned substrates at 3000 rpm for 30 s at an acceleration of 1500 rpm/s^2 using a Laurell WS-650SZ. The curing was performed under nitrogen atmosphere as aforementioned at 140 ºC for 1 h.

The channel dimensions were then defined by using a Q-tip and toothpicks by gently immersing them in DI water, carefully removing excess PEDOT:PSS, with the exception of the desired area as depicted in Figure 3.2.

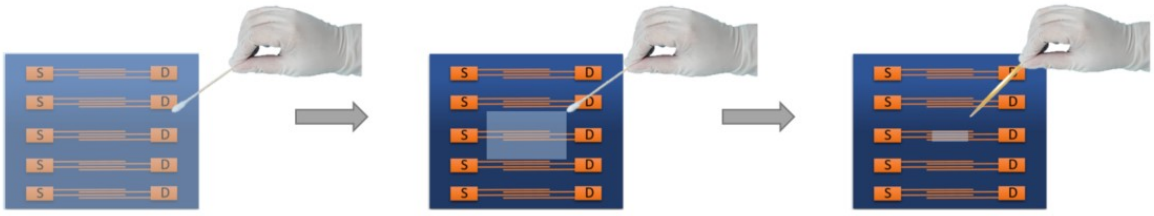

Figure 3.2. Procedure for removing excess ink from active channel deposition. The Q-tip was gently immersed in DI water and then swabbed over the substrate. Excess ink was removed starting from the edges of the substrate until reaching a smaller area as shown in step 2 of the figure. From this and until defining the active channel, the tip of a toothpick was gently immersed in DI and used to carefully further remove excess until the desired dimensions were reached.

3.2 Thin-layer characterization

To characterize the physical properties of the spin-coated PEDOT:PSS inks, representative samples of the mixture were deposited on glass substrates. The thickness was measured through step height of the thin film edges using an Alpha-Step Profilometer with a scan speed of 100 µm/s and a sampling rate of 50 Hz. For the evaluation of resistance and resistivity, a Four-Point Probe Lucus Pro4 4000 with a Keithley 2601A

sourcemeter was used. The software was set up to measure five points on a square wafer with size of 80 and edge exclusion of 8.

3.3 Bacteria and phage preparation

For bacterial overnight culture and phage amplification, Bacto tryptic soy broth (TSB) (DF0370-17-3, BD) was used as the culture broth at a concentration of 30 g/L. Tryptic Soy Agar (TSA) plates were prepared for cell counting and phage titration. TSB at a concentration of 30 g/L was mixed with Bacto Agar (214010, BD) at a concentration of 15 g/L to make TSA. The same process was used to prepare TSB soft agar but with Bacto Agar was added at a concentration of 6 g/L. For all these preparations, Milli-Q water was used and all glassware was sterilized by autoclave at the same time as the broth and agar using a liquid cycle (121 °C, 20 psig) for 20 min.

For the TSA plates, a laminar flow hood was used to prevent contaminations. 20 mL of recently sterilized TSA was poured in sterile 100 mm x 15 mm polystyrene Petri dishes with clear lid (Fisher Scientific) by using a sterile serological 50-mL pipette. The plates were left to air dry until the agar was solidified and then stored at room temperature, piling them with the lid facing down to prevent condensation on the agar, and covering them with aluminum foil to prevent light degradation. Process for TSA plates preparation is shown in Figure 3.3.

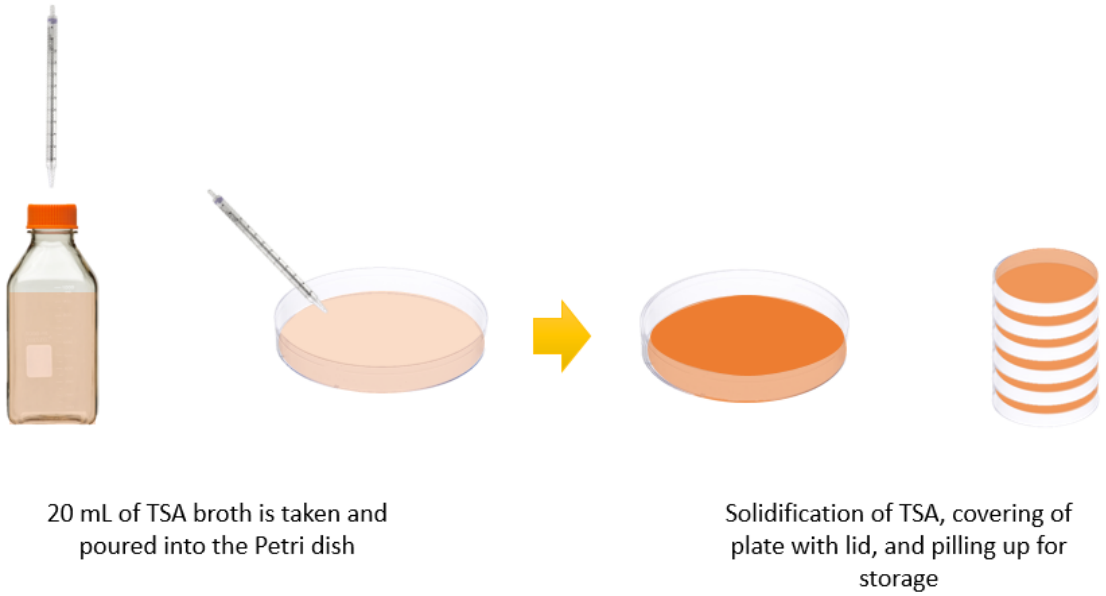

Figure 3.3. Representation of TSA plates preparation.

3.3.1 Bacteria streaking

For the preparation of separated colonies of *E. coli* O157:H7, the streaking plate method was applied (Figure 3.4), using a frozen stock of the pathogen in a ratio of 3:1 with 60% glycerol stored in a 2.0-mL cryogenic vial (typically a stock is prepared using 0.75 mL overnight bacterial culture and 0.25 mL of 60% glycerol (BP229-1, Fisher) and stored at -80 °C). The cryogenic tube was taken out and placed on ice to prevent rapid melting of the stock. A small quantity of the bacterial stock was taken with a sterilized metallic loop and spread in the first quadrant of a TSA plate (black lines in Figure 3.4). To further spread the bacteria to isolate colonies, a small amount of the inoculum was taken and streaked with the sterilized metallic loop (blue lines in Figure 3.4). This step was repeated one more time (green lines in Figure 3.4). Once the streaking was completed, the plate was taken to incubation at 37 °C for overnight growth of the colonies.

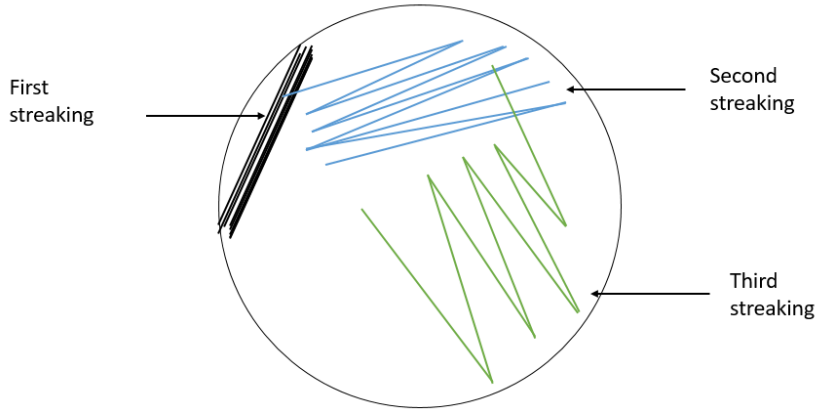

Figure 3.4. Graphical representation of streaking plate method.

3.3.2 Phage PP01 amplification

To obtain a stock of phage PP01, a bacterial culture of *E. coli* O157:H7 was prepared by inoculating one colony from the streaking method mentioned above in 10 mL of TSB, followed by overnight incubation at an orbital speed of 250 rpm and 37 ºC. From this culture, 0.5 mL were inoculated in a 9.5 mL of TSB, and the mixture was incubated for 1-1.5 h at 170 rpm speed and 37 ºC temperature until an optical density at a wavelength of 600 nm (OD_{600nm}) of 0.45-0.55 was reached. To perform the phage initial infection, 1 mL of the host mid-log culture, 0.1 mL of a previously prepared stock of phage PP01 was serially diluted to a titer of 10^5 plaque forming units (PFU)/mL, and 0.5 mL of mTSB (TSB with 10 mM $MgSO_4 \cdot 7H_2O$) were incubated for 15 min at 170 rpm at 37 ºC. After this, the total volume was transferred to 18.4 mL of mTSB, and amplification was allowed to proceed for 5 h at 190 rpm and 37 ºC. During this process, it is expected that the OD_{600nm} value continues increasing until a maximum point where phage infection and its proliferation outcompetes the bacterial growth, resulting in a decrease of the value of

absorbance. The culture was then centrifuged at 6000 x g for 10 min at a temperature of 4 ºC to separate cell debris from the phages, and then filtered using a 0.2-µm SFCA filter (C431219, Fisher-Corning™).

3.3.3 Phage titration method

Phage titration on soft agar was performed to assess the phage titer of stocks and samples. For this method, 10-fold dilution series from the phage stock or sample were prepared, by combining 0.9 mL TSB broth and 0.1 mL of corresponding phage dilution. Subsequently, 4 mL of TSB Soft Agar was inoculated with 0.1 mL overnight bacterial culture and added to the TSA plate. Immediately after, 0.01 mL of each serial dilution was applied on the agar to make a spot. Once the spots were dried, the plate was incubated overnight. The day after, 10-100 plaques were counted from the last dilution where these plaques were well defined and the titer was determined. For instance, if 20 plaques were counted in the serial dilution of 10^8 spot that means the titer is $2x10^9$ PFU/mL. A schematic is shown in Figure 3.5.

The formula for phage titer is (plaque count)*(dilution factor)/volume = titer in PFU/mL.

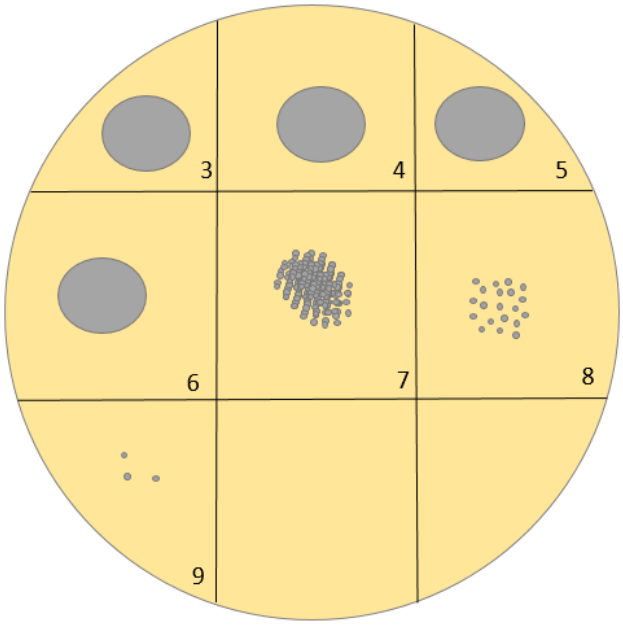

Figure 3.5. Schematic for plaque assay; the serial dilution with at least 10 well-defined phage plaques is the one that is used for counting. In this figure, for serial dilution 8 (number marked at the bottom right of the block) shows 20 plaques for counting.

3.3.4 Deposition of phage PP01 onto gold surface through the MUA-EDC-NHS method

For XPS and antimicrobial activity analyses, representative samples of gold-coated silicon wafers used as gold substrates for the phage deposition through the EDC/NHS chemistry[77]. Gold surfaces were firstly cleaned by sonication with acetone, isopropanol, and ethanol for 5 min, respectively. After this, the cleaned substrates were transferred to sterile polystyrene culture test tubes for 24 h of incubation in 1 mL 10 mM 11- mercaptoundecanoic acid (MUA) (450561, Sigma-Aldrich) in ethanol to form the first part of the self-assembling monolayer (SAM) under room temperature conditions. Subsequently, the substrates were washed two times with ethanol and DI water and

transferred to sterile microcentrifuge tubes for a 30-min incubation in 0.1 M 1-Ethyl-3-[3-dimethylaminopropyl] carbodiimide hydrochloride (EDC, 22980, FisherSci) followed by a second 30-minu incubation with N-hydroxysuccinimide (NHS, 130672, Sigma-Aldrich). Three different concentrations of NHS were tested (0.05, 0.1, and 0.4 M). Both EDC and NHS solutions were prepared in 2-(N-morpholino)ethanesulfonic acid (MES, BP300-100, FisherSci) buffer at pH 5.5, reached by addition of 10 M NaOH. Once this step was finished, the SAM was fully formed (or MUA-EDC-NHS linker). The next step was the incubation of phages for chemical attachment on the gold surface. The substrates were then washed again by pipetting two times with sterile Milli-Q water and incubated in 0.5 mL of PP01 stock at a titer of 10^9 PFU/mL for overnight phage attachment at 4 °C. The next day, the wafers were taken out of incubation with sterile tweezers and washed twelve times by pipetting with sterile 0.02 M PBS and stored in this solution for tests. Before each testing, 12 more washing steps were perform to remove unbound phages.

3.3.5 Preparation of Lactobacillus plantarum samples

To corroborate the performance of the transistor, tests were performed with the non-targeting *Lactobacillus plantarum*. A colony was collected with a sterile loop and cultured overnight in 10 mL of Lactobacillus MRS broth (LMRS, Fisher) at 150 rpm and 30 °C in an orbital incubator. To obtain a concentration of 10^8 CFU/mL, 0.1 mL was taken from the overnight culture and incubated in 10 mL of LMRS for orbital shaking at 150 rpm with a temperature of 30 °C until an OD_{600} in the range of 0.4-0.5 was obtained. Once this absorbance value was reached, bacteria were centrifuged twice at 6000 x g at 4 °C for a period of 10 min to remove the LMRS broth and replace it for the medium to be evaluated.

3.4 X-ray photoelectron spectroscopy

To assess the SAM formation, X-ray photoelectron spectroscopy (XPS) was performed using the PHI 5000 Versa Probe III (U of A Nanofab) with monochromatized Al K_α line, with an X-ray probing size of 200 µm and power of 50 W. The sprectrometer was previously calibrated at a binding energy of 84 eV of $Auf_{7/2}$ with reference to Fermi level. The pressure of the chamber during analysis was lower than $5x10^{-8}$ Pa. For the survey scan, the pass energy applied was 280 eV, and for the high resolution, the energy applied was 55 eV.

For the processing of the spectra, the CasaXPS software was used with a baseline type Shirley or linear, depending on the nature of the peak and the surrounding noise. All graphs and atomic percentages correspond to data taken from high resolution spectra for each element evaluated in the characterization. As well, all spectra were calibrated by compensating the difference between the peak for Au4f7 of each sample with the standard binding energy for metallic gold at 84 eV[78].

3.5 OECT evaluation

3.5.1 Characterization of OECT and conditions

To characterize and evaluate the performance of the PEDOT:PSS-based OECT, the sourcemeter units (SMU) Keithley 2400 and Keithley 2401 controlled by the software Kickstart v 2.6.0 (©Keithley Instruments, LLC) were used. An uninsulated 99.95% gold wire with a 1.0-mm diameter was used as the gate (Product AU00-WR-000171, GoodFellow, Cambridge). To minimize noise during measurements, SMUs were joined through a cable at the backside of the units where the ground is located. The drain and

the source are found on the pre-patterned substrate, made from indium tin oxide (ITO). For these experiments, all electrodes were connected through alligator clips, and the gate electrode was supported by using a laboratory stand support as shown in Figure 3.6.

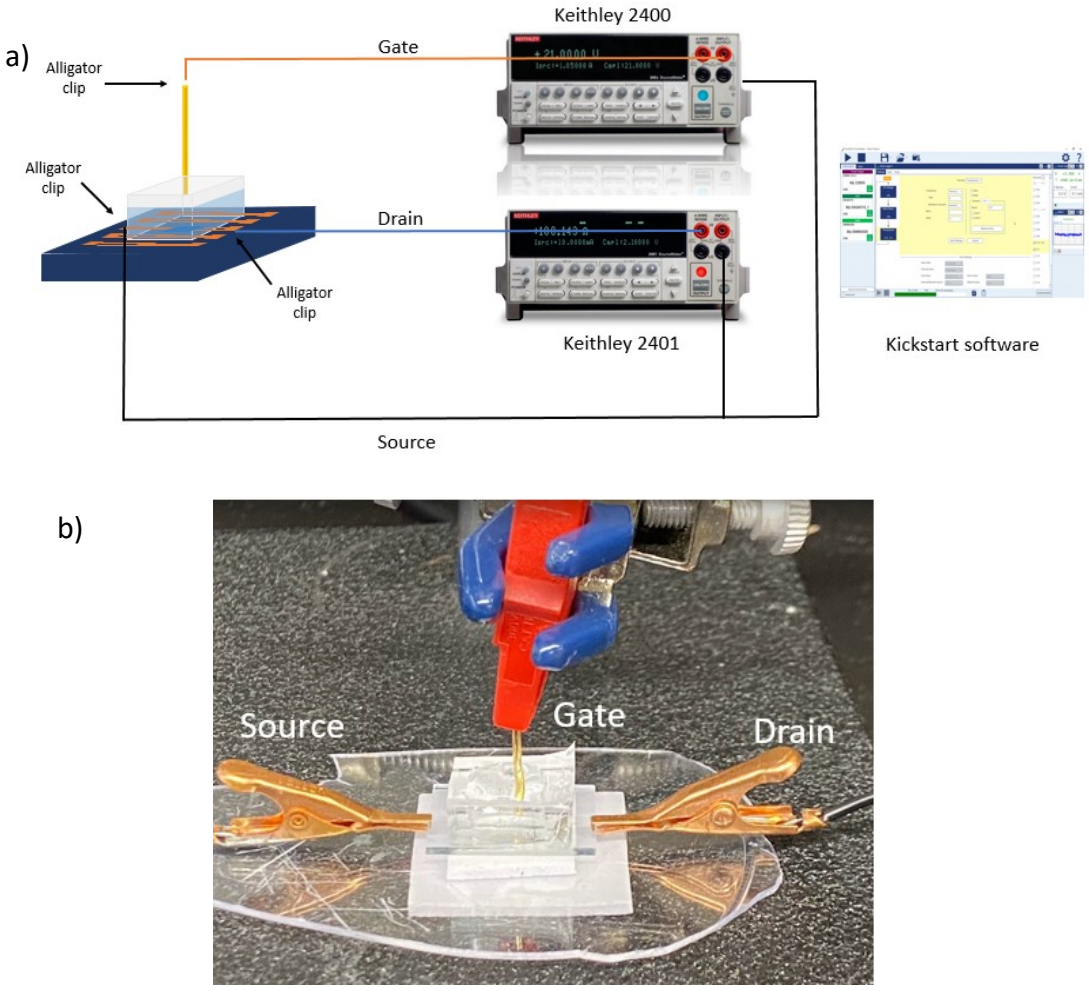

Figure 3.6. Setup for OECT evaluation: a) diagram shows the connections from the sourcemeter units to the transistors and b) picture shows alligator clips and gate electrode positions for evaluations.

To delimit the area of the liquid samples, a PDMS well was prepared by using Sylgard-184 Silicone Elastomer base and curing agent (Sylgard-184, Dow Corning) in a proportion of 10:1, removing the bubbles through vacuum and pouring it in a compartment of a Petri dish with four compartments and letting it cure for 48 h at room temperature. Once the PDMS was cured a portion of the polymer was taken with an X-acto knife and a hole was cut to make a well that covers the active area without fully covering the source and drain electrodes. This procedure is depicted in Figure 3.7.

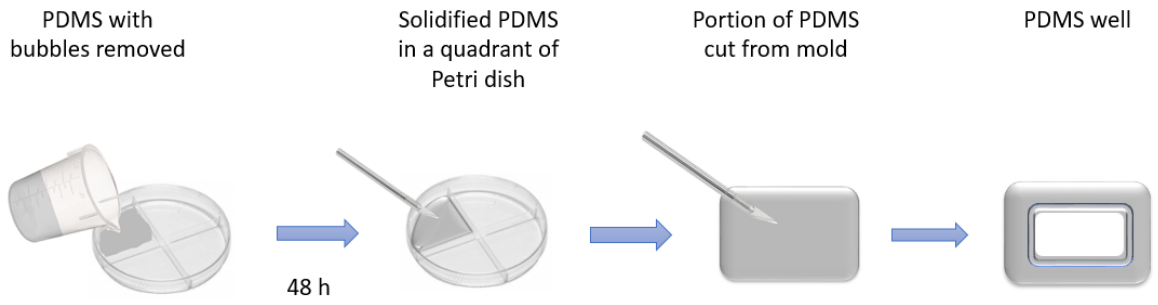

Figure 3.7. Illustration of procedure for the preparation of PDMS well.

Phosphate buffered saline (PBS) and tryptic soy broth (TSB) were used as media. For PBS, tablets were diluted in 200 mL DI to yield a solution of 0.01 M phosphate buffer, 0.0027 M potassium chloride and 0.137 M sodium chloride; for TSB, a solution at 30 g/L was prepared and sterilized. Each liter contains 17 g/L casein peptone (pancreatic), 2.5 g/L dipotassium hydrogen phosphate, 2.5 g/L glucose, 5 g/L sodium chloride, and 3 g/L soya peptone (papain digest).

To measure the output curves, a sweep voltage from -0.5 to 0.5 V with a step rate of 50 mV was applied between the drain and the source, while applying a gate bias that

goes from 0 to 1 V in increments of 0.1 V. For transfer curves, the sweep was applied from 0 to 1 V with a step rate of 50 mV between gate and source electrodes, as well as drain bias from 0 to -1 V with decrements of -0.1 V. All tests were performed with an integration rate of 10 for measurements to decrease the noise effect of the lab-made setup.

3.5.2 Application of OECT for E. coli O157:H7 *detection*

To evaluate the performance of the OECT in contact with bacteria, different tests were performed. For this purpose, different controls were evaluated: (1) media, (2) media + PP01, (3) media + *E. coli* O157:H7, (4) media + *L. plantarum*. As well, experiments with phage PP01 attached to the gold gate electrode were performed, evaluating its performance in (1) media, (2) media + *E. coli* O157:H7 (4) media + *L. plantarum*. Most of the experiments were performed at room temperature without agitation, and the measurements were made every ten minutes with a gate sweep from 0 to 1 V, using a step rate of 50 mV and a constant drain bias of -0.5 V. The overall volume evaluated during each experiment was 0.5 mL.

Regarding to bacteria preparation, overnight cultures were prepared as described in section 3.3.2 for *E. coli* O157:H7, followed by preparing serial dilutions until achieving a final concentration of 10^8 CFU/mL (it is known through growth curves that an overnight culture can reach a maximum concentration of approximately 10^9 CFU/mL)[79]. The dilution was then centrifuged and suspended in the desired medium two times at 6000 x g for 10 min each. For *L.* plantarum, the procedure is described in section 3.3.5. For the gate electrode, chemical attachment was performed using the methodology described in

section 3.3.4 selecting a concentration of 0.1 M NHS for OECT tests. As well, bacteriophages were taken from the lysate prepared (PP01 10^9 PFU/mL) as described in section 3.3.2 with no more than a month from preparation, centrifuged at 21,000 x g for 3 h and resuspended in the desired medium two times.

4. Results and Discussion

In this chapter, results related to three different technical challenges will be addressed: (1) the characterization of the PEDOT:PSS thin layer and its performance in PBS as non-nutrient medium, (2) the characterization of chemical attachment of phage PP01 onto gold surfaces, and (3) the impact of the modified gold wire on the performance of the OECT with the proposed controls mentioned in the objectives, as well as the comparison with TSB as nutrient medium.

4.1 Characterization of PEDOT:PSS-based transistors: film thickness, conductivity and performance

The first goal of this project was to find the most suitable PEDOT:PSS-based ink to be deposited on the substrate and be applied for the OECT fabrication. In the device, the PEDOT:PSS acts as the active channel where charge carriers navigate from the drain to the source electrode when a potential is applied. It is important that PEDOT:PSS has high conductivity, presents the expected operation mode, and remains stable through the measurements in aqueous conditions. In search of the suitable ink for this project, several mixtures were prepared and characterized. The results are discussed based on the suitability of the inks based on conductivity, and output and transfer curves of transistors fabricated in this study. To characterize conductivity, representative thin film samples were deposited onto glass surfaces that went through the same cleaning process as the substrate.

The first ink evaluated was pristine PEDOT:PSS suspension (483905, Sigma Aldrich), which was spin-coated from 1500 to 4000 rpm at an acceleration of 500 rpm/s^2. Four-point probe analysis was used to determine that the conductivity varies from 0.42 to

7.2 mS/cm (Table 4.1). There was no clear trend relating conductivity to thickness in these experiments. By solely using this PEDOT:PSS suspension, conductivity values were substantially lower than values for PEDOT:PSS thin films found in literature, which varies from 0.3 to 1000 S/cm[80].

Table 4.1. Characteristics of first set of experiments with pristine PEDOT:PSS.

Substrate	Spin rate (rpm)	Average thickness (nm)	Average resistivity (ohm-cm)	Average conductivity (S/cm)
1	1500	204.5	138.87	0.0072
2	2000	192	186.89	0.0053
3	2500	160.3	458.72	0.0022
4	3000	92.3	229.66	0.0043
5	3500	84.3	347.07	0.0029
6	4000	84.75	23953.22	0.000042

To improve the conductivity of the films, a commercial PEDOT:PSS formulation, PH1000 (Ossila©), was used since this product is marketed specifically for the fabrication of highly conductive devices,[70] and it was expected that conductivity values obtained would be improved. Given the higher viscosity of the PEDOT:PSS PH1000 suspension, the acceleration for the spin-coating process was increased to 1500 rpm/s^2 for 40 s for the next set of samples. After spin-coating, samples were baked under nitrogen atmosphere by applying three rounds of alternate vacuum and nitrogen cycles using a vacuum oven at approximately 200 ºC for 1 h. Results shown in Table 4.2 show that these changes indeed improved conductivity, with values ranging from 0.07 to 0.17 S/cm, compared to pristine PEDOT:PSS thin films when compared to results in Table 4.1.

Results suggests that baking samples with N_2 improve PEDOT:PSS thin films conductivity compared to annealing with air. From the literature it is known that annealing in N_2 results results in better stability[81].

Table 4.2. Characteristics of with pristine PEDOT:PSS PH1000 baked in inert atmosphere.

Substrate	Spin rate (rpm)	Average thickness (nm)	Average resistivity (ohm-cm)	Average conductivity (S/cm)
7	1500	129.6	6.04	0.17
8	2000	102.6	7.36	0.14
9	2500	86.1	6.49	0.15
10	3000	81.7	9.69	0.10
11	3500	67.6	8.04	0.12
12	4000	74.3	14.50	0.07

Transistors with pristine PEDOT:PSS suspension were prepared by depositing the active channel to cover all the five sets of interdigitated source and drain electrodes fingers (Figure 4.1.a) where the film was spin-coated at 1500 rpm for 40 s. As mentioned in the experimental section, a PDMS well was used to retain the electrolyte during tests. In initial testing, the hydrophobicity of the glass substrate affected the performance of the transistor due to poor interaction between the substrate and PEDOT:PSS. To address this, substrates were treated in a UV-Ozone chamber with a 185 nm lamp for 10-min surface cleaning before moving on to the spin-coating process.

The first experiments for transistor performance were carried out using the Keithley 4200 Semiconductor Characterization System (SCS) (Figure 4.1b) at the nanoFAB at the

University of Alberta. Output and transfer curves are depicted in Figure 4.2. For the output curves (Figure 4.2.a), when the positive gate bias (V_G) is applied, the drain current-drain voltage (I_D-V_D) curves move to more negative voltage values, starting at V_D= -0.02 V at I_D= 0 µA for V_G =0 V and moving towards V_D= - 0.11 at I_D= 0 µA for V_G = 1 V. This suggests that the device is working depletion mode. In the range of 0 to -0.5 V sweep voltage, it can be seen that the transistors is still in the linear range (i.e. saturation has not been reached). Although the saturation region could potentially be reached by applying a higher gate potential difference, the gate voltage was limited to less than 1.5 V as a higher voltage may compromise both the stability of PEDOT:PSS thin films and the integrity of the interdigitated electrodes. Experiments in which applied potentials applied were higher than 2 V damaged the interdigitated fingers, and could also cause water electrolysis when applying a V_G greater or equal to 1.2 V. Transfer curves (Figure 4.2.b) showed a linear trend for the sweep from 0 to 1 V for the evaluated drain bias (V_D). For both cases, the range of biases applied was not broad enough to turn the device OFF, as would be expected for depletion mode transistors. Overall, these curves show that pristine PEDOT:PSS PH1000 was not suitable under these experimental conditions. Considering this, another approach was explored by including additives (widely explored for OECTs semiconductor layers) to the PEDOT:PSS mixture.

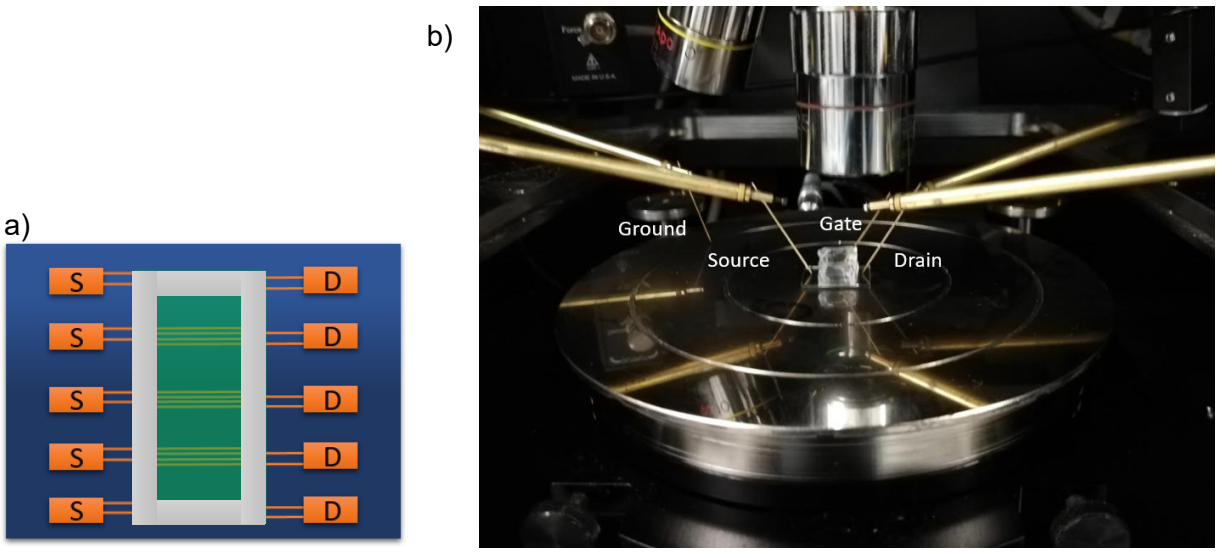

Figure 4.1. a) Coverage area of thin film on substrate using pristine PEDOT:PSS; b) Setup for OECT evaluation using a gold plated tungsten probe as the gate electrode in the Keithley 4200 SCS.

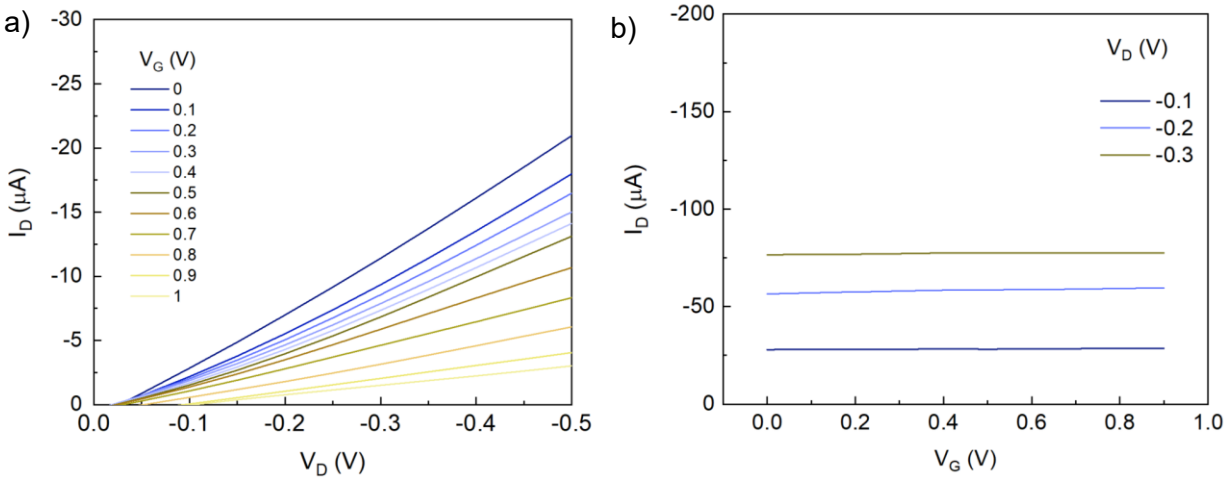

Figure 4.2. a) Output and b) transfer curves for pristine PEDOT:PSS PH1000 OECT using PBS 0.01 M as electrolyte solution and a thin film deposited at 1500 rpm.

Since high conductivity is necessary for good performance of the transistor, and since the output and transfer curves were not satisfactory, secondary dopants or conductivity enhancing agents were added to pristine PH1000. Based on literature, [82–84] an ink was prepared made of 93.5 (v/v)% PEDOT:PSS PH1000 (Ossila©), 5 (v/v)% glycerol, 1(v/v)% (3 glycidyloxypropyl)-trimethoxysilane (GOPS), and 0.5 (v/v)% 4-dodecylbenzenesulfonic acid (DBSA). In this mixture, GOPS acts as cross-linker, glycerol acts as conductivity enhancement agent, and DBSA acts as a surfactant to facilitate film processing and to improve the conductivity of the thin film[84]. Most articles in the literature specify that samples should be baked at a temperature between 130 and 140 ºC after spin coating. Kiebooms *et al*. demonstrated that the presence of dopants could increase the degradation of PEDOT:PSS above 150 ºC, even when this semiconductor is stable up to 250 ºC [81,85]. A set temperature of 140 ºC was selected for the preparation of samples. Results showed that the presence of DBSA, GOPS, and glycerol chemicals indeed increased the conductivity of the thin layer to hundreds of siemens per centimeter as shown in Table 4.3.

Table 4.3. Characteristics of third set of experiments with PEDOT:PSS PH1000, GOPS, and DBSA.

Substrate	Spin rate (rpm)	Average thickness (nm)	Average resistivity (ohm-cm)	Average conductivity (S/cm)
13	1500	243.1	0.0035	283.78
14	2000	202.0	0.0033	301.17
15	2500	182.6	0.0035	284.03
16	3000	175.8	0.0038	261.20
17	3500	167.6	0.0038	263.59
18	4000	119.3	0.0029	340.99

For the pre-patterned substrates, the source and drain electrodes are interdigitated, allowing the active area of the sensor to be varied by varying the size of the area defined by the semiconducting ink. To determine the area that gives the best response, five different areas were explored. A width of approximately 1 mm per pair was maintained in all cases, and the length was varied: 5.74 mm for area 1, 4.55 mm for area 2, 3.2 mm for area 3, 1.48 mm for area 4, and 0.25 mm for area 5. A schematic is shown in Figure 4.3.

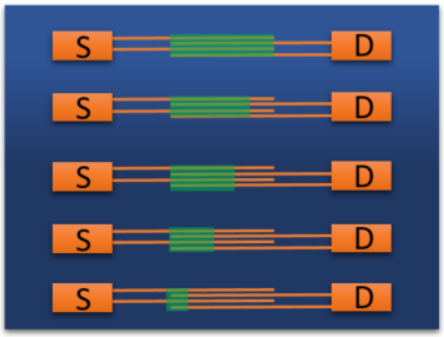

Area 1	Length 1 = 5.74 mm	Width 1 mm
Area 2	Length 2 = 4.55 mm	Width 1 mm
Area 3	Length 1 = 3.20 mm	Width 1 mm
Area 4	Length 1 = 1.48 mm	Width 1 mm
Area 5	Length 1 = 0.25 mm	Width 1 mm

Figure 4.3. Representation of covered areas by ink for each pair of ITO interdigitated electrodes on glass substrate (Ossila©).

Output and transfer curves for each area are shown in Figures 4.4 to 4.8. For area 1 (the largest area), increasing the gate voltage did not cause any decrease of the I_D-V_D curves (Figure 4.4.a), as expected; decreasing the current once V_G= 1.1 V was applied. This could be attributed to the large volume for the area 1 design; the voltage applied was not able to initiate the de-doping process for this PEDOT:PSS film. As well, transfer curves (Figure 4.4.b) confirm that, using these dimensions, the device did not reach the OFF state.

For area 2, the transfer curves (Fig 4.5.b) were slightly better than for Area 1, as it can be seen that applying a gate voltage does cause the current start decreasing, however the device did not reach reach the OFF state under the tested conditions. As well, the threshold potential is non-zero (V_D= -0.11 V) which means that more potential is needed for the output curves to take place (Figure 4.5.a).

For area 3, the transfer curves (Figure 4.6.b) are similar to those collected for area 2, with the main difference being that the threshold potential in the output curves was closer to zero (V_D= -0.02 V, Figure 4.6.a).

As for area 4, the transfer behavior (Figure 4.7.b) was comparable with those observed for areas 2 and 3; but the output curves (Figure 4.7.a) showed that below V_G= 0.5 V, V_D-I_D curves remain similar, which could be due to the channel saturation level remaining the same for V_G= 0.6 to 0.8 V. This was the case even when a higher potential was applied but further investigation is needed to confirm this. However, there is no saturation region in any of the output curves, only linear regions in the V_D-I_D curves.

For the smallest area, area 5 (Figure 4.8), neither output (Figure 4.8.a) nor transfer curves (Figure 4.8.b) showed good performance. For the transfer curves, it was noticed that the registered current increased – instead of decreasing as expected in depletion-mode transistor – above V_G= 0.2 V; the same behavior was observed in output curves. This could be attributed to an over-oxidation of the thin film, leading to the alteration of the conductivity of the polymer due to structure changes, which results in an accumulation-mode PEDOT:PSS transistor. These changes have been reported when a certain critical positive bias is applied or when the device is exposed to sodium hypochlorite[86,87].

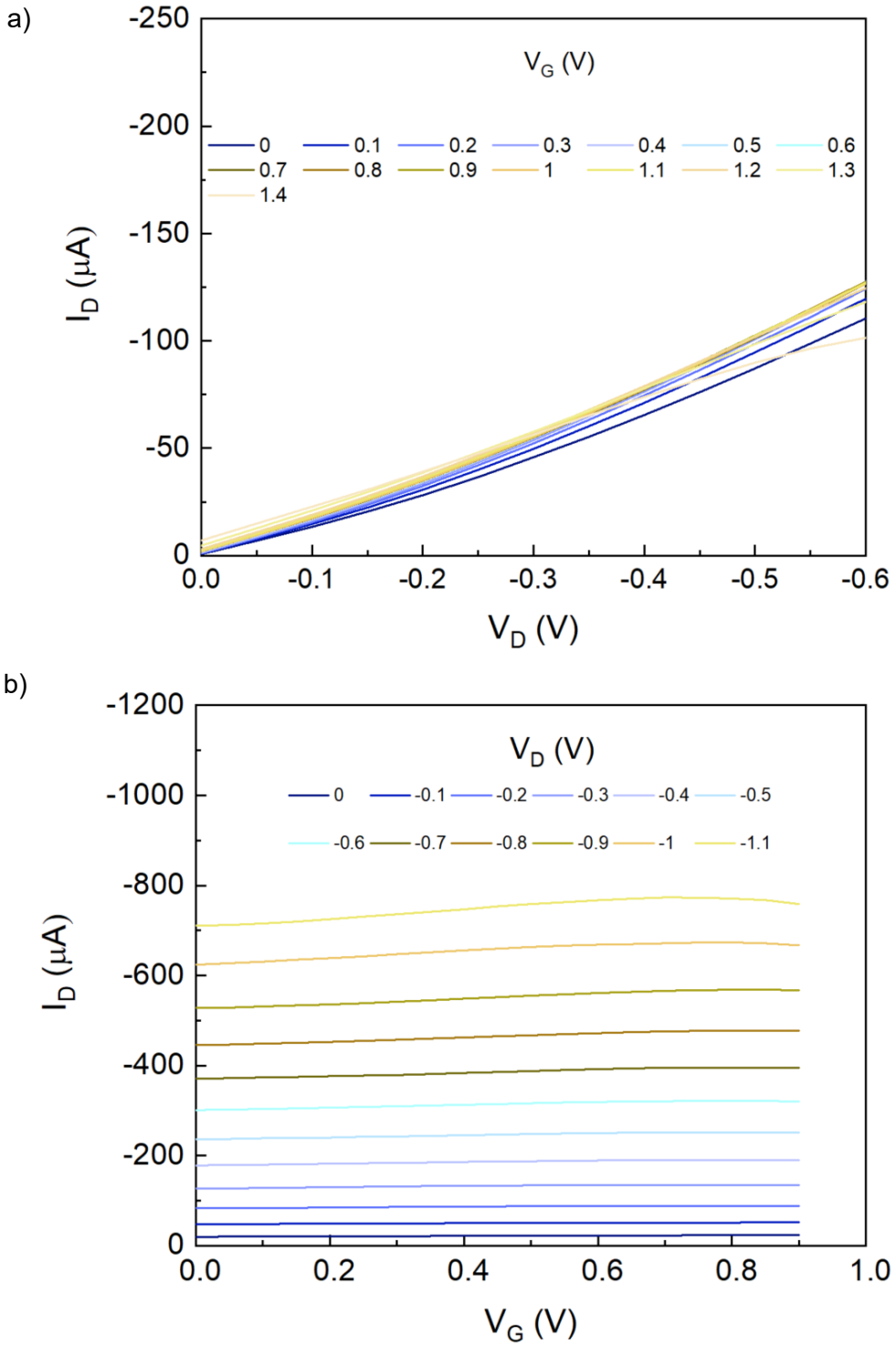

Figure 4.4. a) Output and b) transfer curves for area 1 in Figure 4.3 in 0.01 M PBS at a step rate of 50 mV.

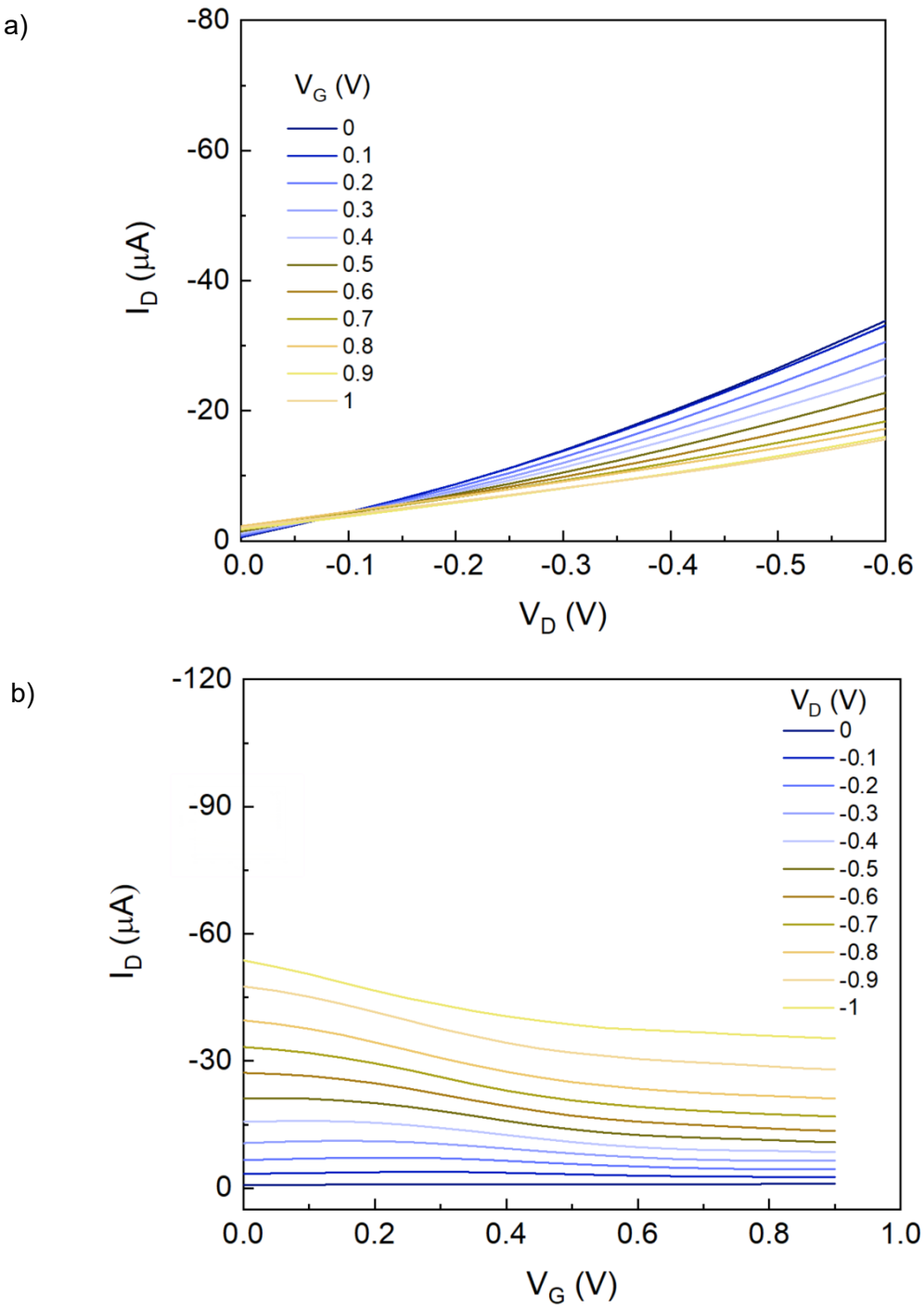

Figure 4.5. a) Output and b) transfer curves for area 2 in Figure 4.3 in 0.01 M PBS at a step rate of 50 mV.

a)

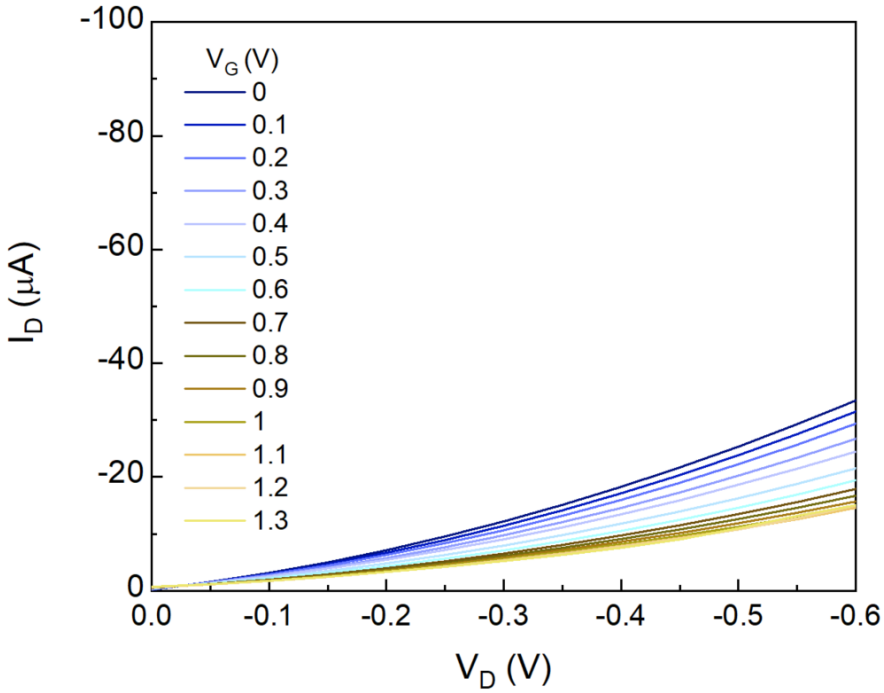

b)

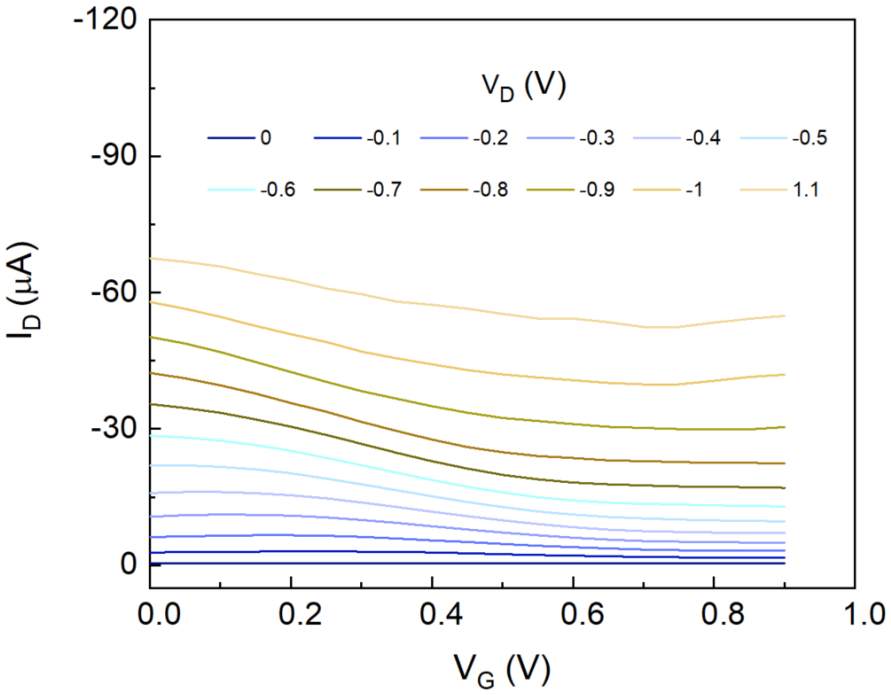

Figure 4.6. a) Output and b) transfer curves for area 3 in Figure 4.3 in 0.01 M PBS at a step rate of 50 mV.

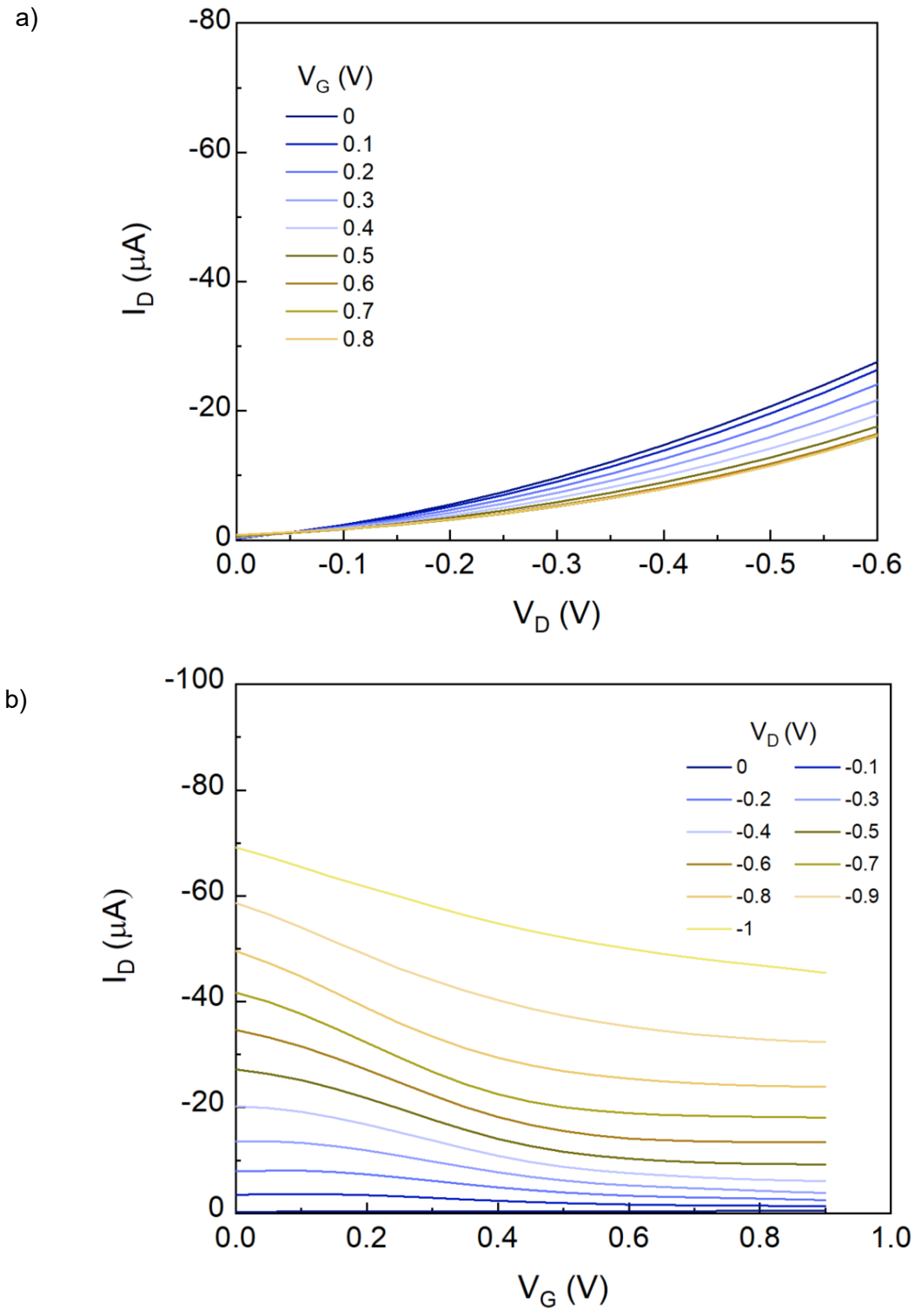

Figure 4.7. a) Output and b) transfer curves for area 4 in Figure 4.3 in 0.01 M PBS at a step rate of 50 mV.

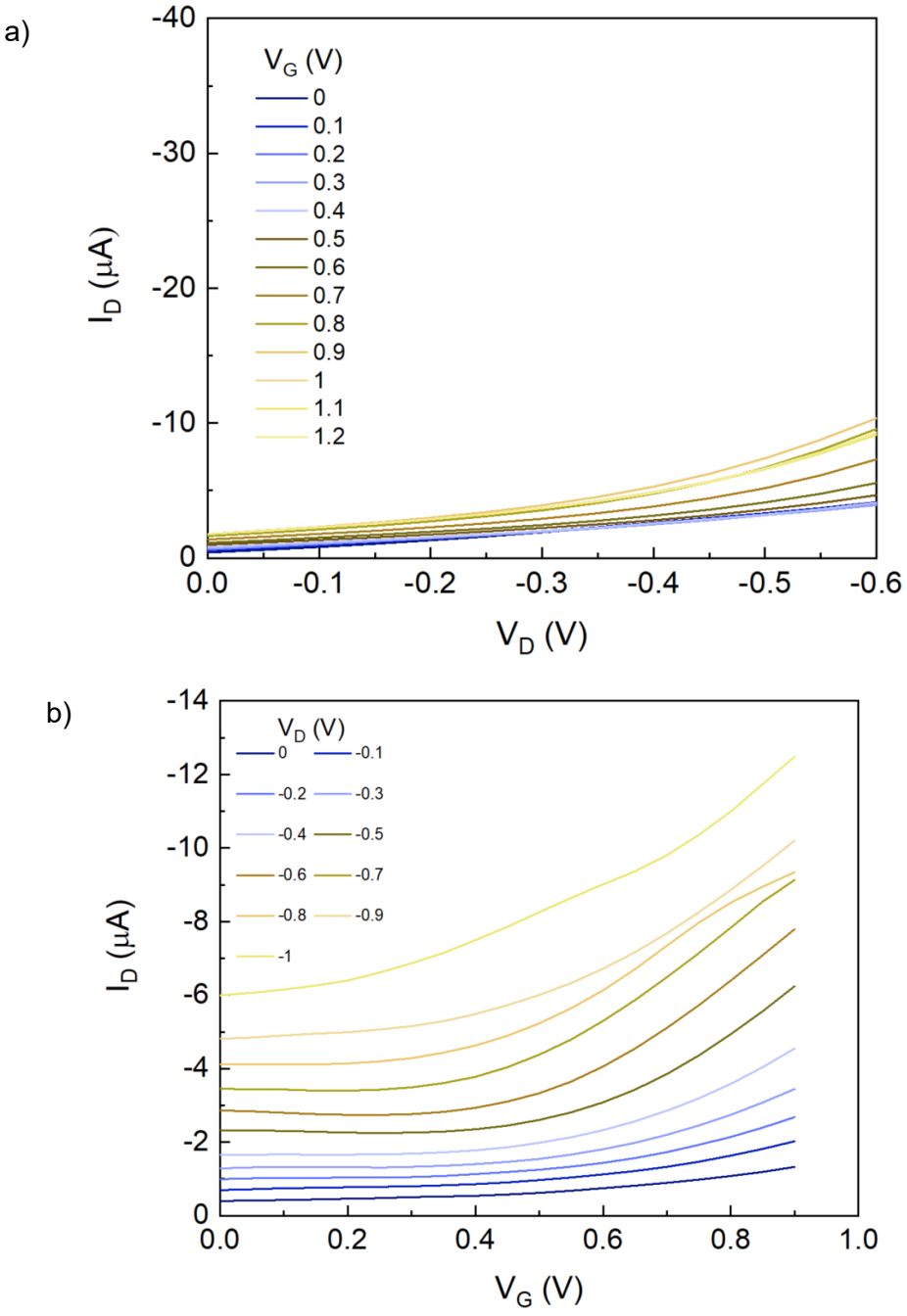

Figure 4.8. a) Output and b) transfer curves for area 5 in Figure 4.3 in 0.01 M PBS at a step rate of 50 mV.

In general, experiments showed that, under the conditions tested, the area of the thin film plays an essential role in the characteristics of the PEDOT:PSS OECT since it defines the quality and stability of the PEDOT:PSS-based channel area. If the area is too large, there is probability that the de-doping process will not happen, and if the area is too small, the stability of the film can be compromised by over-oxidation when it is under an applied voltage.

Based on these curves it was concluded that the best coverage area is between areas 2 and 3 (4.55 mm^2 and 3.20 mm^2). Nevertheless, none of the devices tested during the area study was able to reach an OFF state under the conditions tested, showing that a sufficient number of ions could not be injected into the PEDOT:PSS to cause this transition.

A new formulation of PEDOT:PSS was prepared, following the recipe given in the study by Tang *et al.*[88] , in which an OECT was fabricated to study the effects of cross-linkers on performance. Unlike the ink previously tested, there is no surfactant (DBSA) present and an organic solvent, 2-isopropanol (IPA), is used as conductivity enhancing agent. Substrates were spin-coated using an ink composed of 90 (v/v) % overnight stirred mixture of isopropanol-PEDOT:PSS in a ratio 1:1, and 2 (v/v)% of (3 glycidyloxypropyl)-trimethoxysilane added right before spin coating and mixed for 1 minute through a vortexer. The PEDOT:PSS PH1000 suspension was previously sonicated for 30 min, followed by filtration with a 1.3-µm filter and three subsequent filtrations steps through 0.45-µm nylon filters before mixing with IPA. For the spin-coating deposition, a speed of 3000 rpm was selected for more homogeneity (with a standard acceleration of 1500 rpm/s^2). The samples were then dried under nitrogen atmosphere at 140 ºC for 1 h. The

average values of sheet conductivity for each substrate are summarized in Table 4.4. The average values of sheet conductivity for each substrate are summarized. The expected average deposited thickness of the PEDOT:PSS-based thin film under this procedure is 180 nm, and the selected length and width of the thin-film for transistor fabrication were 4.6 mm and 1.0 mm respectively. The thin film is shown as a blue rectangle in Figure 4.9.

Table 4.4. Characteristics of set of experiments with PEDOT:PSS, IPA, and GOPS.

Substrate	Average thickness (nm)	Average resistivity (ohm-cm)	Average conductivity (S/cm)
18	182.9	0.69	1.45
19	177.4	0.63	1.59
20	180.1	0.82	1.22
21	177.1	0.44	2.27
22	181.6	0.70	1.42

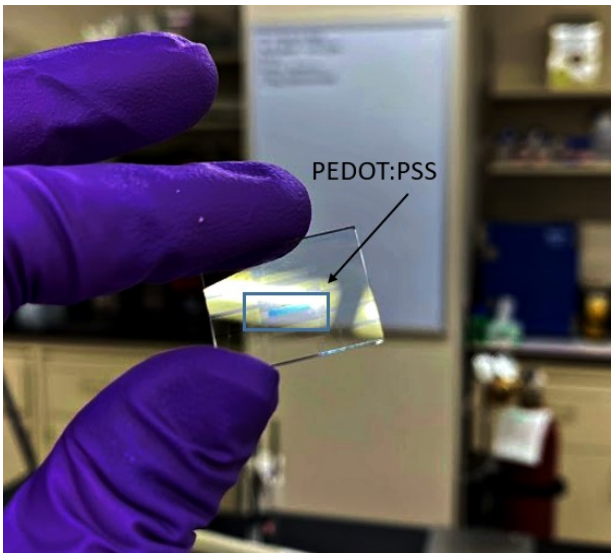

Figure 4.9. PEDOT:PSS-based thin film deposited onto pre-patterned ITO substrate through spin coating.

The curves for the transistor prepared with the active channel using PEDOT:PSS PH1000, IPA, and GOPS are shown in Figure 4.10. Note that, at this point in our work, it was necessary to change analysis systems to one that could be used in the lab, in preparation for our work with biological samples. Two Keithleys were therefore used with the Kickstart software. This led to an increase in noise in the signal (Figure 4.10). These curves exhibit the expected depletion mode, where the I_D values decrease when a positive gate bias is applied, in both output and transfer curves (Figure 4.10.a). In addition, the current increases in the transfer curves where a negative drain bias is applied, while it decreases under a positive gate sweep (Figure 4.10.e), even when the values of sheet conductivity were much lower than values registered for the PEDOT:PSS + DBSA + glycerol + GOPS samples. Dual sweep led to the formation of hysteresis (Figure 4.10.c) at V_G > 0.4 V. This is attributed to the presence of ions and depends on the potential; higher voltage leads to greater hysteresis due to the high amount of ions injected into the thin film[89]. At V_G =0.9 V, the transistor does not fully reach the OFF state. In the ON state, the current is – 97 μA at V_G= 0 and V_D= -0.5 V. As can be seen when the potential V_G= 0-0.4 V, the current increases instead of decreasing, which can be attributed to the fact that this range of potential is too low to push enough ions to reach a saturation region; instead, it contributes to hole mobility in the PEDOT:PSS thin film. These curves suggest that the introduction of IPA as secondary dopant improved the performance of both output curves simultaneously.

On the other hand, the output and transfer curves were evaluated when using TSB as electrolyte. From the output curves (Figure 4.10.b) it can be seen that, unlike in tests using PBS (Figure 4.10.a), the transistor reaches the OFF state by applying V_G = 1.0 V

with a registered I_D = -1.05 µA. In the case of dual output curves (Figure 4.10.d), hysteresis was observed at lower gate bias values compared to tests done in PBS, and the hysteresis area in gate bias values above V_G = 0.7 V started to decrease again. All transfer curves for drain voltage V_D = 0 to -0.6 V converge to similar values when I_D range from -0.4 to -2.6 µA. Even though the curves are not touching each other, improvements are noticeable when using TSB rather than PBS. This is attributed to the components of the broth that contribute to the PEDOT:PSS de-doping process, possibly due to higher load of cations or positively charged components found in the ingredients of TSB.

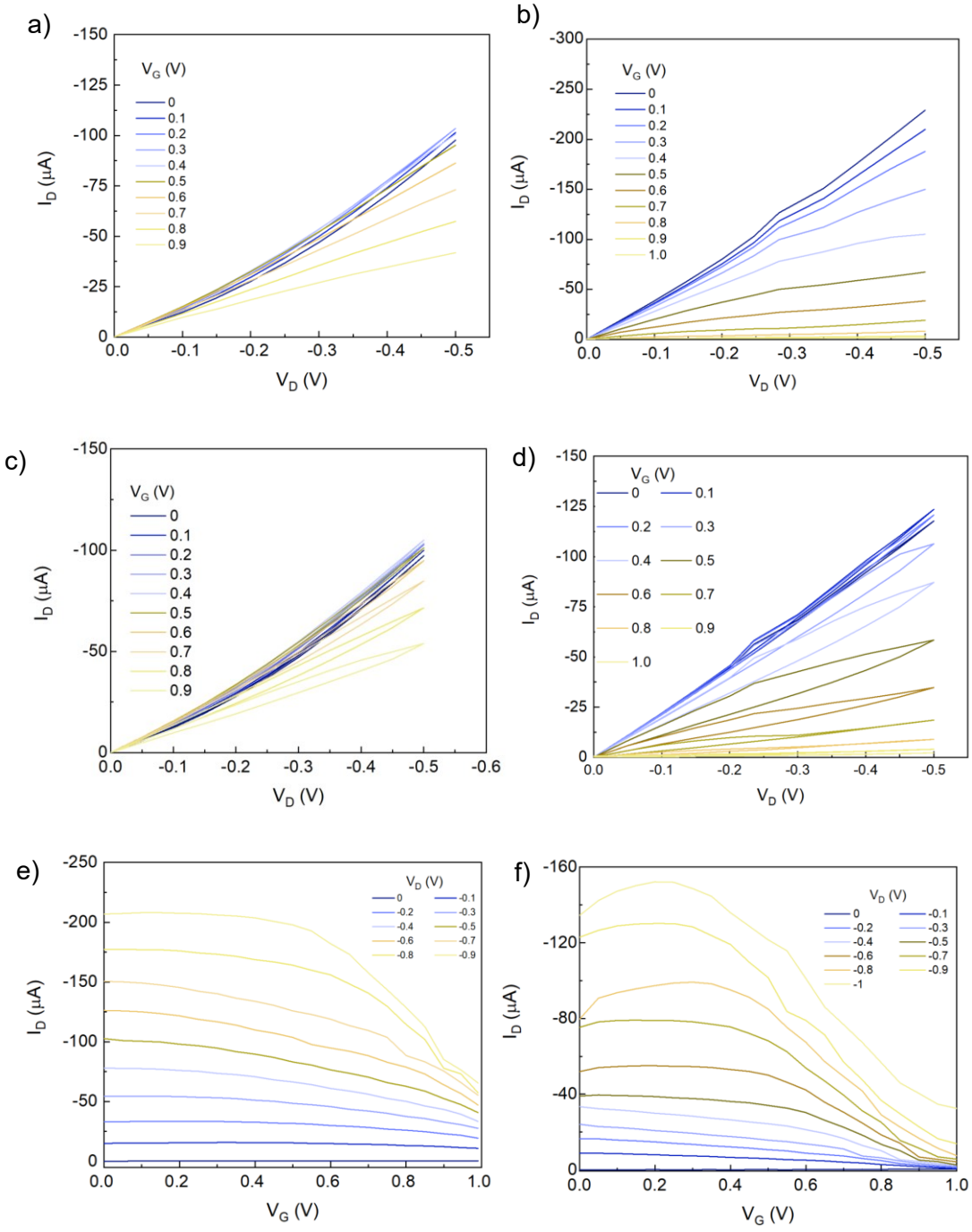

Figure 4.10. a) Linear output, c) dual output, and e) transfer curves for OECT using PBS 0.01 M as the electrolyte; and b) linear output, d) dual output, and f) transfer curves for OECT using TSB as the electrolyte. Step rate of 50 mV.

4.2 Attachment of phage PP01 onto gold surface and antibacterial activity

Phages were immobilized on gold nanowires through chemical bonding. EDC/NHS coupling was selected because of the vast background supporting the chemistry of this coupling when used for biological molecules attached to inorganic surfaces[47,77,90,91]. This method, for gold surfaces, consists on the formation of a SAM that contains a free carboxylic group that reacts with EDC to form an intermediate product (*o*-acylisourea), followed by reacting with NHS to form a semi stable amide bond that interacts with the amino group of the bacteriophage to chemically immobilize it to the gold surface.

In this section, the results regarding the attachment of the bacteriophage PP01 onto gold surfaces and the evaluations will be discussed.

4.2.1 Surface characterization of chemically treated gold surfaces by XPS

The SAM was evaluated through XPS by comparing the atomic percentage of different atoms (Au, C, N, O, and S) in different samples that underwent the EDC/NHS chemistry described in section 3.3.4. Prepared samples and labels are summarized in Table 4.5. Labels “0.4”, “0.1”, and “0.5” refer to samples that only went through the chemical attachment method without exposure to phages; “0.4-PP01”, “0.1-PP01”, and “0.05-PP01” refers to samples that went through chemical modification and PP01 overnight incubation in TSB, and “No C. A.” (i.e. no chemical attachment) denotes wafers without chemical surface modification that were exposed to overnight incubation of phage PP01 in TSB.

Table 4.5. List of samples and its characteristics for solid/liquid phase evaluation.

Label of sample	Chemical treatment	EDC:NHS ratio of concentration (M)	Phage incubation
0.4	No	1:4	No
0.1	No	1:1	No
0.05	No	2:1	No
0.4- PP01	Yes	1:4	Yes
0.1- PP01	Yes	1:1	Yes
0.05- PP01	Yes	2:1	Yes
No C. A.	No	1:1	Yes

Note: No C. A. refers to wafer phages went through physisorption (no chemical attachment).

As shown in Table 4.6, the gold surface atomic percentage decreased when the surface is chemically modified with SAM, and the nitrogen percentage increased when the linker is present in comparison with pristine Au-Si wafers. For the case of oxygen, it can be noticed that the surface atomic percentage value is greater for wafers that were only cleaned for characterization purposes rather than for samples that underwent chemical modification with the linker MUA/EDC/NHS (but not phage attachment). High resolution spectra for O1s shows two peaks at 532 and 533.2 eV (Figure 4.11), which suggests that this oxygen surface atomic percentage is related the linker, and possibly to the presence of water or organic compounds from the atmosphere that were adsorbed to the sample before analysis[92].

The spectra corresponding to S2p were used to confirm the presence of 11-MUA on the gold surface. The presence of the first section of the linker (11-MUA) was confirmed by XPS through two pairs of doublets found in the spectrum: the presence of thiol binding to gold at 161.9 eV, and S-H bonds from the 11-MUA molecule at 163.8 eV[93]

(Figure 4.12.a). Moreover, Figure 4.12.b shows the spectrum of Au4f which was used to calibrate the spectra of other elements (as was described in section 3.4).

High resolution XPS spectra shows one peak for nitrogen (Figure 4.13a), at 400.5 eV, corresponding to C-N bonds [93,94]. For C1s (Figure 4.13c) peaks were found at 285.3 eV corresponding to methylene groups, at 286.9 eV for C-O bonds, and 288.9 attributed to C-O-C*=O bonds [45,91–93]. For the peaks in O1s spectra (Figure 4.13.e), three peaks – at 532.1, 533.1 and 534.1 eV– are found when the spectrum is deconvoluted. These can be attributed to carbonyl, C-O/C-N bonds, and the O*-C=O functional group[78,91] (the asterisk is used to clarify the element where the peak is assigned from), respectively. When the samples were incubated with phage PP01 lysate, the atomic percentages of N and O increased again, while the percentage of Au drastically decreased due to the presence of the phage PP01. For the spectra corresponding to nitrogen (Figure 4.13.b), the peak was shifted to 400.7 eV, corresponding to amide nitrogen, which could be attributed to the nature of the protein-based phage surface[93]. From Figure 4.13.d, it can be seen that the peak corresponding to carboxylic carbon increased compared to the sample without phage PP01 (Figure 4.13.c). As for oxygen (Figure 4.13.e and Figure 4.13.f), the height of the peak corresponding to the O*-C=O functional group increased as well, again likely due to the presence of phages. In overall, HR S2p spectra confirms the formation of the 11-MUA SAM by showing the peak corresponding to the bonding to the gold surface, as well as the increment in atomic percentage for N and O elements in evaluated samples where incubation with PP01 was performed suggest that the bacteriophages are present and attached to the gold surface.

Table 4.6. Atomic surface percentage of different elements in evaluated surfaces.

Samples are labeled according to Table 4.5.

	Sample						
Element	Au-Si wafer	0.4	0.1	0.05	0.4-PP01	0.1-PP01	0.05-PP01
Au	47.39	21.67	25.84	25.45	15.67	15.17	10.58
C	36.04	57.47	54.07	54.77	54.50	56.57	61.34
N	-	4.20	3.72	4.95	11.83	10.53	10.48
O	14.58	13.37	13.61	12.25	16.48	16.13	15.75
S	1.98	3.29	2.76	2.58	1.51	1.59	1.85

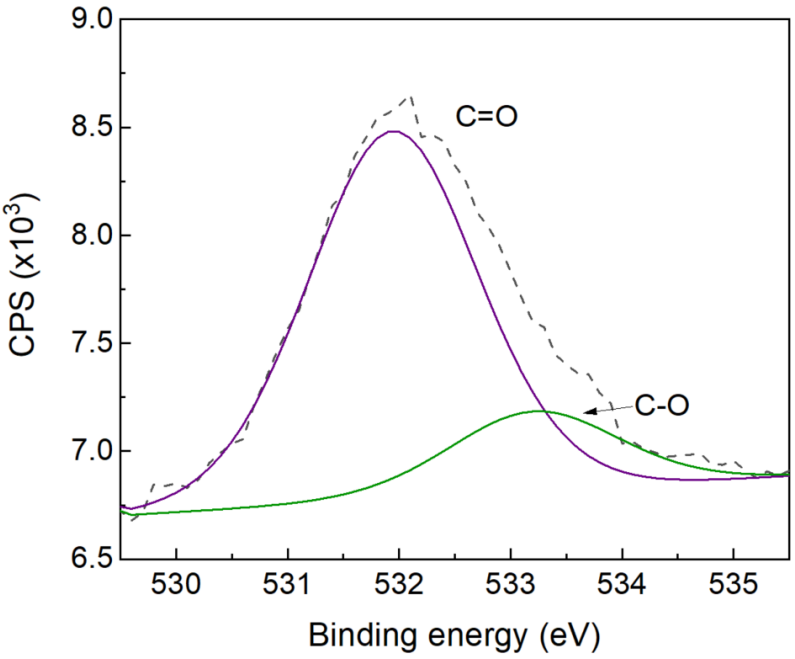

Figure 4.11. High resolution XPS spectra (dotted line) and deconvoluted peaks for O1s element in Au-Si wafer.

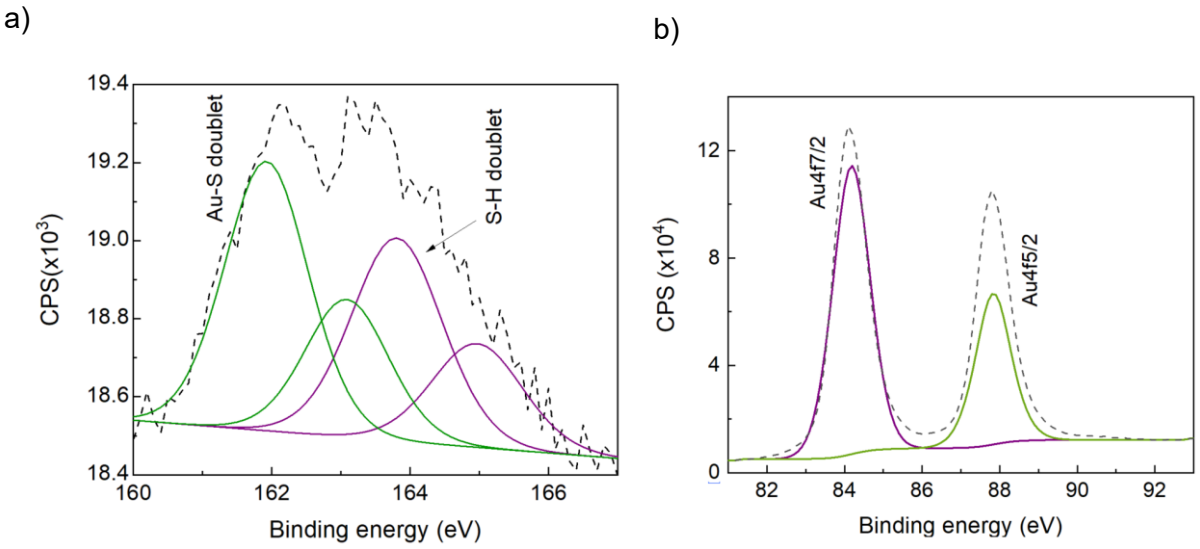

Figure 4.12. High resolution XPS spectra and deconvoluted peaks for a) S2p and b) Au4f for sample 0.1-PP01.

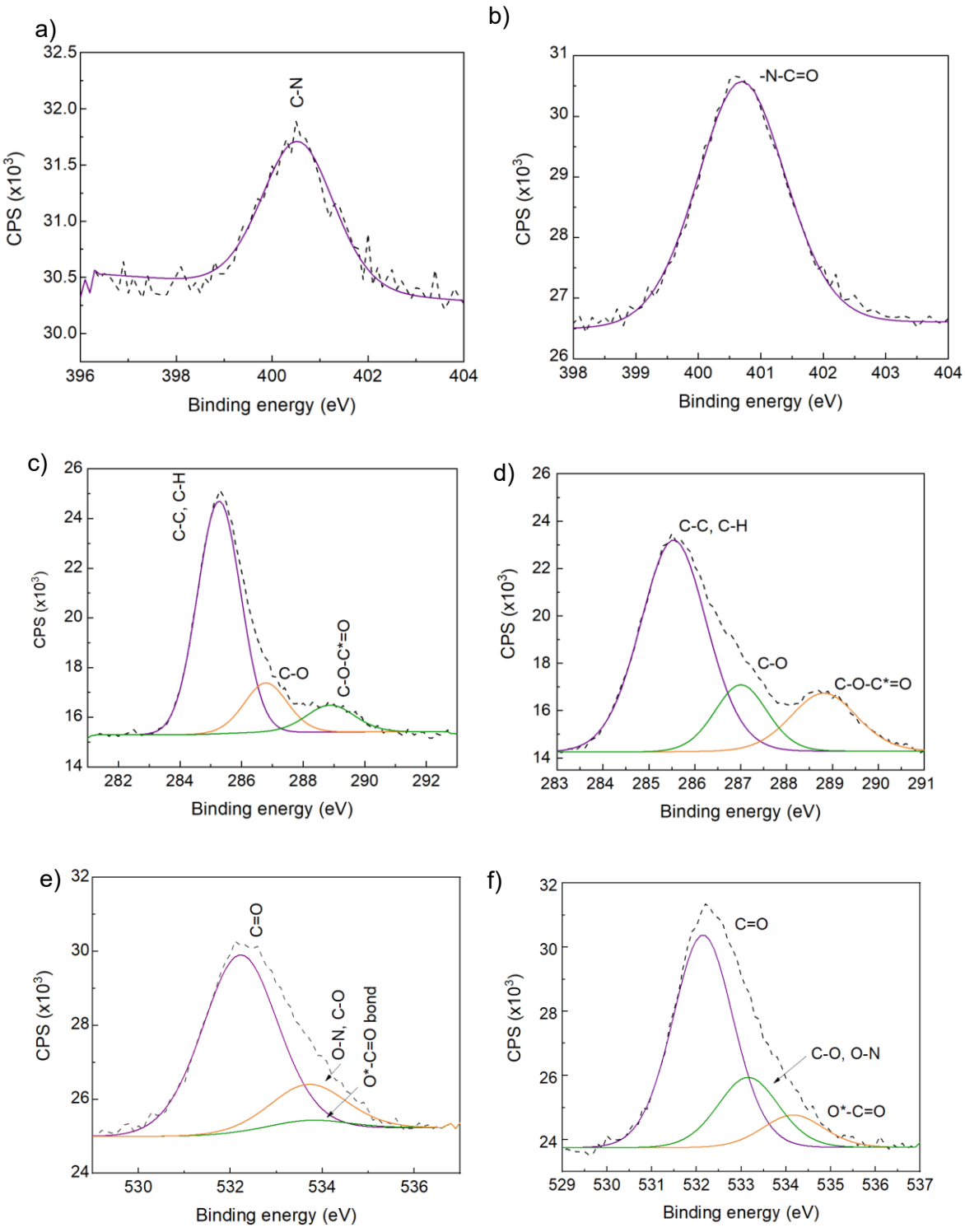

Figure 4.13. High resolution XPS spectra and deconvoluted peaks for (a,c,e) chemically modified Au-Si wafers for sample 0.1-No PP01, and (b,d,f) chemically modified Au-Si wafers with attached PP01 (sample 0.1-PP01) for N1s, C1s, and O1s.

4.2.2 Antibacterial activity of phage PP01 immobilized on Au-coated wafers on solid agar

Immobilized phage orientation is important because the tail fibers need to be free to detect and anchor to the target bacteria. Since bacteriophage orientation is not controlled by the selected attachment method, it is expected that some of the immobilized phages may not be in a convenient orientation for bacterial infection. To determine whether the immobilized phages are able to infect bacteria, experiments in TSA (solid phase) and TSB (liquid phase) were performed by using chemically modified gold wafers with attached phage PP01. For solid-phase evaluation, 0.1 mL of overnight culture of the host *E. coli* O157:H7 was added to TB soft agar and poured to the agar plate. Once the agar was dried, three different types of substrates with and without phages were tested: (1) Gold-coated silicon wafers treated with 0.1 M EDC-0.4 M NHS without phage incubation; (2) gold-coated silicon wafers treated with 0.1 M EDC-0.4 M NHS immersed overnight in phage solution; (3) gold-coated silicon wafers treated with 0.1 M EDC-0.1 M NHS without phage incubation; (4) gold-coated silicon wafers treated with 0.1 M EDC-0.1 M NHS immersed overnight in phage solution; (5) gold-coated silicon wafers treated with 0.1 M EDC-0.05 M NHS without phage incubation; (6) gold-coated silicon wafers treated with 0.1 M EDC-0.05 M NHS immersed overnight in phage solution; and (7) control wafers, which were made by immersing non-chemically treated wafers (no EDC/NHS chemical functionalization) overnight in phage solution. These samples were placed on the soft agar and incubated overnight for phage infection.

The samples on the left side of the petri dishes in Figures 4.14.a, 4.14.b, and 4.14.c show that chemical modification (EDC/NHS 1:4, EDC/NHS 1:1, and EDC/NHS 2:1) alone did not lead to bacterial cell lysis; however, samples incubated overnight with phage

solution (samples on the right side of the petri dishes) exhibited antimicrobial activity through the formation of clear lysis areas around the substrates. This suggests that even if a portion of phages were not immobilized with controlled orientation, at least some of the phages were in a proper direction (tail free) to perform infection activity on bacteria present in the agar.

For the control wafers without chemical treatment (Figure 4.14.d), zones of clearing also appeared around the substrates, suggesting that phage PP01 also can be attached through physisorption when interacting with the gold surfaces. This behavior was also reported by Tawil *et al.* where phages were present on gold surfaces through electrostatic interaction when exposed to gold surfaces[46].

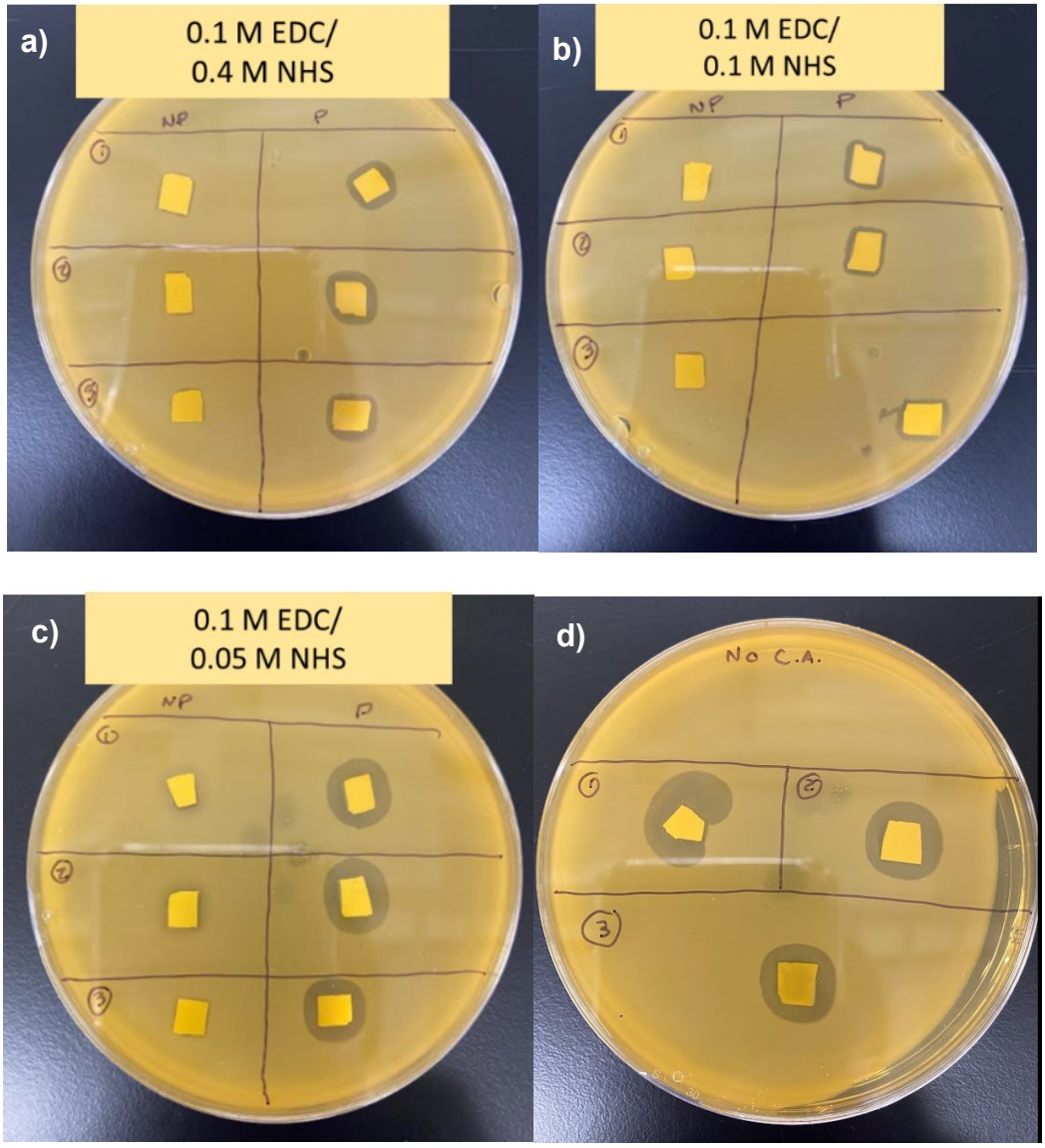

Figure 4.14. Lytic activity in TSA plaques of substrates with and without phage PP01 attached using a) 0.1 M EDC-0.4 M NHS; b) 0.1 M EDC-0.1 M NHS; c) 0.1 M EDC-0.05 M NHS; and d) no chemical attachment (No C. A. as shown in agar plate).

P= Phage attached to wafer surface, NP= No phages attached at the surface.

4.2.3 Antibacterial activity of phage PP01 on Au-coated wafers in liquid phase

The second part of the evaluation of antibacterial activity consisted on testing the lytic activity of phages attached to gold surface (same substrates as in section 5.2.1) by adding the substrates to mid-log cultures of *E. coli* O157:H7 and monitoring OD_{600}, a proxy for cell density, for 8 h. Table 4.5 summarizes the samples that were evaluated through this experiments and corresponding labels for Figure 4.16. The results of antibacterial activity of these substrates were compared to infections of cultures by free phages at a multiplicity of infection (MOI) of 0.01. The MOI is described as the ratio of phage to bacteria. It is an important parameter as it dictates, in many ways, the infection dynamics; the higher the value, the faster the infection will overtake the host population. This MOI was selected so the phage infection was in a relatively similar velocity as for the samples tested. The results from this free phage infection culture were used as a control sample.

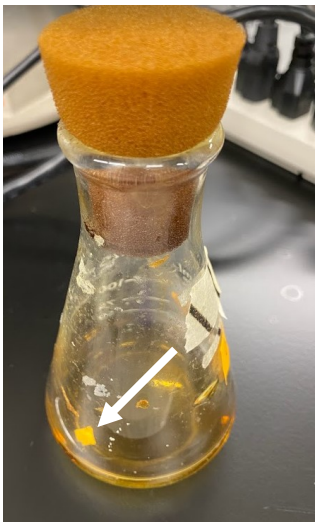

Figure 4.15. Sterilized flask with bacterial culture and wafer being tested.

Figure 4.16 shows the results obtained through the measurement of OD_{600}. The results for the first three curves, corresponding to wafer with chemical treatment at 0.4, 0.1, and 0.05 but without phages), suggest chemical treatment alone did not impart any antibacterial activity towards *E. coli* O157:H7 cultures. The cultures showed a constant increase in OD_{600} values over the 8-h range, which means that *E. coli* O157:H7 was continuously growing. For samples that were both chemically treated and incubated with phage PP01 (labeled as (0.4-PP01, 0.1-PP01, and 0.05-PP01) the lytic activity, evidenced by the drop inOD_{600}, started at approximately 5 h, around the same time as for sample with non-chemically attached phages (labeled as “No C. A.”). However, OD_{600} values were lower with the latter samples compared to 0.4-PP01, 0.1-PP01, and 0.05-PP01 samples, which could be attributed to the fact that more phages were available to infect the bacteria in the culture.

An important question for the work at hand is whether the phages are chemically bonded to the gold surface, or just weakly physisorbed. To clarify this, it is necessary to look at the OD_{600} values for each set of samples. For the sample comprised of phages in solution (MOI 0.01), it is seen that bacterial infection starts at 3 h, and reached a plateau after 5 h, indicating the end of the infection process. The OD_{600} of the sample labelled No C. A. (the control sample with physisorbed phages) decreases after 5 h, indicating that infection is occurring. The OD_{600} of samples with chemically-attached phages (0.4-PP01, 0.1-PP01, and 0.05-PP01) also began to decrease after 5 h, but at a slower rate, while the absorbance of the samples without phages continued to increase over the duration of the experiment. This shows that for samples without phages, no infection occurs and the bacteria continue to grow unchecked, while for the chemically-attached phages, infection

led to the number of bacteria to decrease. The rate of OD_{600} decrease for samples with chemically-attached phages occurred at a lower rate than the No C. A. curve. This observation could be attributed to the nature of the bonding and the conditions of the experiment: constant agitation from the orbital shaker in the incubator may have led to the detachment of phages that were physisorbed to gold surfaces, leaving them free, increasing the probability to find a host and infect it, whereas for chemically bonded phages, it is probable that a certain percentage were not properly oriented for infection.

Overall, results suggest that phages may be chemically attached to gold surfaces, able to perform bacterial infection even though this is a method that does not control the orientation of the phages. For the immobilization of phages PP01 on the gold wire surface, it was decided that the coupling reaction will be performed on a concentration ratio 0.1 M EDC and 0.1 NHS (1:1 in molarity). Results showed that antibacterial activity was relatively similar with the three selected ratios, especially for the liquid phase evaluation, which was the phase of interest for followed experiments in the fabricated OECT.

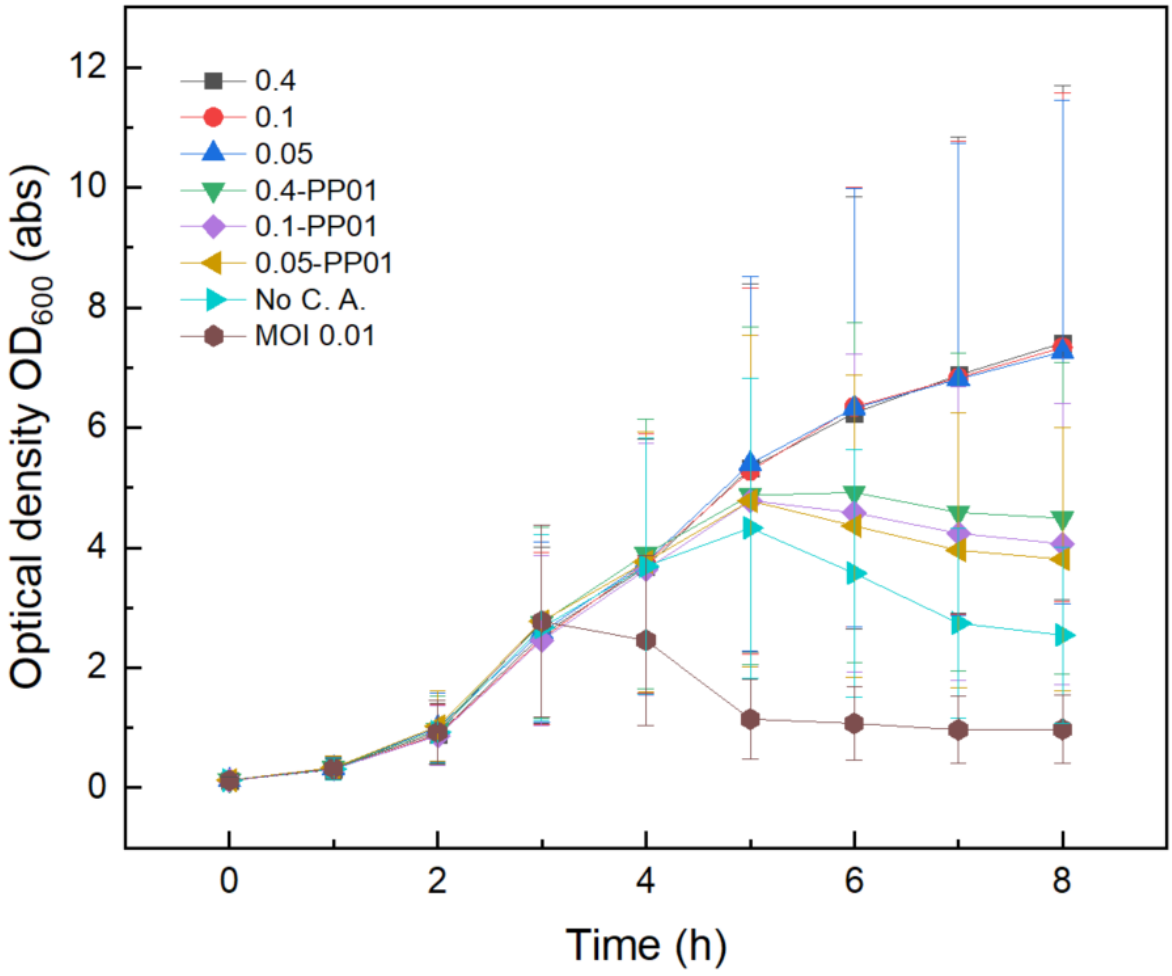

Figure 4.16. Phage activity in E. coli O157:H7 cultures at three different linker ratios. Error bars correspond to standard deviation for the measurements. Legends: 0.4, 0.1, and 0.05 refer to chemically modified gold surfaces; 0.4-PP01, 0.1-PP01, and 0.05-PP01 refer to chemically immobilized PP01 on gold surfaces; No C.A. refers to sample that underwent on phage incubation with no chemical surface modification; and MOI 0.01 refers to the ratio between the phage PP01 titer and *E. coli* O157:H7 concentration.

4.3 Incorporation of phage PP01 and E. coli O157:H7 *to OECT measurements*

Once the OECT, the gate wire and the effect of the phage immobilized on a gold surface were separately studied and characterized, it was necessary to evaluate the performance of these elements altogether in comparison to different controls: (1) medium; (2) medium and phage PP01 free in medium and immobilized on gold wire; (3) medium and *E. coli* O157:H7; and (4) medium and non-target bacteria, *Lactobacillus plantarum*.

To engineer a sensor for bacteria, it was important to consider the environment of analyte (bacteria). For an OECT, the liquid medium is especially important since ions from the medium diffuse into the thin layer and de-dope the PSS side chains, decreasing the overall current of the active channel. To determine the effect of medium on device performance, two media were explored: PBS, a non-nutrient medium and TSB, a nutrient medium. PBS, a buffer commonly used for biological applications, was utilized as medium because of its ability to maintain a constant pH around 7.0 and to stabilize proteins[95]. TSB is a complex medium used for culture growth.

First, the response of the transistor was measured using the bare gold electrode as the gate. Measurements of the blank for the medium at a constant V_D = -0.5 V in a 1-h window, taking measurements every 10 min, were performed. As shown in Figure 4.17.a, throughout the 60 min timeframe the measurements of the blank were stable at a drain bias of -0.5 V. Similar behavior was found when the medium was TSB (Figure 4.17.b). It is important to note that evaluation at time = 0 led to different curves than those collected at other time points, which could be attributed to stabilization of the gate electrode with the electrolyte. Through these measurements it was concluded that the device is stable for both media under the test conditions.

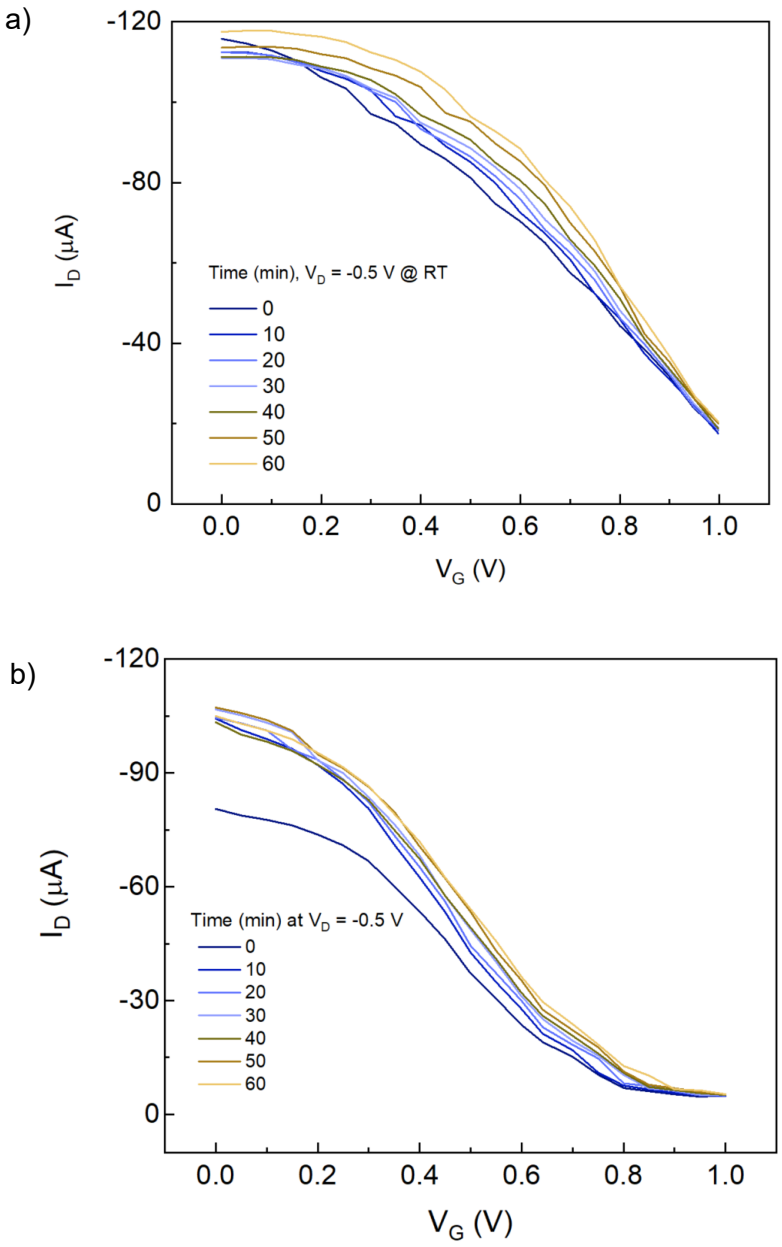

Figure 4.17. Transfer curves for blank gold wires in a) 0.01 M PBS, and B) TSB at V_D= -0.5 V at a step rate of 50 mV. Curves are shown for wires equilibrated in media at different times.

The response of the transistor when in contact with free bacteria *E. coli* and PP01 in PBS were evaluated through V_G-I_D curves on a constant drain potential of V_D= -0.5 V, using a bare gold wire, and testing in a timeframe of 30 min for each experiment. The transfer curves at time = 0 for exposure to either bacteria or phages in PBS (Figures 4.18.a and 4.18.b, respectively) show the lowest drain current (I_D) through the gate positive sweep. Again, after 10, 20 and 30 min the I_D increased compared to time = 0, which could be attributed to stabilization/equilibration of the system. For the curves corresponding to *E. coli* O157:H7 (Figure 4.18.a), it can be seen that after 10 min, all the curves have the same trajectory, whereas for phage PP01 (Figure 4.18.b) the trajectory was most similar at times t = 20 and 30 min. For the case of *E. coli* O157:H7 in TSB (Figure 4.18.c), V_G-I_D curves shows similar trends from 20 min onwards. In general, the V_G-I_D set of curves for all experiments show stability through the selected time frame for exposure to phage and pathogen in separate measurements.

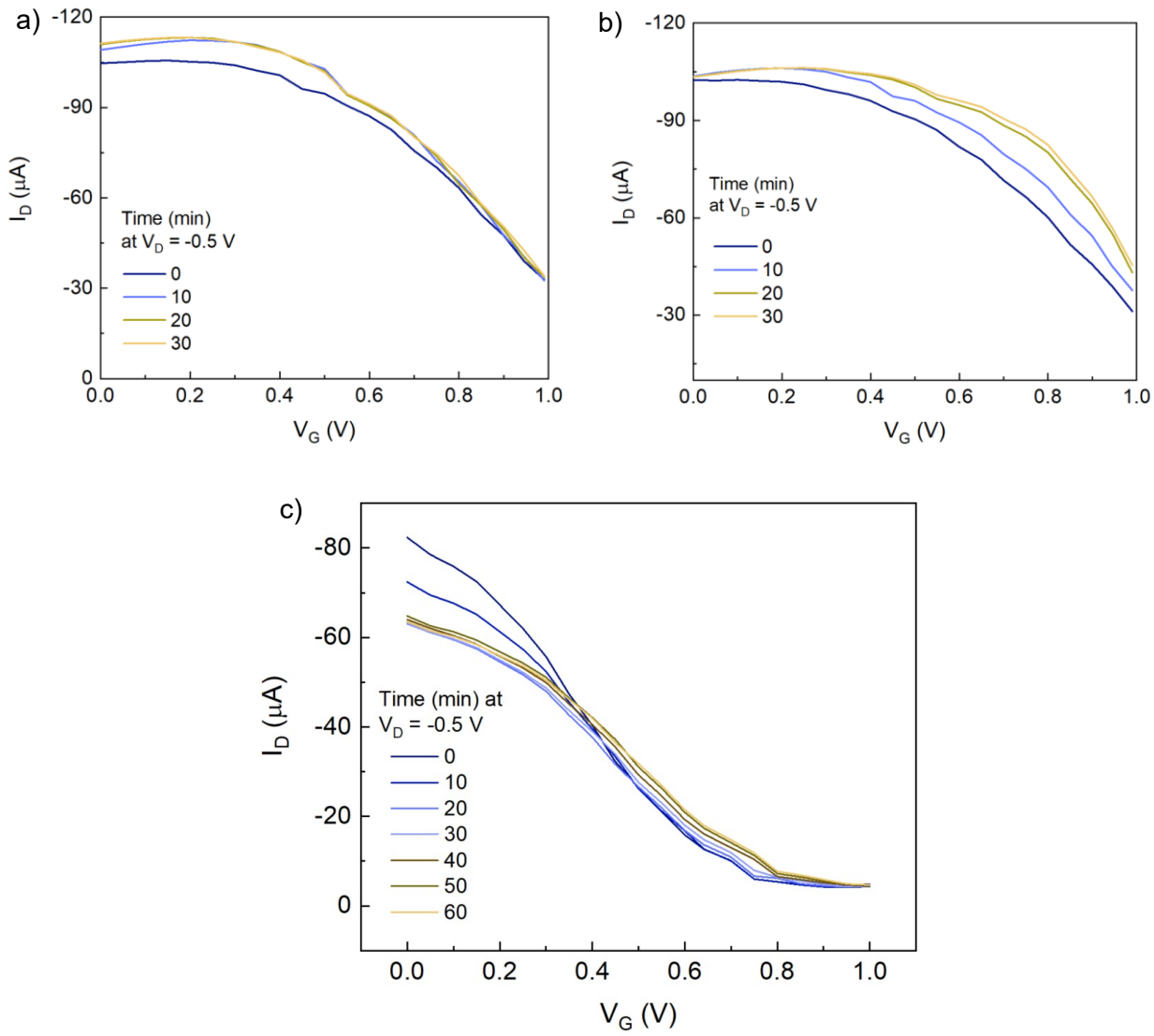

Figure 4.18. Transfer curves with a) *E. coli* O157:H7 at 1x10^8 CFU/mL in 0.01 M PBS; b) phage PP01 1x10^7 PFU/mL in 0.01 M PBS; and c) *E. coli* O157:H7 1x10^8 CFU/mL in TSB. V_D= -0.5 V at a step rate 50 mV.

Further experiments were performed to evaluate the transistor response when in presence of both phage PP01 and *E. coli* O157:H7. For this, aliquots were prepared as followed: 0.25 mL of *E. coli* O157:H7 at 1x10^8 CFU/mL and 0.25 mL PP01 at 1x10^7 PFU/mL (MOI of 0.1) were added into the PDMS well, and measurements were carried

every 10 minutes for 1h under a constant V_D = -0.5 at room temperature. Transfer curves showed no response indicating ionic change as a result of the infection presumably occurring in the medium (Figure 4.19.a) – the I_D had similar values curves of 10 to 60 min. This is surprising since lysis was expected by showing a change in the ionic environment of the electrolyte that would affect the transfer curves, which typically occurs after approximately 20 to 40 min[41].

To explain this lack of response in transfer curves V_G-I_D after 1 h of phage-pathogen exposure, a new test was performed. For this, the temperature was increased to 37 °C to create an environment more favorable to cell growth and phage infection. Two samples were prepared for this experiment: (1) the first one consisted of 1 mL of 0.01 M PBS, 1 mL of *E. coli* O157:H7 at 10^8 CFU/mL suspended in PBS, and 0.3 mL of PP01 at 10^9 PFU/mL suspended in PBS (MOI = 3), and (2) the second sample consisted of a control prepared with 1.3 mL of 0.01 M PBS and 1 mL of *E. coli* O157:H7 at 10^8 CFU/mL suspended in PBS. The final volume was 2.3 mL for both types of samples. The volume of phage added to the solution was 0.3 mL; this relatively large volume was chosen to ensure that lysis would occur rapidly (larger MOI). For sample 1, both I_D and OD_{600} were measured to evaluate the evolution of the interaction in a time frame of 300 min simultaneously, and the control sample (sample 2) was used to compare OD_{600} measurements.

Figure 4.19.b shows a significant instability of the transfer curves when a V_D= -0.5 V is applied. This could be attributed to the fact that, in order to keep the temperature high, it was necessary to keep the PBS containing the phages and bacteria in an incubator, and to transfer them to the transistor for measurements. This procedure likely

affected the measurements of the transistor because of temperature fluctuations, and the system may still have been stabilizing during initial measurements. Moreover, the OD_{600} of the sample (Figure 4.19.c) remained relatively constant and similar to the control without phages, suggesting that no infection was occurring over the time frame of the measurement. This could be due to the absence of nutrients allowing cells to actively grow in PBS, which impedes the lytic cycle[96]. Based on the results of this experiments, it can be concluded that liquid samples tested should remain in the PDMS well to not alter the performance of the test, and that 0.01 M PBS does not offer favorable conditions for the lytic infection to take place; however, the fact that there is not lytic cycle does not rule out the possibility that the phages are able to attach to the bacterial membrane.

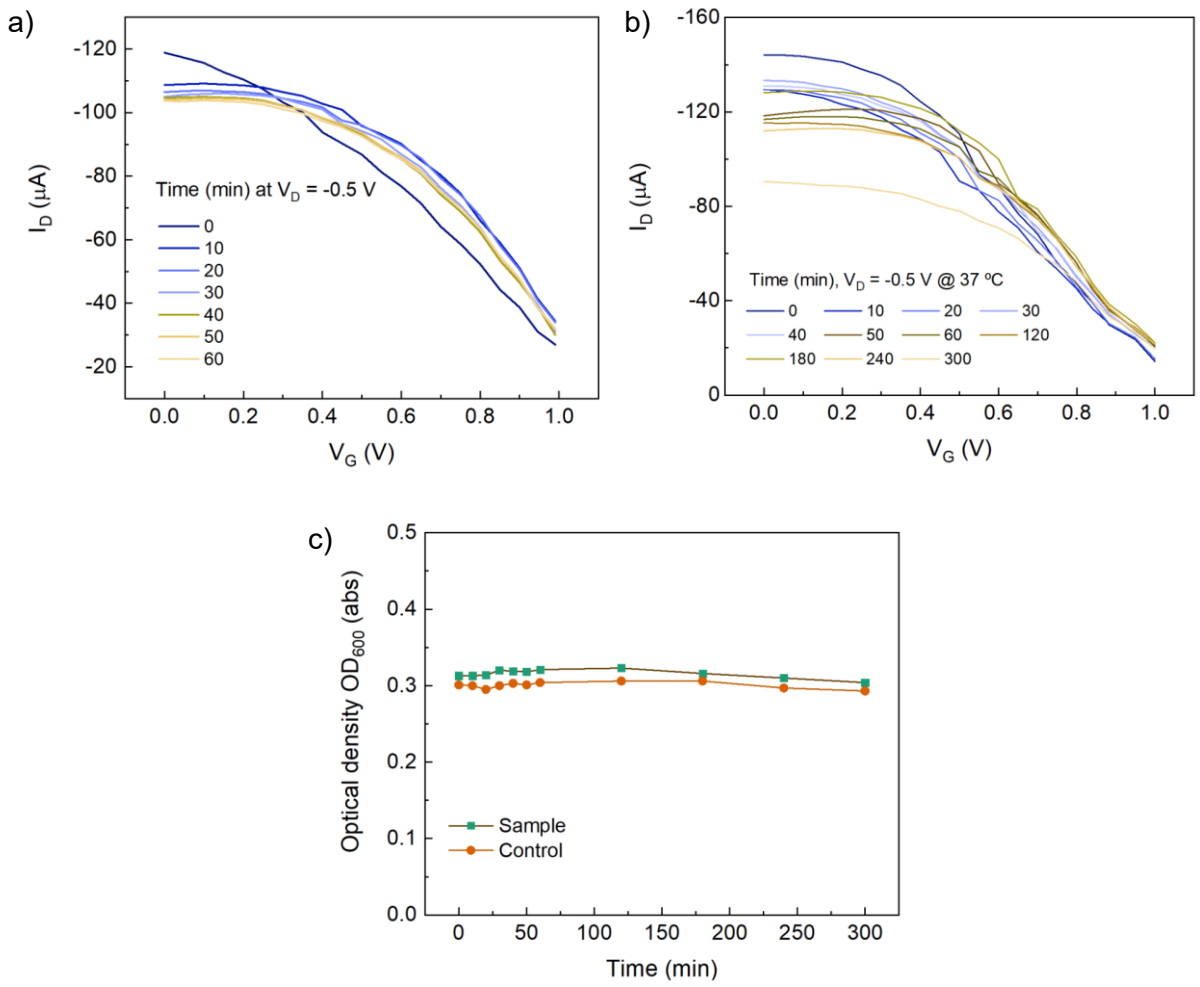

Figure 4.19. Transfer curves for a) bacteria *E. coli* O157:H7 at 1x10^8 CFU/mL and PP01 at 1x10^7 PFU/mL at RT; b) bacteria *E. coli* O157:H7 at 1x10^8 CFU/mL and PP01 at 1x10^9 PFU/mL at 37 °C; and c) Optical density OD_{600} comparison for sample (*E. coli* O157:H7 and PP01) and control (*E. coli* O157:H7). V_D= -0.5 V at a step rate 50 mV in 0.01 M PBS.

The stability of the transistor (as assessed by transfer curves) when using a chemically immobilized gold electrode with phage PP01 was studied by using both PBS and TSB as the electrolyte. Experiments were performed by measuring transfer curves

(V_G-I_D) using a constant potential of V_D= -0.5 V. The curves shown in Figure 4.20.a correspond to the measurements of modified gate electrodes in 0.01 M PBS, and show that drain current was increasing with time; this suggests that phage PP01 were released from the surface of the wire over time, and, due to their charged nature, contributed to the ionic load in the solution; providing charges that could increase the drain current under the same bias in the transfer curves. Another possibility to consider is that detachment of phage PP01 decreased the surface coverage, decreasing as well the charge-transfer resistance of the gold wire. On the contrary, when similar experiments were run using TSB as the medium (Figure 4.20.b), the drain current curves remained fairly constant from t= 0 to 60 min. As the only difference between these experiments was the medium, these results suggest that the current increment in PBS was likely caused by the release of phages that were weakly adsorbed on the electrode's surface, and the ionic strength of TSB was sufficiently to not show these variations over time. This suggestion was further confirmed by doing a plaque assay of liquid samples measured in TSB after the experiment, where it is seen that phages were present in the media (Figure 4.20.c). At the same time, this demonstrated that at least some phages in the media after 1h of experiment possibly were not damaged by the constant voltage applied, which is shown their ability to infect and form plaques in the agar.

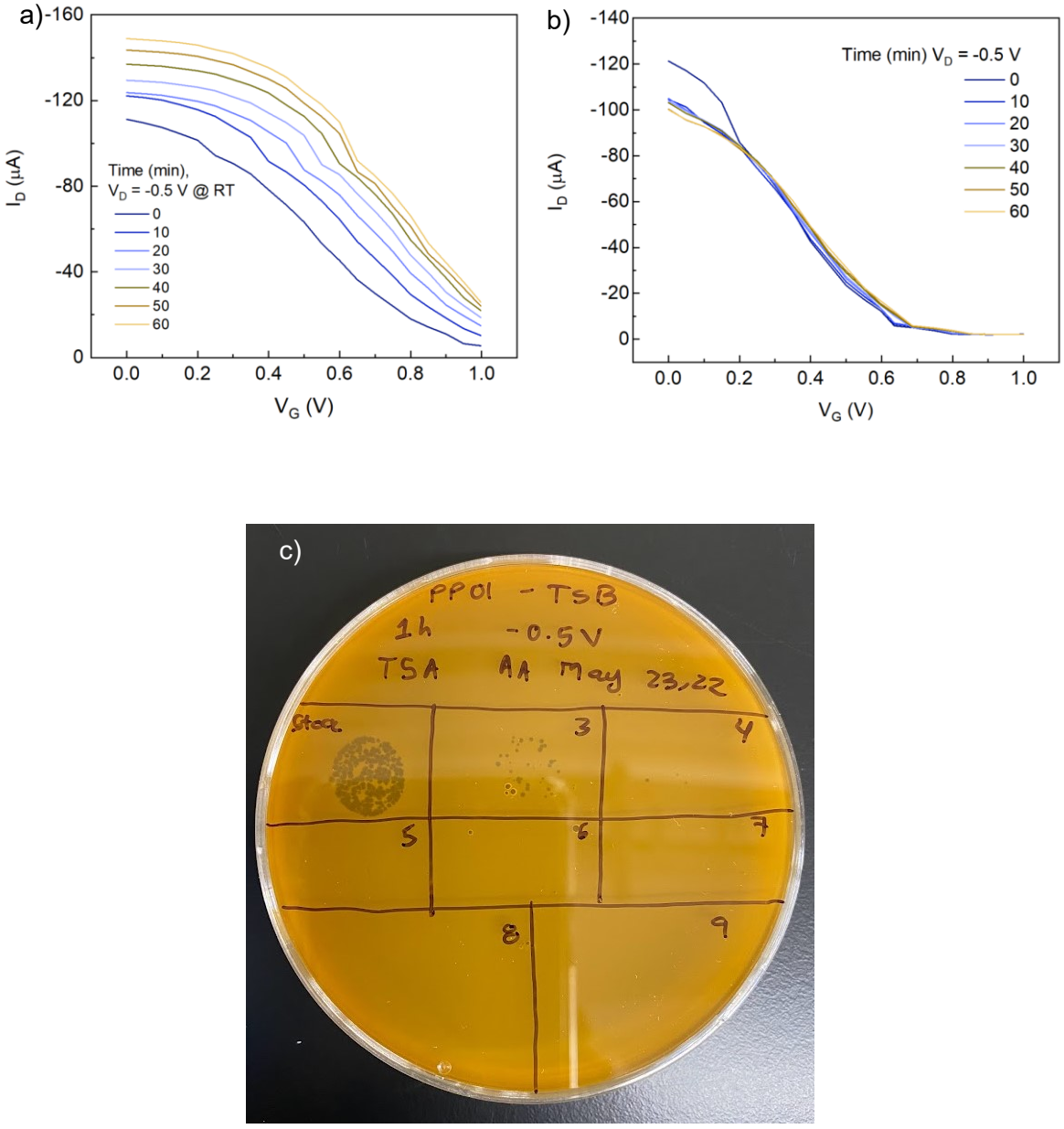

Figure 4.20. Transfer curves using immobilized PP01 on gold wire in a) 0.01 PBS medium, and b) TSB medium; c) plaque assay of TSB sample after 1 h experiments.

The response of the transistor in the presence of *E. coli* O157:H7 when using a gold electrode with chemically immobilized phage PP01 for targeted detection was studied. Experiments were performed by measuring transfer curves (V_G-I_D) using a constant potential of V_D= -0.5 V in both PBS and TSB media. Experiments were performed with *E. coli* O157:H7 (the target bacterium) and *Lactobacillus plantarum* (a non-target bacterium) at a concentration of 10^8 CFU/mL. Results are shown in Figure 4.21. When using 0.01 M PBS as the medium, transfer curves showed that after 20 min all curves were recorded at relatively the same I_D (Figure 4.21.a), which suggests that phages in fact were attaching the bacteria without cell lysis happening during the timeframe of the experiment. Meanwhile, when using TSB as the electrolyte (Figure 4.21.b), there was a reduction of the drain current in the set of transfer curves which could be attributed to the interaction of phage PP01, both attached and detached from the gold wire, with *E. coli* O157:H7; the process between these two biological entities requires an infection where the tail of the phage will be inserted into the bacterial membrane. Since the bacteria is anchored to the electrode through the bioreceptor, it is probable that the electron-transfer resistance of the electrode would increase, leading to a decrease in the recorded drain current over time[74]. Another factor that may have influenced the decrease of current in OECTs is the decreasing amount of bacteria during cellular lysis. Butina *et al.* showed that I_D changes over time corresponded to bacterial growth (*S. Enteritidis* 3934 and the isogenic mutant Δ*csgD*) when compared to I_D results when M9 minimal medium was measured with no inoculated bacteria[75,97]. Here, the curves shifted upwards from 0 to 30 min as the device stabilized. It can be seen that at 40 min there was a sudden increase of the current, which suggests that these changes could have occurred as a

result of lysis. Through this experimental setup, it is not possible to conclude which interaction is happening at the experimental point, but if compared to Figure 4.20.b, it can be seen that the OECT can recognize that an interaction is indeed taking place.

As a control *L. plantarum* was added to PBS along with phages. The phages should not be able to infect or attach to this bacterium. Indeed, there was no significant change in the drain current when PBS was used as the medium (Figure 4.21.c), but this result was not conclusive since the same effect was shown for *E. coli* O157:H7. However, performance in TSB confirmed that phage PP01 is selective and only attaches to *E. coli* O157:H7, as shown in Figure 4.21.d. In fact, unlike for *E. coli*, no significant change of current was observed for the set of curves with *L. plantarum*. This demonstrates that the I_D changed due to the targeted interaction between the bacteria and phages in *E. coli* experiments. From these experiments it is concluded that phage PP01 can selectively attach to this bacterium when TSB is used as the media, but nutrients are necessary to reach lysis that would show a change in current in the V_G-I_D set of curves. Thus, this device can potentially be used to detect the presence of *E. coli* O157:H7 in liquid samples. Further studies are required to verify the reproducibility, selectivity and sensitivity of the transistor, but it is believed that this project acts as a starting point for the development of a new biosensor.

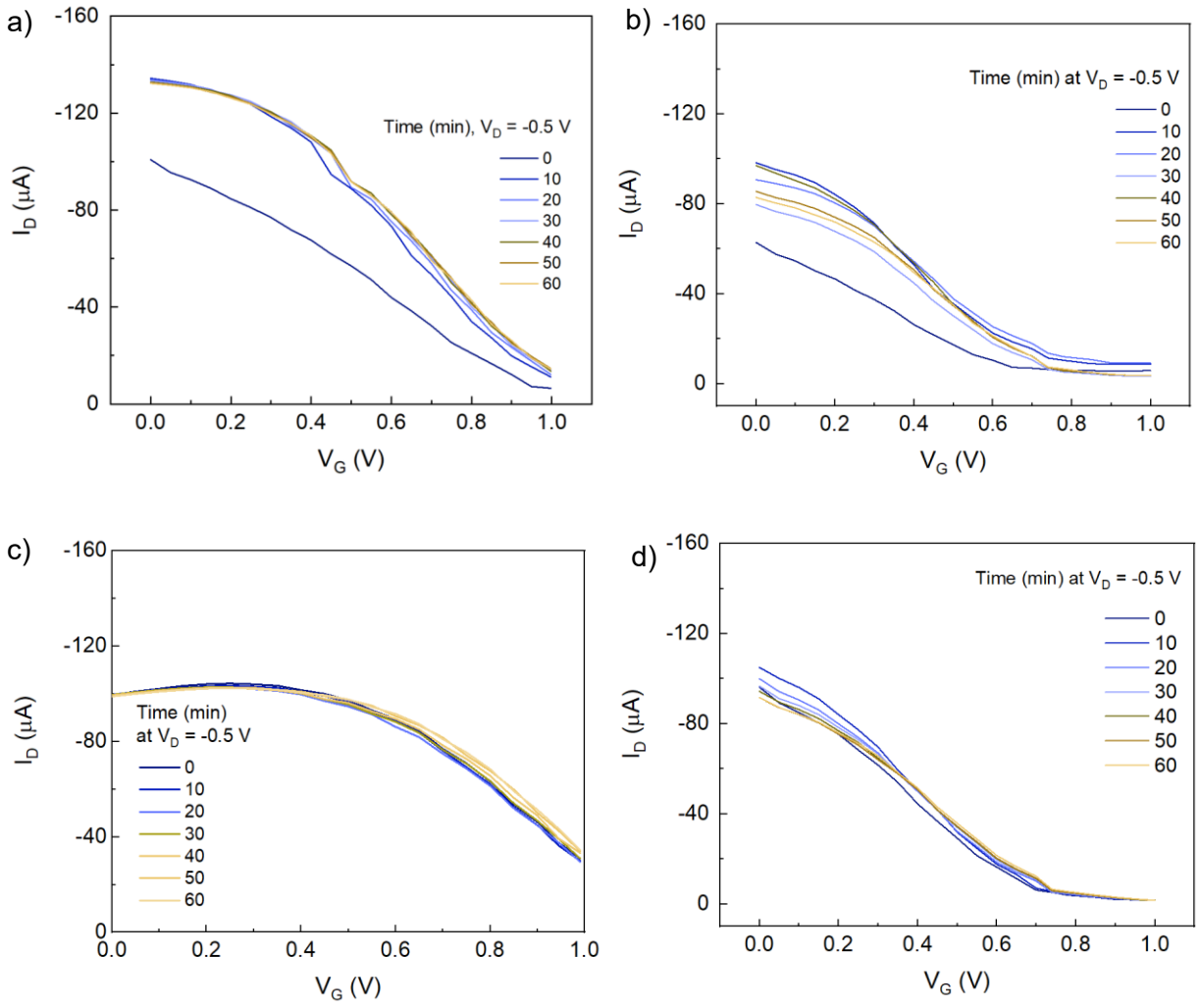

Figure 4.21. Transfer curves using immobilized PP01 on gold wire for *E. coli* O157:H7 10^8 CFU/mL in a) 0.01 M PBS and b) TSB media. Curves for *L. plantarum* 10^8 CFU/mL evaluation are shown in transfer curves using c) 0.01 PBS + PP01 in media using a bare gold wire; and d) TSB as the media using the chemically modified electrode with PP01.

5. Conclusions

5.1 Summary

In this report, results regarding the fabrication of an organic electrochemical transistor and its potential application in the detection of bacterial pathogens in liquid samples were presented. A pre-patterned ITO substrate with interdigitated fingers for source-drain electrode pairs was used as the substrate. The best performance for the active channel for this device was observed when using an ink prepared with PEDOT:PSS PH1000, IPA, and GOPS with dimensions of 180 nm thickness x 4.6 mm length x 1.0 mm width. As expected, the transistor operated in depletion mode where cations from the electrolyte are injected into the thin film, de-doping the PEDOT:PSS structure and decreasing the drain current registered for the device. In this study, two electrolyte solutions were tested: PBS and TSB. Results showed that the load of positively charged ions and molecules found in TSB were enough to bring the transistor into the OFF state at a V_G = 1.0 V with a registered I_D = -1.05 µA. TSB contains ionic species (sodium chloride and dipotassium phosphate), as well as carbon and nitrogen sources for the bacterium *E. coli* O157:H7 to grow. In PBS it was not possible to detect phage-pathogen interactions; however when TSB was used as the electrolyte solution, the transfer curves (V_G-I_D) showed a change in drain current during the evaluation period with the modified gold gate electrode with immobilized PP01. Meanwhile no changes were seen when the OECT with immobilized phages was used to assess a sample containing the non-target bacterium *L. plantarum*, showing that the device is selective to the bacteria of interest.

5.2 Strengths and weaknesses

The devices that exhibited the best performance were made with the PEDOT:PSS PH1000/ IPA/ GOPS ink; even though the sheet conductivity of this ink is 2-fold lower than that of samples with glycerol and DBSA. As well, it is important to highlight that the width and length of the active channel are in the order of millimeters, which is larger than for examples of transistors in literature. However, this can also be an important factor in the quality of output and transfer curves and the observation that the OECT did not reach a common OFF state as expected. More studies are need to redefine the channel dimensions.

With regards to the modification of the gate electrode, it was shown that the MUA/EDC/NHS method potentially works for the chemical attachment of phage PP01 to the surface; further studies are needed to fully confirm this immobilization. However, this method did not avoid the fact that phages can be also physisorbed – physisorbed phages can be released from the surface with time as shown through plaque assay. This leads to questioning whether the recorded change in the transfer curves was due to the interaction with phages attached to the gold surface as required or with phages released to the medium. Nevertheless, results show, in general, that a biological interaction can be sensed in this transistor when a bacterial concentration of 10^8 CFU/mL is present in TSB.

5.3 Applicability and future work

The present work can be a starting point for new OECTs where the bio-receptor, located in the gate electrode (and not on the active channel), can let the transistor be reused for bacterial detection, since the bacteria is not attached to the thin film surface.

However, a methodology must be proposed for surface cleaning and re-immobilization of phages on the gold wire. Also, channel dimensions in the order of the millimeters may represent an advantage for the potential fabrication of PEDOT:PSS-based transistors in the far future.

This project has several areas that can be improved. One of the future recommendations is the evaluation of the volumetric capacitance for the transdoconductance calculation, which is considered a figure of merit for these devices. Through this evaluation, this device can be fully compared with others in literature, and the results should enable the identification of other areas of improvement for the ink and thin film dimensions. Also, another path of exploration is the relationship between gate electrode and thin film, testing different wire diameters and the role that the gate electrode plays for both output and transfer curves.

As for the characterization of the modified gold electrode, even though it was confirmed that phages were immobilized on the gold surface, it may be beneficial to image the gold wire and the representative samples to calculate the phage density over a specific area through this attachment method.

In terms of bacterial evaluation, the device was only studied for high cell concentrations (10^8 CFU/mL). It is suggested to repeat the performed experiments to understand the interaction happening on the gate electrode as a function of time, as well as its performance in presence of lower concentrations, and determine the limit of detection of the device.

In conclusion, this work has shown a potential application for *E. coli* O157:H7 detection in complex media when phage PP01 is used as the bioreceptor in an OECT

sensing platform. It is expected that this work brings a new perspective for a new generation of transistors where phages play an important role to selectively detect pathogens in a fast response, easy-to-use and with relatively easy fabrication methodology.

References

(1) Moghtader, F.; Congur, G.; Zareie, H. M.; Erdem, A.; Piskin, E. Impedimetric Detection of Pathogenic Bacteria with Bacteriophages Using Gold Nanorod Deposited Graphite Electrodes. *RSC Advances* **2016**, *6*, 97832.

(2) Development, O. of R. &. *Standard Analytical Protocol for Escherichia coli O157:H7 in Water*. https://cfpub.epa.gov/si/si_public_record_report.cfm?Lab=NHSRC&address=nhsrc/&dirEntryId=224124 (accessed 2021-06-01).

(3) Essendoubi, S.; Stashko, N.; So, I.; Gensler, G.; Rolheiser, D.; Mainali, C. Prevalence of Shiga Toxin-Producing Escherichia Coli (STEC) O157:H7, Six Non-O157 STECs, and Salmonella on Beef Carcasses in Provicionally Licensed Abattoirs in Alberta, Canada. *Food Control* **2019**, *105*, 226–232.

(4) Wiwanitkit, V. The Type of E. Coli. In *Escherichia Coli Infections*; Internet Medical Publishing: United States, 2011; pp 8–10.

(5) *CDC | E. coli Outbreak From Fresh Spinach | CDC Foodborne and Diarrheal Diseases Branch*. https://www.cdc.gov/ecoli/2006/spinach-10-2006.html (accessed 2021-06-01).

(6) Ch. Bindu Kiranmayi; Krishnaiah, N.; Mallika, E. N. Escherichia Coli O157:H7 - An Emerging Pathogen in Food of Animal Origin. *Veterinary World 3* (8), 382–389.

(7) News ·, C. B. C. *Inside Walkerton: Canada's worst-ever E. coli contamination | CBC News*. CBC. https://www.cbc.ca/news/canada/inside-walkerton-canada-s-worst-ever-e-coli-contamination-1.887200 (accessed 2021-06-01).

(8) Acharya, M.; Kalischuk, R. G.; Klein, K. K.; Bjornlund, H. Farmstead Drinking Water Sources, Concerns and Safety Practices of Livestock Farm Families in Southern

Alberta, Canada. *WIT Transactions on Ecology and the Environment* **2008**, *111*, 627–636.

(9) Gannon, V. P. J.; Graham, T. A.; Read, S.; Ziebell, K.; Muckle, A.; Mori, J.; Thomas, J.; Selinger, B.; Townshend, I.; Byrne, J. Bacterial Pathogens in Rural Water Supplies In Southern Alberta, Canada. *Journal of Toxicology and Environmental Health, Part A* **2004**, *67*, 1643–1653.

(10) Yao, L.; Lamarche, P.; Tawil, N.; Khan, R.; Aliakbar, A. M.; Hassan, M. H.; Chodavarapu, V. P.; Mandeville, R. CMOS Conductrimetric System for Growth Monitoring and Sensing of Bacteria. *IEEE Transactions on Biomedical Circuits and Systems* **2011**, *5* (3), 223–230.

(11) Decataldo, F.; Grumiro, L.; Marino, M. M.; Faccin, F.; Giovannini, C.; Brandolini, M.; Dirani, G.; Taddei, F.; Lelli, D.; Tessarolo, M.; Calienni, M.; Cacciotto, C.; Lavazza, A.; Fraboni, B.; Scagliarini, A.; Sambri, V. Fast and Real-Time Electrical Transistor Assay for Quantifying SARS-CoV-2 Neutralizing Antibodies. *Communication Materials* **2022**, *3*, 5.

(12) *Definition of depletion mode*. PCMAG. https://www.pcmag.com/encyclopedia/term/depletion-mode (accessed 2022-07-12).

(13) Janardhanan, J. A.; Chen, Y.-L.; Liu, C.-T.; Tseng, H.-S.; Wu, P.-I.; She, J.-W.; Hsiao, Y.-S.; Yu, H. Sensitive Detection of Sweat Cortisol Using an Organic Electrochemical Transistor Featuring Nanostructured Poly(3,4-Ethylenedioxythiophene) Derivates in the Channel Layer. *Analytical Chemistry* **2022**, *94*, 7584–7593.

(14) *Biological Recognition Element - an overview | ScienceDirect Topics*. https://www.sciencedirect.com/topics/engineering/biological-recognition-element (accessed 2022-07-12).

(15) Abdullah Lim, S.; Uddin Ahmed, M. Introduction to Food Biosensors. In *Food Biosensors*; Food Chemistry, Function and Analysis; Royal Society of Chemistry, 2016; pp 1–21.

(16) *bacteriophage / phage | Learn Science at Scitable*. https://www.nature.com/scitable/definition/bacteriophage-phage-293/ (accessed 2022-07-12).

(17) Zhang, L.; Wang, G.; Wu, D.; Xiong, C.; Zheng, L.; Ding, Y.; Lu, H.; Zhang, G.; Qiu, L. Highly Selective and Sensitive Sensor Based on an Organic Electrochemical Transistor for the Detection of Ascorbic Acid. *Biosensors and Bioelectronics* **2018**, *100*, 235–241.

(18) Pourakbari, R.; Yousefi, M.; Khalilzadeh, B.; Irani-nezhad, M. H.; Khataee, A.; Aghebati-Maleki, L.; Soleimanian, A.; Kamrani, A.; Chakari-Khiavi, F.; Abolhasan, R.; Motallebnezhad, M.; Jadidi-Niaragh, F.; Yousefi, B.; Kafil, H. S.; Hojjat-Farsangi, M.; Rashidi, M.-R. Early Stage Evaluation of Colon Cancer Using Tungsten Disulfide Quantum Dots and Bacteriophage Nano-Composite as an Efficient Electrochemical Platfom. *Cancer Nanotechnology* **2022**, *13* (1), 7.

(19) Canada, H. *Guidelines for Canadian Drinking Water Quality: Guideline Technical Document – Escherichia coli*. https://www.canada.ca/en/health-canada/services/publications/healthy-living/guidelines-canadian-drinking-water-quality-guideline-technical-document-escherichia-coli.html (accessed 2021-06-01).

(20) Eccoña Sota, A.; Cap, M.; Rodriguez, A.; Szerman, N.; Speroni, F.; Vaudagna, S. R. Effects of High Hydrostatic Pressure and Beef Patty Formulations on the Inactivation of Native Strains of Shiga Toxin-Producing Escherichia Coli O157:H7. *Food and Bioprocess Technology* **2021**, *14*, 1194–1198.

(21) | *E. coli* | *CDC*. https://www.cdc.gov/ecoli/general/index.html (accessed 2021-06-01).

(22) Olsen, S. J.; Miller, G.; Breuer, T.; Kennedy, M.; Higgins, C.; Walford, J.; McKee, G.; Fox, K.; Bibb, W.; Mead, P. A Waterborne Outbreak of Escherichia Coli O157:H7 Infections and Hemolytic Uremic Syndrome: Implications for Rural Water Systems. *Emerg Infect Dis* **2002**, *8* (4), 370–375. https://doi.org/10.3201/eid0804.000218.

(23) Naught, M. D.; Wilkinson, A. *IUPAC. Compendium of Chemical Terminology*, 2nd ed.; Oxford, 1997.

(24) Rana, J. S.; Jindal, J.; Beniwal, V.; Chhokar, V. Utility Biosensors for Applications in Agriculture - A Review. *Journal of American Science* **2010**, *6* (9), 353–375.

(25) Anik, U. Electrochemical Medical Biosensors for POC Applications. In *Medical biosensors for point of care (POC) applications*; Woodhead Publishing, 2016; pp 275–276.

(26) Luka, G.; Ahmadi, A.; Najjaran, H.; Alocilja, E.; DeRosa, M.; Wolthers, K.; Malki, A.; Aziz, H.; Althani, A.; Hoorfar, M. Microfluidics Integrated Biosensors: A Leading Technology Towards Lab-on-a-Chip and Sensing Applications. *Sensors* **2015**, *15*, 30011–30031.

(27) Lin, M.-H.; Gupta, S.; Chang, C.; Lee, C.-Y.; Tai, N.-H. Carbon Nanotubes/Polyethylenimine/Glucose Oxidase as a Non-Invasive Electrochemical Biosensor Performs High Sensitivity for Detecting Glucose in Saliva. *Microchemical Journal* **2022**, *180*, 107547.

(28) *Enzyme*. Genome.gov. https://www.genome.gov/genetics-glossary/Enzyme (accessed 2022-07-12).

(29) Liang, Y.; Wu, C.; Figueroa-Miranda, G.; Offenhausser, A.; Mayer, D. Amplification of Aptamer Sensor Signals by Four Orders of Magnitude via Interdigitated Organic Electrochemical Transistors. *Biosensors and Bioelectronics* **2019**, *144*, 111668.

(30) Hao, X.; Yeh, P.; Qin, Y.; Jiang, Y.; Qiu, Z.; Li, S.; Le, T.; Cao, X. Aptamer Surface Functionalization of Microfluidic Devices Using Dendrimers as Multi-Handled Templates and Its Application in Sensitive Detections of Foodborne Pathogenic Bacteria. *Analytica Chimica Acta* **2019**, *1056*, 96–107.

(31) Gervais, L.; Gel, M.; Allain, B.; Tolba, M.; Brovko, L.; Zourob, M.; Mandeville, R.; Griffiths, M.; Evoy, S. Immobilization of Biotinylated Bacteriophages on Biosensor Surfaces. *Sensors and Actuators B* **2007**, *125*, 615–621.

(32) Wang, H.; Zhao, Y.; Bie, S.; Suo, T.; Jia, G.; Liu, B.; Ye, R.; Li, Z. Development of an Electrochemical Biosensor for Rapid and Effective Detection of Pathogenic Escherichia Coli in Licorice Extract. *Appl. Sci.* **2019**, *9*, 925.

(33) Bhalla, N.; Jolly, P.; Estrela, P. Introduction to Biosensors. *Essays Biochem* **2016**, *60* (1), 1–8.

(34) Razmi, N.; Hasanzadeh, M.; Willander, M.; Nur, O. Recent Progress on the Electrochemical Biosensing of Escherichia Coli O157:H7: Materials and Methods Overview. *Biosensors* **2020**, *10* (5), 54.

(35) Harper, D. R.; Abedon, S. T.; Burrowes, B. H.; Mc Conville, M. L. Introduction to Bacteriophages. In *Bacteriophages*; Springer Nature: Switzerland, 2021; pp 3–16.

(36) Bertozzi Silva, J.; Storm, Z.; Sauvageau, D. Host Receptors for Bacteriophage Adsorption. *FEMS Microbiology Letters* **2016**, *363*, fnw002.

(37) Kurtboke, I. *Bacteriophages*; InTech, 2012.

(38) Doekes, H. M.; Mulder, G. A.; Hermsen, R. Repeated Outbreaks Drive the Evolution of Bacteriophage Communication. *eLife* **2021**. https://doi.org/10.7554/eLife.58410.

(39) Ripp, S. Whole Cell Sensing System II. In *Advances in Biochemical Engineering/Biotechnology*; Springer, 2009; pp 66–67.

(40) Richter, L.; Janczuk-Richter, M.; Niedziolka-Jonsson, J.; Paczesny, J.; Holyst, R. Recent Advances in Bacteriophage-Based Methods for Bacteria Detection. *Drug Discovery Today 23* (2), 448–455.

(41) Zhou, Y.; Marar, A.; Kner, P.; Ramasamy, R. P. Charge-Directed Immobilization of Bacteriophage on Nanostructured Electrode for Whole-Cell Electrochemical Biosensors. *Analytical Chemistry 89*, 5734–5741.

(42) Bone, S.; Alum, A.; Markovski, J.; Hristovski, K.; Bar-Zeev, E.; Kaufman, Y.; Abbaszadegan, M.; Perreault, F. Physisorption and Chemisorption of T4 Bacteriophages on Amino Functionalized Silica Particles. *Journal of Colloid and Interface Science* **2018**, *532*, 68–76.

(43) Yorganci, E.; Akyilmaz, E. Alkaline Phosphatase Based Amperometric Biosensor Immobilized by Cysteamine-Glutaraldehyde Modified Self-Assembled Monolayer. *Artificial Cells, Blood Substitutes, and Biotechnology* **2011**, *39* (5), 317–323.

(44) Singh, A.; Glass, N.; Tolba, M.; Brovko, L.; Griffiths, M.; Evoy, S. Immobilization of Bacteriophages on Gold Surfaces for the Specific Capture of Pathogens. *Biosensors and Bioelectronics* **2009**, *24*, 3645–3651.

(45) Stettner, J.; Frank, P.; Griesser, T.; Trimmel, G.; Schennan, R.; Gilli, E.; Winkler, A. A Study on the Formation and Thermal Stability of 11-MUA SAMs on Au(111)/Mica and on Polycrystalline Gold Foils. *Langmuir* **2009**, *25*, 1427–1433.

(46) Tawil, N.; Sacher, E.; Mandeville, R.; Meunier, M. Strategies for the Immobilization of Bacteriophages on Gold Surfaces Monitored by Surface Plasmon Resonance and Surface Morphology. *The Journal of Physical Chemistry C* **2013**, *117*, 6686–6691.

(47) Tsai, T.-C.; Liu, C.-W.; Wu, Y.-C.; Ondevilla, N. A. P.; Osawa, M.; Chang, H.-C. In Situ Study of EDC/NHS Immobilization on Gold Surface Based on Attenuated Total Reflection Surface Enhanced Infrared Absorption Spectroscopy (ATR-SEIRAS). *Colloids and Surfaces B: Biointerfaces* **2019**, *175*, 300–305.

(48) *Blood Glucose Meters*. https://www.maximintegrated.com/en/design/technical-documents/tutorials/4/4659.html (accessed 2022-07-20).

(49) Ling, P.; Yan, F.; Yu, J.; Chan, H. L. W.; Yang, M. The Application of Organic Electrochemical Transistors in Cell-Based Biosensors. *Adv. Mater.* **2010**, *22*, 3655–3660.

(50) Romele, P.; Gkoupidenis, P.; Koutsouras, D. A.; Lieberth, K.; Kovacs-Vajna, Z. M.; Blom, P. W. M.; Torricelli, F. Multiscale Real Time and High Sensitivity Ion Detection with Complementary Organic Electrochemical Transistors Amplifier. *Nature Communications* **2020**, *11*, 3743.

(51) Zhou, Y.; Han, S.-T.; Roy, V. A. L. Nanocomposite Dieletric Materials for Organic Flexible Electronics. In *Nanocrystalline Materials: Their Synthesis-Structure-Property Relationship and Applications*; Elsevier: Hong Kong, 2014; pp 195–197.

(52) Kaushik, B. K.; Kumar, B.; Prajapati, S.; Mittal, P. *Organic Thin-Film Transistor Applications: Materials to Circuits*; Taylor & Francis, CRC Press: United States, 2017.

(53) Mabeck, J. T.; Malliaras, G. G. Chemical and Biological Sensors Based on Organic Thin-Film Transistors. *Anal. Bioanal. Chem* **2006**, *384*, 343–353.

(54) Liao, C.; Yan, F. Organic Semiconductors in Organic-Thin Film Transistor-Based Chemical and Biological Sensors. *Polymer Reviews* **2013**, *53* (3), 352–406.

(55) Lin, P.; Yan, F.; Yu, J. J.; Chan, H. L. W.; Yang, M. The Application of Organic Electrochemical Transistors in Cell-Based Biosensors. *Adv. Mater.* **2010**, *22*, 3655–3660.

(56) Yan, F.; Mok, S. M.; Yu, J.; Chan, H. L. W.; Yang, M. Label-Free DNA Sensor Based on Organic Thim Film Transistors. *Biosensors and Bioelectronics* **2009**, *24*, 1241–1245.

(57) Rivnay, J.; Inal, S.; Salleo, A. Organic Electrochemical Transistors. *Nature Review Materials* **2018**, *3*, 17086.

(58) White, H. S.; Kittlesen, G. P.; Wrighton, M. S. Chemical Derivatization of an Array of Three Gold Microelectrodes with Polypyrrole: Fabrication of a Molecule-Based Transistor. *J. Am. Chem. Soc.* **1984**, *106*, 5375–5377.

(59) Shen, H.; Abtani, A.; Lussem, B.; Boudouris, B. W.; Mei, J. Device Engineering in Organic Electrochemical Transistors toward Multifunctional Applications. *ACS Appl. Electron. Mater.* **2021**, *3* (6), 2434–2448.

(60) Kim, Y.; Lim, T.; Kim, C.-H.; Yeo, C. S.; Seo, K.; Kim, S.-M.; Kim, J.; Park, S. Y.; Ju, S.; Yoon, M.-H. Organic Electrochemical Transistor-Based Channel Dimension-Independent Single-Strand Wearable Sweat Sensors. *NPG Asia Materials* **2018**, *10*, 1086–1095.

(61) Bai, L.; García Elósegui, C.; Li, W.; Yu, P.; Fei, J.; Mao, L. Biological Applications of Organic Electrochemical Transistors: Electrochemical Biosensors and Electrophysiology Recording. *Frontiers in Chemistry* **2019**, *7*, 313.

(62) Coppede, N.; Villani, M.; Gentile, F. Diffusion Driven Selectivity in Organic Electrochemical Transistors. *Scientific Reports* **2014**, *4*, 4297.

(63) Donahue, M. J.; Proctor, C. M.; Strakosas, X. Polymers/PEDOT Derivates for Bioelectronics. In *Redox Polymers for Energy and Nanomedicine*; Royal Society of Chemistry, 2020; pp 488–545.

(64) Tong, C. Semiconducting Materials for Printed Flexible Electronics. In *Advanced Materials for Printed Flexible Electronics*; Springer, Cham, 2021; Vol. 317, pp 159–220.

(65) Mcbride, J. W.; Lam, L. A Review of Conducting Polymers in Electrical Contact Applications. **1970**.

(66) Sanchez-Sanchez, A.; del Agua, I.; Malliaras, G. G.; Mecerreyes, D. Conductive Poly(3,4-Ethylenedioxythiophene)(PEDOT)-Based Polymers and Their Applications in Bioelectronics. In *Smart Polymers and their Applications*; Woodhead Publishing in Materials, 2019; pp 191–218.

(67) Kim, S.-M.; Kim, C.-H.; Kim, Y.; Kim, N.; Lee, W.-J.; Lee, E.-H.; Kim, D.; Park, S.; Lee, K.; Rivnay, J.; Yoon, M.-H. Influence of PEDOT:PSS Crystallinity and Composition on Electrochemical Transistor Performance and Long-Term Stability. *Nature Communications* **2018**, *9*, 3858.

(68) Inal, S.; Rivnay, J.; Suiu, A.-O.; Malliaras, G. G.; McCulloch, I. Conjugated Polymers in Bioelectronics. *Accounts of Chemical Research* **2018**, *51*, 1368–1376.

(69) Stritesky, S.; Markova, A.; Vitecek, J.; Safarikova, E.; Hrabal, M.; Kubac, L.; Kubala, L.; Weiter, M.; Vala, M. Printing Inks of Electroactive Polymer PEDOT:PSS: The Study of Biocompatibility, Stability, and Electrical Properties. *J Biomed Mater Res Part A* **2018**, *106A*, 1121–1128.

(70) *PEDOT:PSS | PH1000, AI4083, HTL Solar & HTL Solar 3, F HC Solar*. Ossila. https://www.ossila.com/products/pedot-pss (accessed 2022-02-22).

(71) El-Moghazy, A.; Wisuthiphaet, N.; Yang, X.; Sun, G.; Nitin, N. Electrochemical Biosensor Based on Genetically Engineered Bacteriophage T7 for Rapid Detection of Escherichia Coli on Fresh Produce. *Food Control* **2022**, *135*, 108811.

(72) Ashiani, D.; Keihan, A. H.; Rashidiani, J.; Dashtestani, F.; Eskandari, K. Oriented T4 Bacteriophage Immobilization for Recognition of Escherichia Coli in Capacitance Method. *International Journal of Electrochemical Science 11*, 10087–10095.

(73) Zhu, Z. T.; Mabeck, J. T.; Zhu, C. C.; Cady, N. C.; Batt, C. A.; Malliaras, G. G. A Simple Poly(3,4- Ethylene Dioxythiophene)/Poly(Styrene Sulfonic Acid) Transistor for Glucose Sensing at Neutral PH. *Chem. Commun* **2004**, 1556–1557.

(74) Demuru, S.; Marette, A.; Kooli, W.; Junier, P.; Briand, D. Flexible Organic Electrochemical Transistor with Functionalizaed Inkjet-Printed Gold Gate for Bacteria Sensing; 2019; pp 2519–2522.

(75) He, R.-X.; Zhang, M.; Tan, F.; Leung, P. H. M.; Zhao, X.-Z.; Chan, H. L. W.; Yang, M.; Yan, F. Detection of Bacteria with Organic Electrochemical Transistors. *Journal of Materials Chemistry* **2012**, *22*, 22072.

(76) *ITO Glass Substrates, 20 x 15 mm, OFET and Sensing*. Ossila. https://www.ossila.com/en-ca/products/interdigitated-ito-ofet-substrates (accessed 2022-07-20).

(77) Leppanen, M.; Maasilta, I. J.; Sundberg, L.-R. Antibacterial Efficiency of Surface-Immobilized Flavobacterium-Infecting Bacteriophage. *ACS Appl. Bio. Mater* **2019**, *2*, 4720–4727.

(78) X-Ray Photoelectron Spectroscopy (XPS) Reference Pages.

(79) Duffy, G.; Whiting, R. C.; Sheridan, J. J. The Effect of a Competitive Microflora, PH and Temperature on the Growth Kinetics of Escherichia Coli O157:H7. *Food Microbiology* **1999**, *16*, 299–307.

(80) Elschner, A.; Lövenich, W. Solution-Deposited PEDOT for Transparent Conductive Applications. *MRS Bulletin* **2011**, *36*, 794–798.

(81) Huang, J.; Miller, P. F.; de Mello, J. C.; de Mello, A. J.; Bradley, D. D. C. Influence of Thermal Treatment on the Conductivity and Morphology of PEDOT/PSS Films. *Synthetic Materials* **2003**, *139*, 569–572.

(82) ElMahmoudy, M.; Inal, S.; Charrier, A.; Uguz, I.; Malliaras, G. G.; Sanaur, S. Tailoring the Electrochemical and Mechanical Properties of PEDOT:PSS Films for Bioelectronics. *Macromolecular Materials and Engineering* **2017**, *302*, 1600497.

(83) Zhang, S.; Hubis, E.; Girard, C.; Kumar, P.; DeFranco, J.; Cicoira, F. Water Stability and Orthogonal Patterning of Flexible Micro-Electrochemical Transistors on Plastic. *J. Mater. Chem. C* **2016**, *4*, 1382.

(84) Zhang, S.; Kumar, P.; Nouas, A. S.; Fontaine, L.; Tang, H.; Cicoira, F. Solvent-Induced Changes in PEDOT:PSS Films for Organic Electrochemical Transistors. *APL Materials 3*, 014911.

(85) Kiebooms, R.; Aleshin, A.; Hutchison, K.; Wudl, F.; Heeger, A. Doped Poly(3,4-Ethylenedioxythiophene) Films: Thermal, Electromagnetical and Morphological Analysis. *Synthetic Materials* **1999**, *101*, 436–437.

(86) Fan, J.; Rezaie, S. S.; Facchini-Rakovich, M.; Gudi, D.; Montemagno, C.; Gupta, M. Tuning PEDOT:PSS Conductivity to Obtain Complementary Organic Electrochemical Transistor. *Organic Electronics 66*, 148–155.

(87) Kamensky, M. A.; Eliseeva, S. N.; Lang, G.; Ujvari, M.; Kondratiev, V. V. Electrochemical Properties of Overoxidized Poly-3,4-Ethlenedioxythiophene. *Russian Journal of Electrochemistry* **2018**, *54* (11), 893–901.

(88) Tang, K.; Miao, W.; Guo, S. Crosslinked PEDOT:PSS Organic Electrochemical Transistors on Interdigitated Electrodes with Improved Stability. *ACS Appl. Polym. Mater.* **2021**, *3*, 1436–1444.

(89) Salmani-Rezaie, S. Organic Electrochemical Transistor, Understanding and Modifying for Sensing Applications. Thesis for the degree of Master of Science in Materials Engineering, University of Alberta, Edmonton Alberta, 2016.

(90) Kelestemur, S.; Altunbek, M.; Culha, M. Influence of EDC/NHS Coupling Chemistry on Stability and Cytotoxicity of ZnO Nanoparticles Modified with Proteins. *Applied Surface Science* **2017**, *403*, 455–463.

(91) Wang, C.; Sauvageau, D.; Elias, A. Immobilization of Active Bacteriophages on Polyhydroxyalkanoate Surfaces. *ACS Appl. Mater. Interfaces* **2016**, *8*, 1128–1138.

(92) *Table of Elements | Thermo Fisher Scientific - CA*. https://www.thermofisher.com/ca/en/home/materials-science/learning-center/periodic-table.html (accessed 2022-08-08).

(93) Goon, I. Y.; Lai, L. M. H.; Lim, M.; Amal, R.; Gooding, J. J. 'Dispersible Electrodes': A Solution to Slow Response Times of Sensitive Sensors. *Chemical Communications* **2010**, *46* (46), 8821–8823.

(94) Yang, X.; Li, C.; Hiang, J.; Liu, Y. Nitrogen-Doped Fe3C@C Particles as an Efficient Heterogeneous Photo-Assisted Fenton Catalyst. *RSC Advances* **2017**, *7* (25), 15168–15175.

(95) Pavani, P.; Kumar, K.; Rani, A.; Venkatesu, P.; Lee, M.-J. The Influence of Sodium Phosphate Buffer on the Stability of Various Proteins: Insights into Protein-Buffer Interactions. *Journal of Molecular Liquids* **2021**, *331*, 115753.

(96) Kadavi, D. R.; Shaffer, J. J.; Lott, S. E.; Wolf, T. A.; Bolton, C. E.; Gallimore, W. H.; Martin, E. L.; Nichelson, K. W.; Kokjohn, T. A. Influence of Infected Cell Growth State on Bacteriophage Reactivation Levels. *Applied and Environmental Microbiology* **2000**, *66* (12), 5206–5212.

(97) Butina, K.; Filipovic, F.; Richter-Dahlfors, A.; Parlak, O. An Organic Electrochemical Transistor to Monitor Salmonella Growth in Real-Time. *Adv. Mater.* **2021**, *8*, 2100961.

Appendix A: Permissions to Reproduce

Figure 1.2 is reprinted (adapted) with permission from Sensitive Detection of Sweat Cortisol Using an Organic Electrochemical Transistor Featuring Nanostructured Poly(3,4-Ethylenedioxythiophene) Derivatives in the Channel Layer. Janardhanan, J. A.; Chen, Y.-L.; Liu, C.-T.; Tseng, H.-S.; Wu, Po.-I.; She, J.-W.; Hsiao, Y.-S.; Yu, H.-h *Anal. Chem.* 2022, 94, 21, 7584–*7593*. Copyright 2022 American Chemical Society

Figure 2.3 is reprinted from Drugs Delivery Today, Vol 23, Issue 2, Łukasz Richter,Marta Janczuk-Richter,Joanna Niedziółka-Jönsson,Jan Paczesny,and Robert Hołyst, Recent advances in bacteriophage-based methods for bacteria detection, pages no. 448-455.; Copyright 2018, with permission from Elsevier (License # 5370951497089)

Figure 2.6 is reprinted from Nature Review Materials, Vol. 3, Jonathan Rivnay *et al.*, Organic electrochemical transistors, article no. 17086; Copyright 2018, with permission from Springer Nature (License # 5370950997005)

Figure 2.9 is reprinted from Food Control, Vol. 135, Ahmed Y. El-Moghazy, Nicharee Wisuthiphaet, Xu Yang, Gang Sun, Nitin Nitin, Electrochemical biosensor based on genetically engineered bacteriophage T7 for rapid detection of Escherichia coli on fresh produce, start page 108811; Copyright 2022, with permission from Elsevier (License # 5370951364692)

Figure 2.11 is reprinted (adapted) with permission from Detection of bacteria with organic electrochemical transistors. He, Rong-Xiang; Zhang, Meng; Tan, Fei; Leung, Polly H. M.; Zhao, Xing-Zhong; Chan, Helen L.W.; Yang, Mo; Yan, Feng *Journal of materials chemistry.* 2022, Vol. 22, Issue 41, 22072. Copyright 2012 Royal Society of Chemistry (Licenses #1258583-1, and # 1258584-1)